ANALYSIS, DESIGN AND CONTROL OF DIRECT-DRIVE MANIPULATORS

by

Kamal Youcef-Toumi

BSME, Mechanical Engineering
University of Cincinnati.
(1979)
MSME, Mechanical Engineering
Massachusetts Institute of Technology
(1981)

SUBMITTED TO THE DEPARTMENT OF MECHANICAL ENGINEERING IN PARTIAL FULFILLMENT OF THE REQUIREMENTS FOR THE DEGREE OF

DOCTOR OF SCIENCE

IN

MECHANICAL ENGINEERING

at the

MASSACHUSETTS INSTITUTE OF TECHNOLOGY

May 1985

Signature of Author _____
Department of Mechanical Engineering
May 17, 1985

Certified by _____
Prof. Haruhiko Asada
Thesis Supervisor

Accepted by _____
Prof. A. A. Sonin
Chairman, Department Graduate Committee

ANALYSIS, DESIGN AND CONTROL OF DIRECT-DRIVE MANIPULATORS

by

Kamal Youcef-Toumi

Submitted to the Department of Mechanical Engineering on May 17, 1985 in partial fulfillment of the requirements for the degree of Doctor of Science in Mechanical Engineering.

Abstract

The direct-drive arm exhibits several advantageous properties including no backlash, low friction, and high mechanical stiffness. These advantages are a consequence of eliminating the actuator transmission. The manipulator, however, becomes extremely massive and highly sensitive to the linear and nonlinear inertial interactive forces when the actuators are mounted between adjacent links.

This thesis presents effective design methods for articulated direct-drive arms, specifically for application to high-speed and high-accuracy trajectory control tasks. The inherent difficulties of the direct-drive concept are overcome and the potential advantages are fully exploited.

First, an analytical tool is developed to evaluate the static force characteristics of mechanisms. The effectiveness of different kinematic structures is evaluated in terms of the power dissipation in the actuators.

Second, a new approach is developed for arm linkage design. The goal is to simplify the controller design by reducing the effects of complicated manipulator dynamics and to further improve performance by increasing the load capacity. A method for designing an arm linkage with small inertial load changes and small interactive forces is developed by analyzing the kinematic structure, actuator locations and the mass properties. This design methodology achieves a decoupled and invariant manipulator inertia tensor in joint space. As a result, each actuator experiences completely decoupled dynamics as well as a constant load which is independent of the arm configuration.

These design tools are applied in the development of the 3 d.o.f M.I.T direct-drive arm. The manipulator, with a decoupled and nearly invariant arm inertia tensor, shows a substantial improvement in control performance. The arm performance is evaluated in terms of speed, acceleration and torque control capability.

Thesis Supervisor and Chairman: Prof. Haruhiko Asada
Title: Associate Professor of Mechanical Engineering

Thesis Committee Members: Prof. Steven Dubowsky
Prof. Neville Hogan
Prof. John Hollerbach

ACKNOWLEDGEMENTS

I would like to thank my thesis supervisor, Professor Haruhiko Asada, for his constant encouragement during this research. His professional advice, patience and very useful criticisms are sincerely appreciated. Many thanks go to the members of my thesis committee: Prof. S. Dubowsky, Prof. N. Hogan and Prof. J. Hollerbach for their sharp criticisms and suggestions.

I express my sincerest gratitude to my sponsor, Shin Meiwa Industry Co. LTD. of Japan, for their support which made this work possible. Special thanks go to Dr. M. Kaga and Mr. H. Koyama. I am also greateful to Mr. H. Yamamoto for the useful suggestions, help at odd hours in the laboratory, and friendship.

I thank all members of the robotics group for their support. Special thanks go to Andre By, Jose Cro Granito, Richard Ramirez, Paul Ro and Harry West for the enlightening discussions, Paul Fillipski for the valuable discussions on dynamics, Neil Goldfine for his comments and reviews of this thesis and other documents, and Swee-Keng Lim for his comments and help with the torque estimation experiments.

The administrative help from Sandra Williams Tepper and Anne Diamond are sincerely acknowledged.

Finally and foremost to my wife Fawzia, my son Zakaria and parents for their love, patience, constant support and encouragement.

Table of Contents

List of Figures

List of Tables

Chapter 1
INTRODUCTION

1.1 Background

The dynamic characteristics of a manipulator often determine its ability to perform complex tasks. High speed and precision are essential in many advanced applications of robot manipulators [Dubowsky 83]. An example is the high speed laser cutting application for which the required robot speeds and accelerations are on the order of 3 m/sec and 3 to 5 G, respectively, which are an order of magnitude higher than obtainable with conventional robots. In order to meet such severe requirements, hardware limitations in today's robots must be overcome.

Electromechanical drives for robots typically employ gearing to match the impedances of the motors with their corresponding loads. These mechanisms often introduce serious problems that degrade the control performance of the robot. Harmonic drives, for example, which are widely used in existing robots, have insufficient mechanical stiffness and cause a significant fluctuation in the torque transmitted. Other robots have conventional gear trains for which backlash is the main problem [Unimation 80]. A common technique for eliminating backlash is the preloading of gears. A large preload, however, leads to large friction which causes gears to wear quickly. Also, these gears must be adjusted regularly to keep the backlash to a minimum.

Furthermore, conventional electromechanical robots are essentially positioning devices and are not suitable for torque control. Sophisticated control

schemes recently developed, such as bilateral control [Inoue 71], generalized springs and dampers [Nevins and Whitney 74], grasping compliance control [Hanafusa and Asada 77], hybrid position/force control [Raibert and Craig 80], impedance control [Hogan 81], and compliant motion control [Mason 81] are all dependent on the actuators ability to control torque, directly or indirectly. Primarily, these control schemes have been implemented on conventional electromechanical robots, which were not designed as torque-controlled devices. Consequently, performance has been limited by friction and deflection in the gearing.

1.2 Direct-drive Concept

Direct-Drive is an innovative design approach which shows great promise in control performance. A direct-drive arm is a mechanical manipulator in which high-torque, low-speed motors are directly coupled to their respective loads [Asada and Kanade 83, Asada, Kanade and Takeyama 83]. A basic construction for a direct-drive joint is shown in Figure 1-1. Since no gearing is employed in the mechanism, the joint has low friction, high mechanical stiffness and no backlash. Therefore, the direct-drive arm has the potential for fast and accurate positioning as well as precise torque control.

Consequently, direct-drive arms meet the critical requirements of many advanced robot applications. High speed is a crucial requirement in high production-rate manufacturing. Traditional robots are not suitable for such production lines because of severe task time requirements. Fast but simple positioning devices such as pneumatic cylinders have been used for high production-rate lines, but limited flexibility is a major problem for these simple devices. Thus direct-drive arms with higher speeds and greater flexibility are appropriate for high

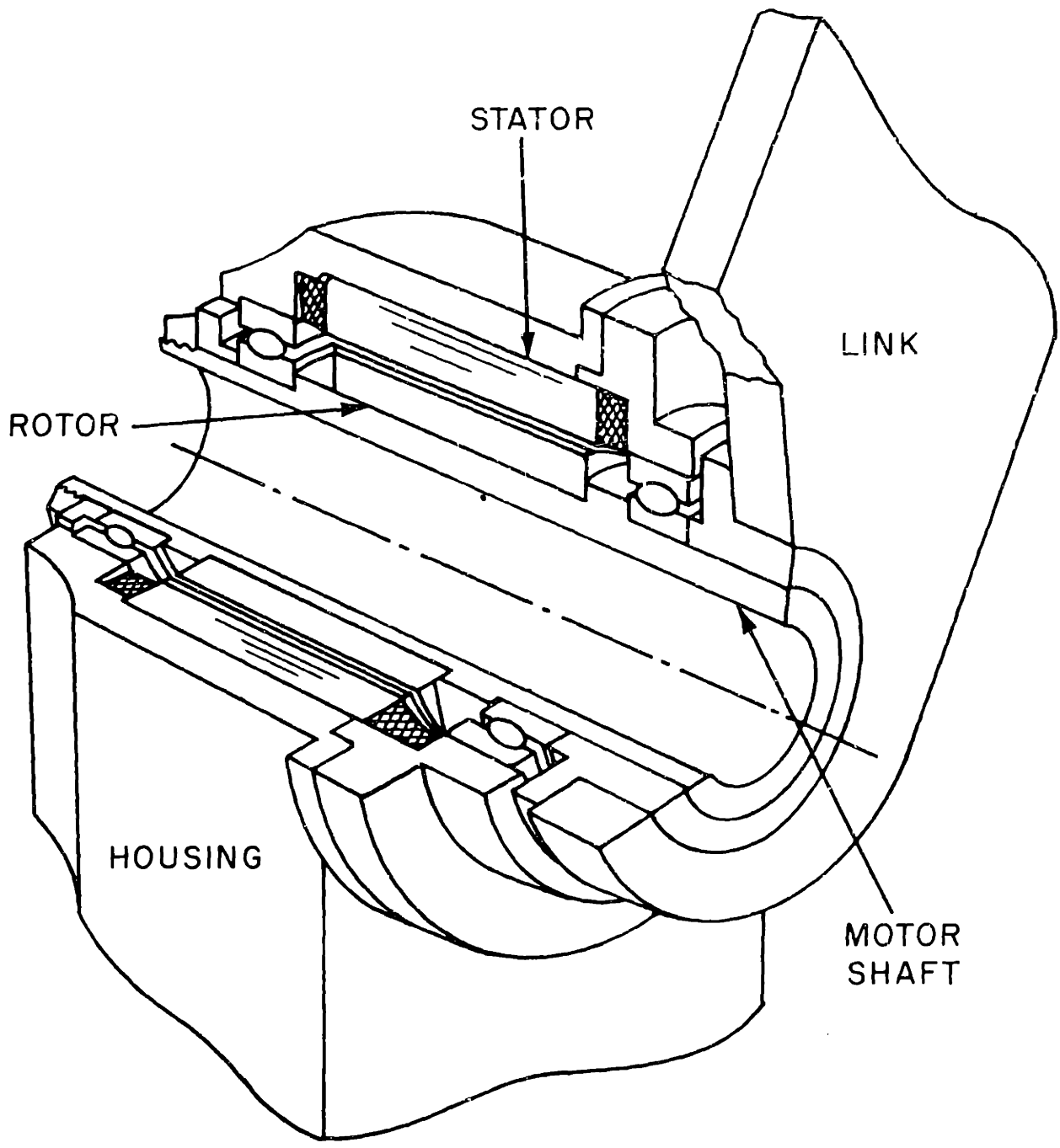

Figure 1-1: Basic construction of a direct-drive joint

production-rate flexible manufacturing systems.

There is also an increasing need for high accuracy robots, particularly in the microelectronics industry. Assembly of optical fibers, for example, requires accuracy on the order of 3 to 10 μm. Such high accuracy operations are out of the range of today's industrial robots which use reducers. As the size of the electronic devices decreases and the density of chips increases, still higher accuracy is required for positioning devices. The direct-drive method meets such increasing accuracy requirements.

Both high speed and high accuracy are required for some advanced robot applications. Sheet metal cutting using a laser or plasma cutter requires a speed of over 1 m/s with 3 to 5 G acceleration with trajectory tracking errors of less than 0.05 mm. Even a small amount of backlash or deflection at the gearing is not acceptable when such severe specifications must be met.

1.3 Issues and Objectives

Although the direct-drive method provides some desirable characteristics, it also has several drawbacks. First, since the drive system has no means of amplifying the motor output torque, hence the robot can not exert a large force for a long time without overheating the motors. Second, if the motors are mounted at the joints of a serial linkage arm, the weight of each motor is a load to the other motors. Therefore, the required motor sizes increase rapidly from the distal joint to the proximal joint. This rapid increase results in a heavy arm with a relatively small load capacity [Asada and Kanade 83]. The third drawback is the high sensitivity of direct-drive motors to arm inertia changes or disturbances. The inertial load of each axis varies with the arm configuration and, interactive and

nonlinear forces also act on each axis of the manipulator arm. These varying loads and disturbance forces are all reflected directly to the motor axes and consequently affect the dynamic behavior of the direct-drive motors significantly [Asada, Kanade and Takeyama 83]. Finally, the major difficulty in designing the control system is to maintain stability in the face of a wide range load conditions. Because of the direct coupling, the inertial load reflected to the motor axis is significantly large in comparison with its damping factor. This results in a slow response (large mechanical time constant). In addition, the direct-drive motors use large windings in order to exert a large torque, thus the electrical time constant is also large.

The goal of this thesis is then to explore effective *design methods* for articulated direct-drive arms applied in high-speed high-accuracy trajectory control tasks. The inherent difficulties, mentioned above, must be overcome so that the potential advantages can be fully exploited. These design methods include a power efficiency analysis for the kinematic structure design and a dynamic analysis of articulated direct-drive arms.

A new approach is developed for the arm linkage design in order to increase the load capacity and reduce the effect of the complicated manipulator dynamics, thereby simplifying the controller design. The kinematic structure and mass properties are analyzed. Then a method for designing an arm linkage with small inertial load changes and small interactive and nonlinear forces is developed. One desirable feature is a decoupled and invariant inertia tensor in joint space. The joint axes dynamics are completely decoupled from each other and experience a constant load independently of the arm configuration, under this condition.

1.4 Overview of the Thesis

Chapter 2 deals with two major issues of direct-drive arm design, namely overheating and small load capacity. A power efficiency analysis is presented to address these issues. First, an analytical tool based on the motor constants is formulated in order to evaluate the end point static force characteristics of arm mechanisms. Second, the traditional serial configuration of the direct-drive arm is compared with a parallel drive configuration that avoids the large arm weight. The parallel drive configuration improves the load capacity to arm weight ratio and minimizes the power dissipation in the actuators. The effectiveness of these kinematic structures is evaluated in terms of power dissipation.

The direct-drive motors are highly sensitive to the complicated arm dynamics. A mass distribution technique is developed in Chapter 3 to minimize these effects on the drive system. The inertia of the different links are redistributed to achieve a decoupled and invariant inertia tensor for the articulated direct-drive arm. Each joint actuator of such an arm experiences a constant inertial load with no inertial coupling or nonlinear velocity torques from other joints throughout the whole workspace. In this Chapter, necessary conditions and, necessary and sufficient conditions for achieving this ideal dynamic behavior are derived for open loop kinematic chains with revolute joints.

In the previous Chapter, each actuator was located at the corresponding joint where it exerted a torque between the adjacent links. This type of drive system limits the number of degrees of freedom that can be decoupled. The actuator, however can be located on other links if an appropriate transmission can be used. Chapter 4 discusses the decoupling problem for a mechanism where the actuators are relocated to other links with the use of a transmission. It will be shown that the

decoupling condition as previously obtained can be significantly relaxed by the relocation of actuators. When actuators are mounted remotely and joints are driven through a transmission, the torque exerted by one actuator is not necessarily applied to one joint but can affect several joints. Thus, the effects of relocating the actuators on the manipulator kinematics and dynamics, is also studied. First, the relationship between the actuator displacements and their corresponding joint displacements are set up. Then the linear and angular velocity vectors of each link are determined in order to examine the new manipulator dynamics. Second, the manipulator mass properties are considered. The analysis of Chapter 3 shows that the effects due to rotation about the centroid of a link are of primary concern. It is necessary to determine which link mass properties affect the coupling between any given two actuators. Specifically, the moments of inertia are of special interest. A useful notation is introduced to facilitate this task and help in the understanding of coupling.

Chapter 5 presents the design guidelines using the theorems and the corollaries of Chapter 3 and, the set notation of Chapter 4. The decoupling conditions derived are then expressed as a design rule for decoupling serial spatial mechanisms. Also, the sufficient conditions for a decoupled and invariant n degree-of-freedom planar mechanism are derived. Finally, a discussion on mechanisms using parallel drives is given. It will be shown that merely locating the actuators at the base does not guarantee decoupling.

The guidelines, described in Chapter 5, are applied in the design of the 3 d.o.f M.I.T direct-drive arm. The mass distributions for decoupling the arm inertia tensor are derived. Discussions on the design trade-offs are given.

The overall control performance of the M.I.T direct-drive arm is then evaluated in Chapter 7. On the basis of the simplified arm load condition, the

design of the drive control system is discussed. This includes (i) the modeling of the actuator and position control system, and (ii) the modeling of joint torque sensor, where the torque developed at the joint is estimated using phase currents, and the torque control performance at the joint level. The overall dynamic performance of the M.I.T direct-drive arm is then evaluated experimentally, including the decoupled arm inertia tensor. Finally, Chapter 8 gives a summary of conclusions and recommendations.

Chapter 2
POWER EFFICIENCY ANALYSIS

2.1 Introduction

This Chapter presents an analytical tool for evaluating mechanisms in terms of the power dissipation in the actuators and the end point force generated. This is particularly important in evaluating the overheating of direct-drive actuators. Two different mechanisms are selected and compared for use in the direct-drive approach.

2.2 Power Efficiency Analysis

One of the problems with the direct drive approach is that the robot can not exert a large force. Because of the direct coupling of motors to their loads, the output torques of motors are not amplified through reducers. In consequence, the motors have to bear the loads directly, and can overheat, particularly in a stall condition. In this section, we analyze the power dissipated in the motors when a force is exerted at the tip of the arm.

An important parameter for torque motors is the motor constant, that is, the ratio of output torque τ to the square root of power dissipated in the motor P [Electro-Craft 80],

$$k_m = \frac{\tau}{\sqrt{P}} \tag{2.1}$$

The motor constant represents how efficiently the motor converts its input power into output torque. If k_m is small, the motor dissipates a large amount of power to exert torque.

When a robot bears a load at the arm tip, the load is distributed among all the motors of the arm mechanism. In addition to the individual motor characteristics, the efficiency of exerting a force at the arm tip also depends on the kinematic structure of the arm mechanism. Let **F** be the end point force exerted at the arm tip represented in cartesian coordinates, and let τ be the vector of equivalent torques of n motors, then one obtains [Paul 81]

$$\tau = \mathbf{J}^t \mathbf{F} \tag{2.2}$$

where **J** is the jacobian matrix associated with the coordinate transformation from the joint coordinates to the cartesian coordinates of the arm tip.

Let P be the total power dissipated in the n motors driving the arm mechanism and k_{mi} be the motor constant of the i-th motor, then the total power dissipation P is given by the following quadratic form of end point force **F**,

$$P = \sum_{i=1}^{n} \frac{\tau_i^2}{k_{mi}^2} = \mathbf{F}^t \mathbf{L} \mathbf{F} \tag{2.3}$$

where **L** is given by

$$\mathbf{L} = \mathbf{J}\ diag\left(\frac{1}{k_{m1}^2}, \ \cdots\ , \frac{1}{k_{mn}^2} \right) \mathbf{J}^t \tag{2.4}$$

Thus the power dissipation depends not only on the kinematic structure but also on the motor constants of the actuators.

The relation given by (2.4) is a congruence transformation, and thus the

matrix **L** is positive definite as long as the Jacobian matrix is nonsingular [Strang 80]. Therefore the matrix **L** has all real, positive eigenvalues, $\lambda_i > 0$, and the quadratic form can be rewritten as

$$P = \sum_{i=1}^{n} \lambda_i F_i^2 \tag{2.5}$$

where F_i is the component of end point force along the eigenvector corresponding to λ_i. The geometrical interpretation of equ.(2.3) is obtained by fixing the total power *P*. In this case , the quadratic form of equ.(2.3) is that of an ellipsoid as shown in Figure 2-1. The principal axes of such an ellipsoid are aligned with the eigenvectors of the matrix **L**, and the length of each principal axis is equal to the reciprocal of the square root of the corresponding eigenvalue. Since the smallest (largest) eigenvalue of **L** corresponds to the major (minor) axis of the ellipsoid, the maximum (minimum) force **F** acts along the major (minor) axis. Therefore, along the major axis, the input power is most effectively converted into a force at the arm tip. Since the matrix **L** involves the Jacobian matrix **J**, which varies with the arm configuration, the static characteristics vary as well. By examining the ellipsoid for different arm configurations, one can analyze the global characteristics of the power to force conversion.

To evaluate the overall efficiency of the arm-motor combination, we define the mean power dissipation ratio, λ_m, which is the mean of the eigenvalues and is given by

$$\lambda_m = \frac{1}{n} \mathit{trace}(\mathbf{L}) \tag{2.6}$$

The units of λ_m are Watts per square Newton.

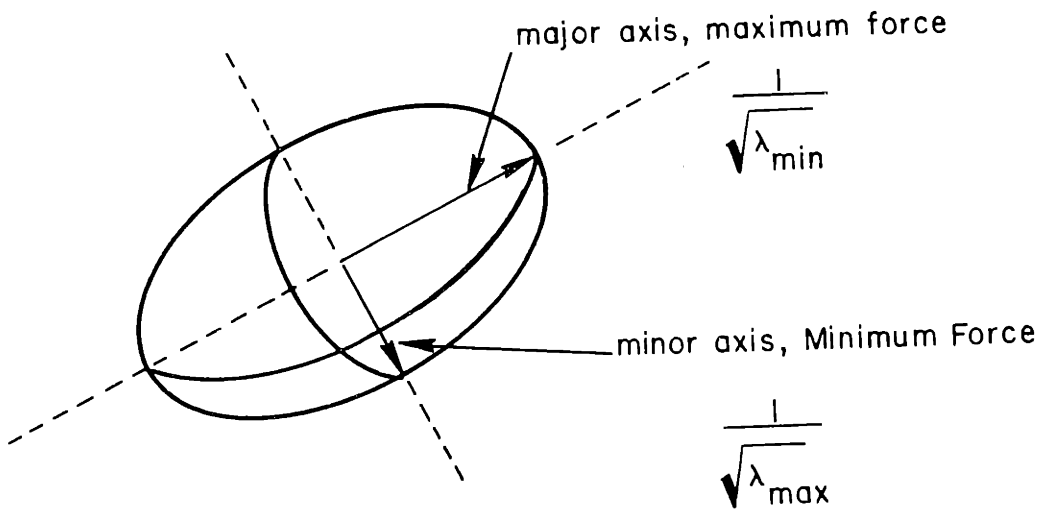

Figure 2-1: Force ellipsoid.

2.3 Kinematic Structure Design

2.3.1 Parallel Drive Mechanism

In order to select a suitable kinematic structure for a direct-drive arm, we consider the following basic structures : a simple serial drive mechanism, as shown in Figure 2-2; and a general five-bar-link parallel drive mechanism, shown in Figure 2-3.

In this section we define these two drive system methods: serial drive and parallel drive. Figure 2-2 shows the typical construction of a serial drive arm mechanism, in which the lower link is driven by a motor fixed on the base and the upper link is driven by a motor attached at the tip of the lower link. In this serial configuration, the weight of the second motor is a load to the first motor. Moreover, the reaction torque of the second motor acts on the first motor. When the second motor accelerates in the clockwise direction, a counter-clockwise torque acts on the first motor, and vise versa. Thus the two motors have significant interactions. In this thesis, an arm mechanism in which each motor is located at a joint of a serial linkage between the adjacent links is referred to as a serial drive mechanism.

Figure 2-3 shows an alternative arm construction consisting of a five-bar-link. Two motors fixed on the base drive the two input links and cause a two-dimensional motion at the tip of the arm. The weight of one motor is not a load on the other. Also the reaction torque of one motor does not act directly upon the other, because the motors are fixed on the base . An arm mechanism in which motors are mounted on a fixture and the weight and reaction torque of one motor do not affect the other motors directly is referred to as a parallel drive mechanism.

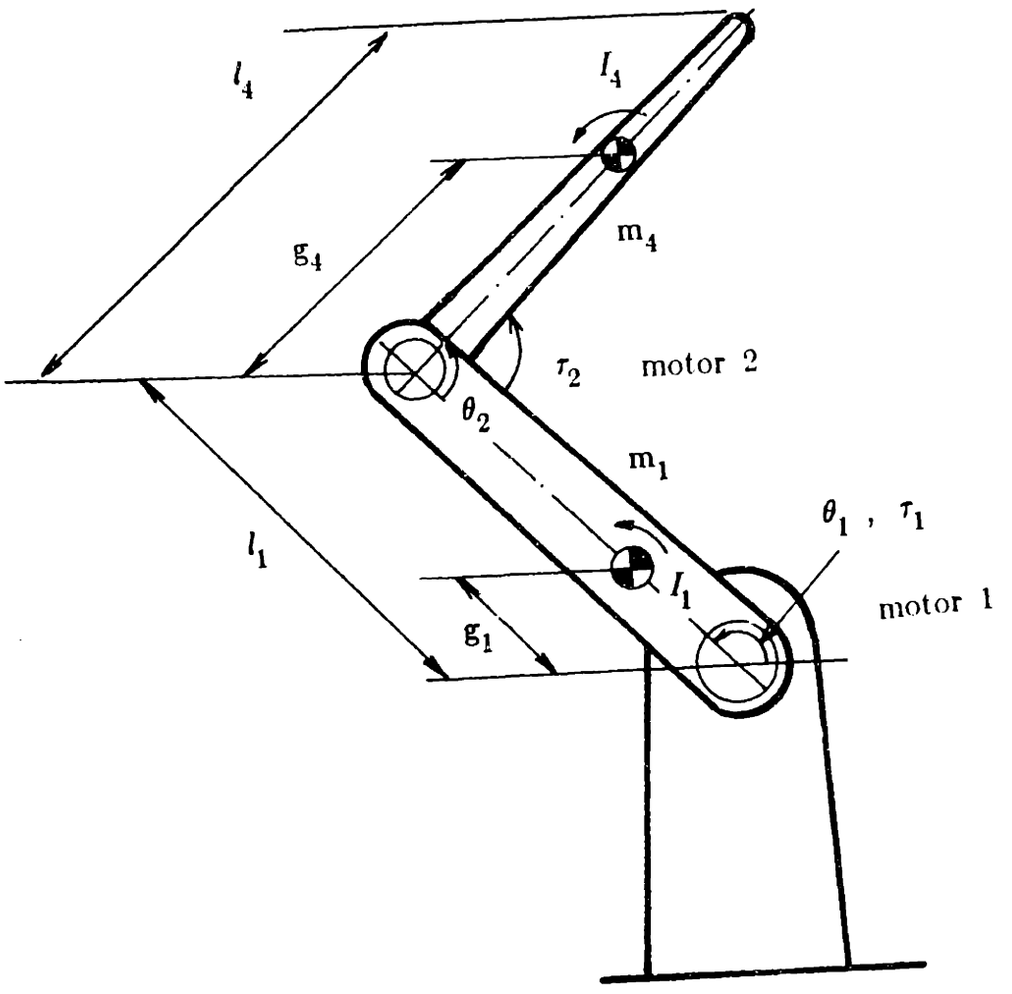

Figure 2-2: 2 d.o.f serial drive arm mechanism.

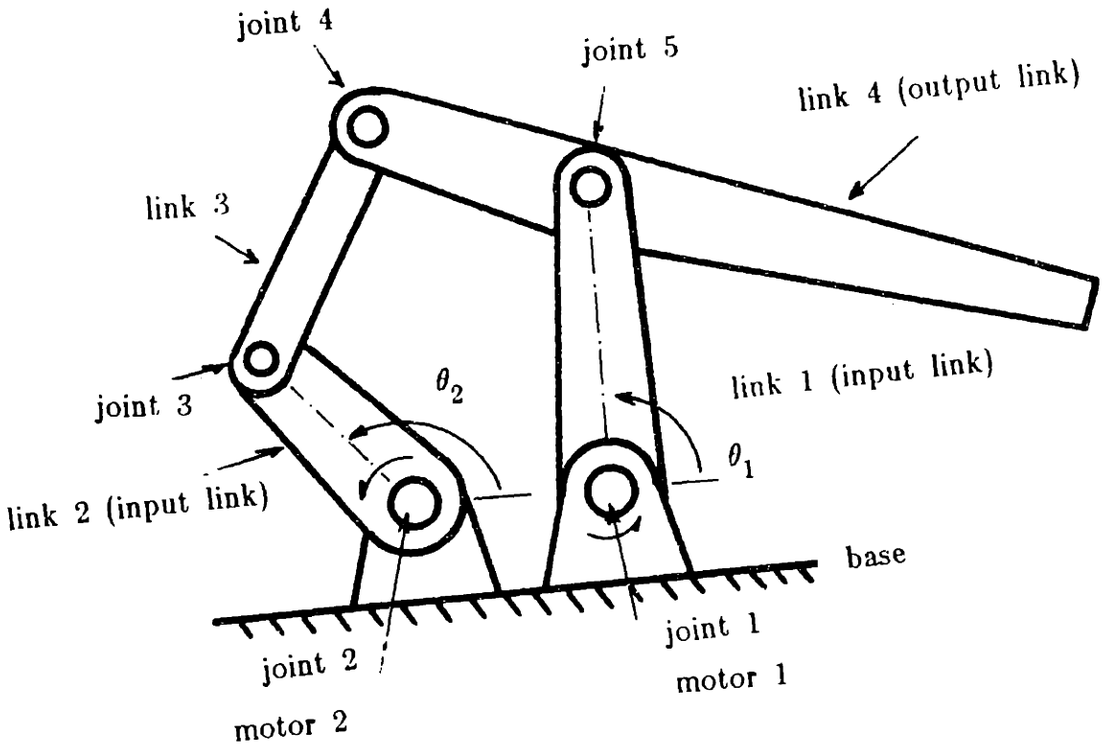

Figure 2-3: A general five-bar-link mechanism

The parallel drive mechanism has been used in several models of commercial robots that have conventional electromechanical drives with gearings. The five-bar-link mechanism, however, is particularly useful for overcoming the inherent difficulties of the direct drive method.

2.3.2 Motor Constant Identification

In order to use the analysis of the previous section, the motor constants, k_{mi}, have to be determined. The following experiment was conducted to identify the motor constant of a single active joint. First, a position control system is set up to permit the arbitrary positioning of the motor rotor using a computer terminal (see Chapter 7). This position control system is needed since the relationships derived in the previous section are valid at stall condition. Second, known torque loads were applied to the motor shaft while under position control and the power input to the system was calculated using the corrected phase currents in the motor (Appendix A). Figure 2-4 provides a plot of the experimental data. The square root of power measured is plotted against the torque applied. A least square fit yields a motor constant of 2.366 $Nm/\sqrt{Watts}$.

2.3.3 Kinematic Structure Evaluation

The end point force for the serial drive mechanism in comparison with the parallel drive mechanism of Figure 2-5 is evaluated. These characteristics were analyzed in [Asada and Youcef-Toumi 83, Asada and Youcef-Toumi 84].

For the five-bar-link parallel drive mechanism, matrix **L** is given by

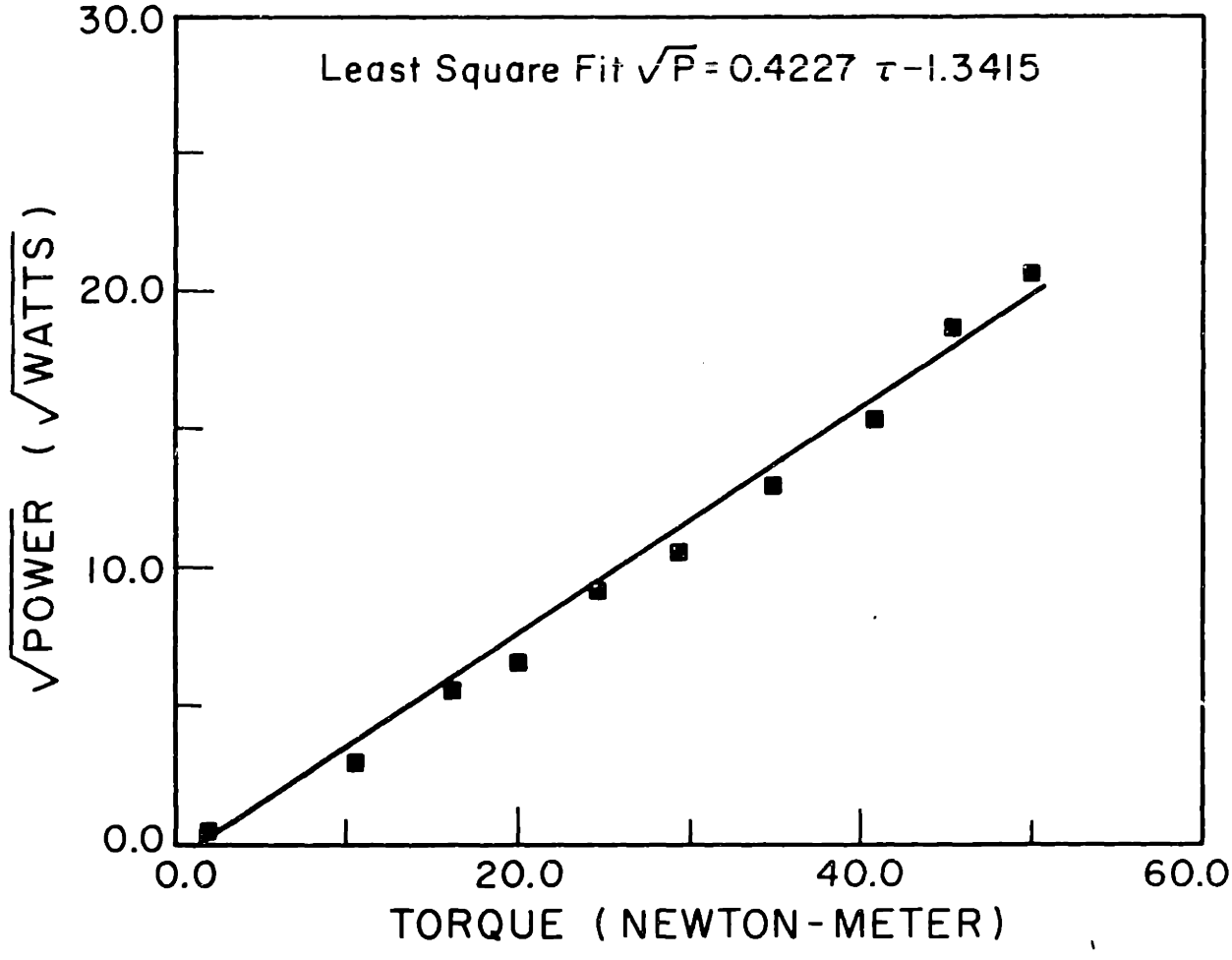

Figure 2-4: Motor constant.

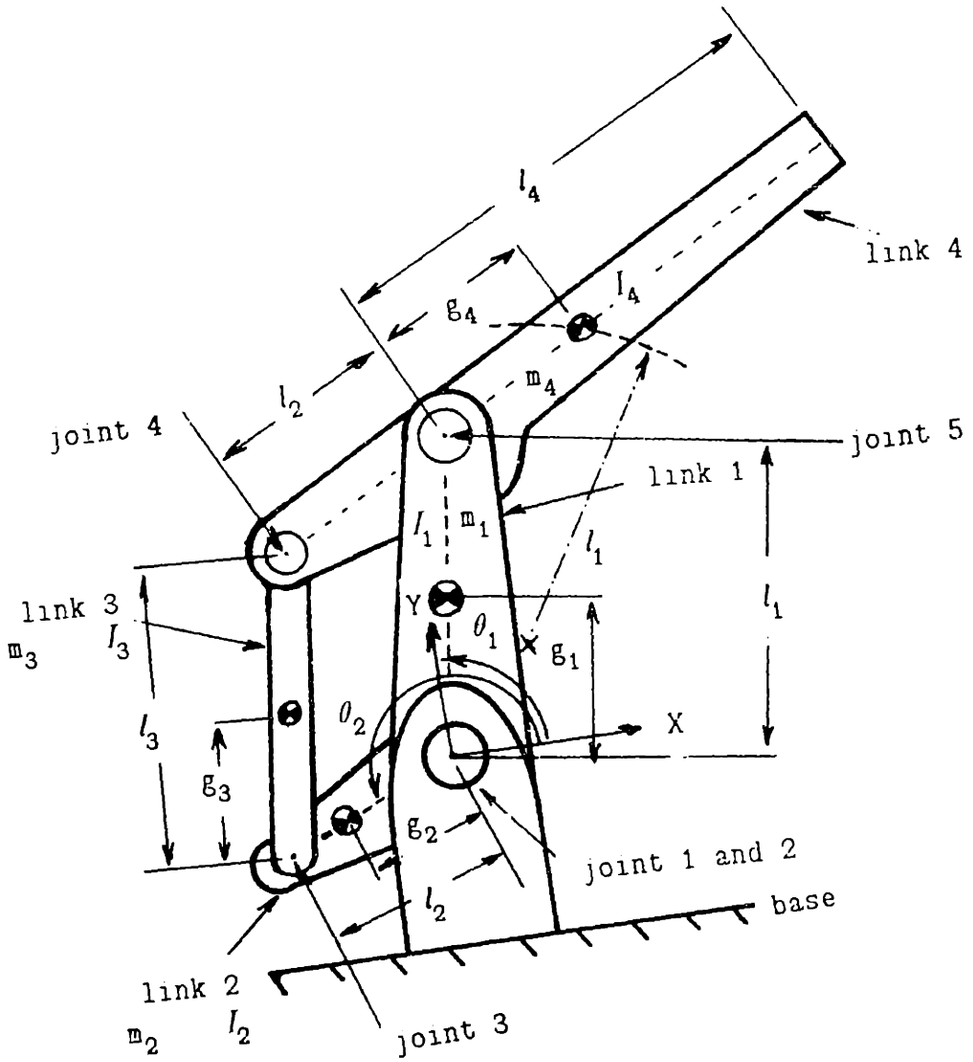

Figure 2-5: 2 d.o.f parallel drive five-bar-link mechanism

$$\mathbf{L} = \begin{bmatrix} L_{11} & L_{12} \\ L_{12} & L_{22} \end{bmatrix}$$

where

$$L_{11} = \frac{l_1^2}{k_{m1}^2}\sin^2(\theta_1) + \frac{l_4^2}{k_{m2}^2}\sin^2(\theta_2)$$

$$L_{12} = -\frac{l_1^2}{k_{m1}^2}\sin(\theta_1)\cos(\theta_1) - \frac{l_4^2}{k_{m2}^2}\sin(\theta_2)\cos(\theta_2)$$

$$L_{22} = \frac{l_1^2}{k_{m1}^2}\cos^2(\theta_1) + \frac{l_4^2}{k_{m2}^2}\cos^2(\theta_2)$$

where the end point force **F** is represented in the coordinate system fixed at the base as shown in Figure 2-5.

Figure 2-6 illustrates the static force characteristics, equ.(2.3), for the parallel configuration. The maximum (minimum) force produced is along the major (minor) axis of the ellipsoid at the tip of the arm. Note that in this parallel configuration the force appears to be nearly isotropic in a wide region . The maximum force based on a total power of 1 KW is estimated to be 190 N. This value is obtained by taking the square root of the ratio of the power to the minimum eigenvalue.

The mean power dissipation ratio is then given by

$$\lambda_m = \frac{1}{2}\left(\frac{l_1^2}{k_{m1}^2} + \frac{l_4^2}{k_{m2}^2}\right) \tag{2.7}$$

Although the matrix **L** varies with the arm configuration, the mean power

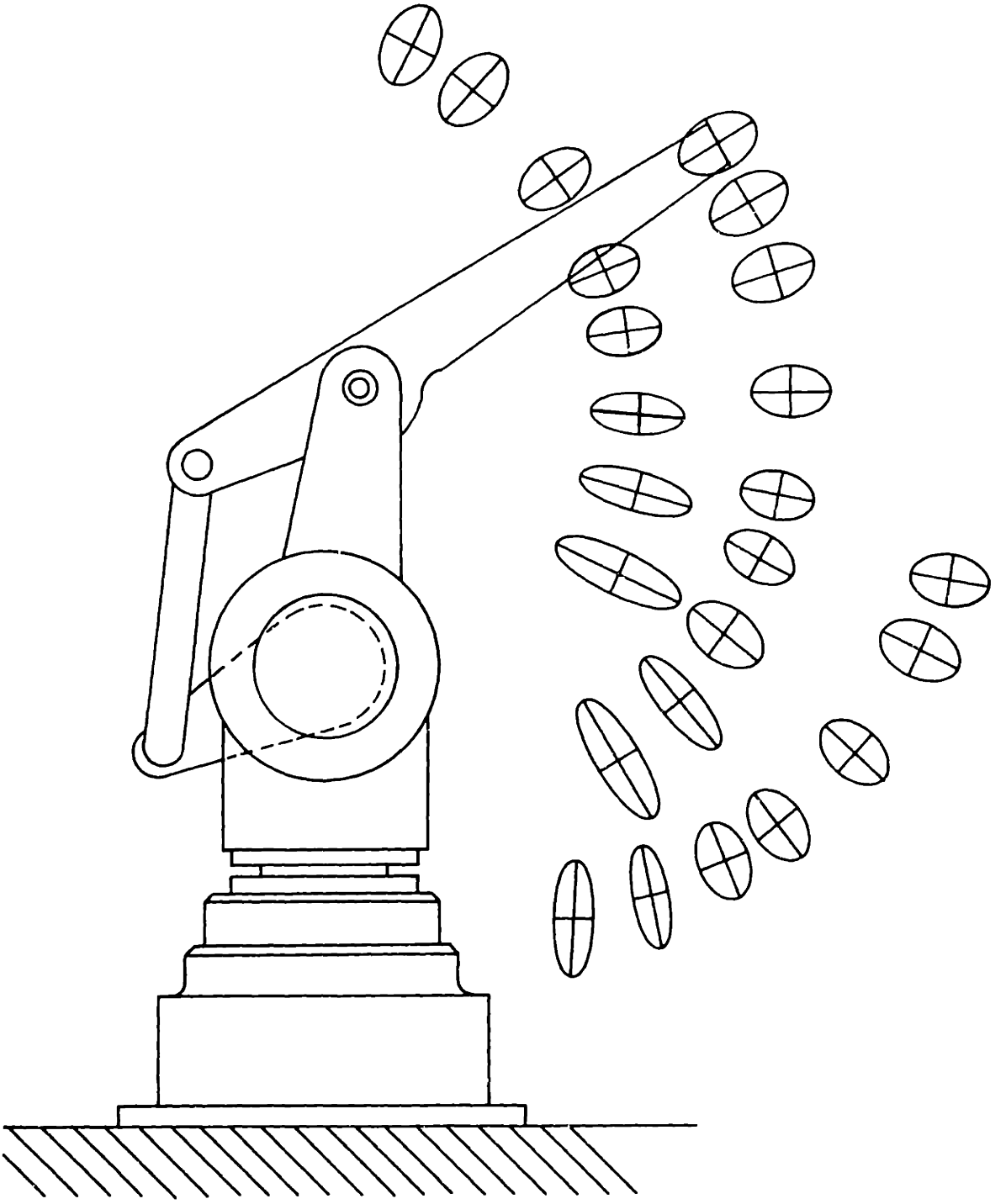

Figure 2-6: Static force characteristics

dissipation λ_m is uniform for all the configurations. For shorter link lengths, l_1 and l_4, and larger motor constants, k_{m1} and k_{m2}, the arm-motor combination has a better efficiency having a small mean power dissipation ratio.

Let us compare the parallel drive mechanism with the serial drive in terms of the value of λ_m. The mean power dissipation ratio of the serial drive mechanism of Figure 2-2 is

$$\lambda_m = \frac{1}{2}\left(\frac{l_1^2}{k_{m1}^2} + \frac{l_4^2}{k_{m2}^2} + \frac{l_4^2}{k_{m1}^2}\right) - \frac{l_1 l_4}{k_{m1}^2}\cos(\theta_2) \qquad (2.8)$$

In this case, λ_m varies depending on the arm configuration. As θ_2 increases, λ_m becomes larger, namely, the efficiency becomes lowe. • Comparing equ.(2.7) with equ.(2.8), one finds the parallel drive has a smaller mean power dissipation ratio than the serial drive except when

$$|\theta_2| \leq \cos^{-1}\left(\frac{l_4}{2l_1}\right)$$

The mean power curves are shown in Figure 2-7.

In the case of the prototype I robot described in Figure 2-5 [Asada and Youcef-Toumi 83, Asada and Youcef-Toumi 84], link lengths, l_1 and l_4, are 0.40 m and 0.65 m respectively, and the angle of joint 2 is limited by 35 Deg $\leq \theta_2 \leq$ 170 Deg. Then the parallel drive mechanism has a better efficiency for all arm configurations within the limit. This is another important advantage of the parallel drive mechanism over the serial drive. Having the same motor constants and the same link lengths covering the same workspace, the parallel drive mechanism can more efficiently exert force at the arm tip.

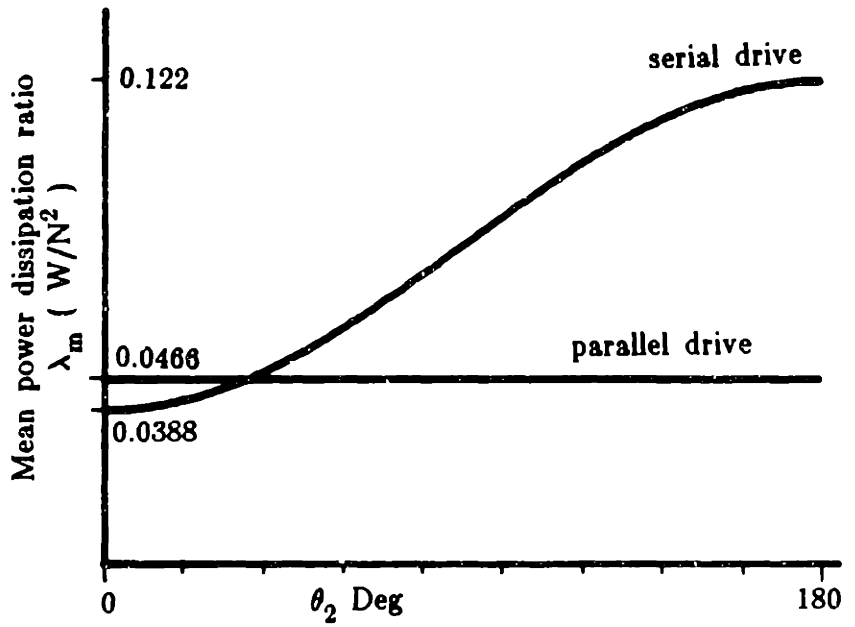

Figure 2-7: Mean power dissipation ratio for the parallel and serial drives.

2.4 Conclusion

By analyzing the internal power dissipation at the motors when exerting a force at the tip of the arm, it was shown that the parallel drive mechanism has a lower power dissipation than a serial drive that has the same motors and covers the same workspace.

Chapter 3
DECOUPLING OF MANIPULATOR INERTIA TENSORS

3.1 Introduction

This Chapter introduces the concept of simplification of manipulator dynamics through decoupling the inertia tensor, as well as by making it invariant for different arm configurations. First, a serial arm linkage with all revolute joints is analyzed and the conditions, for the arm structure and mass distributions, to have decoupled inertia tensors are derived. The necessary and sufficient conditions for decoupled and invariant inertia tensors are then derived for a group of arm mechanisms.

3.2 Simplification of Manipulator Dynamics

Robot manipulators are highly nonlinear and coupled dynamic systems. The motion of one actuator is disturbed by other actuator motions, and the dynamic behavior varies with the arm configuration. The *coupling* effects become even more prominent when the speed increases, and the required accuracy becomes more severe. The interactions and nonlinear forces have been shown to cause errors in position response even at low speeds [Brady, Hollerbach et al 83]. Therefore, compensation for such complicated dynamics is necessary in order that the manipulator follows the planned trajectory accurately.

High speed direct-drive robots surely experience very significant dynamic interactions and nonlinearities. An example is the M.I.T direct-drive arm [Asada and Youcef-Toumi 84] where the maximum speed and maximum acceleration are on the order of 10 m/sec and 5 G respectively. This inertial coupling was experienced in the early version of the CMU direct-drive arm [Asada, Kanade and Takeyama 83]. Recently, [Kanade, Khosla and Tanaka 84] reported that in the CMU direct-drive arm model II, errors of the order of 0.25 and 1.1 degrees were induced in the proximal joints that were servoing at a sampling rate of 1 ms. These errors will undoubtedly cause errors of the order of millimeters at the end effector if not compensated for.

Several schemes have been adopted in the control of manipulators. A model-referenced adaptive control law has been used to maintain a uniform dynamic performance over a wide range of system configurations and payloads [Dubowsky and Des Forges 79]. Feedforward compensation of nonlinear and interactive torques has been combined with optimal regulators for linearized systems to improve the control performance [Vukobratovic and Stokic 80]. Feedforward control can effectively compensate for the predictable motions of a direct-drive arm whose characteristics can be identified accurately [Asada, Kanade and Takeyama 83]. Recent progress in fast real-time computing algorithms have greatly reduced the computational burden. They have made it possible to compute the inverse dynamics of serial manipulators in real time by using recursive equations based on the Newton-Euler formulation [Luh, Walker and Paul 80], and also on the Lagrangian formulation [Hollerbach 80]. Other Methods for achieving dynamically decoupled manipulator motions have also been proposed. Using a nonlinear control law [Freund 82], and a model-referenced adaptive control [Takegaki and Arimoto 81] to obtain decoupled arm dynamics in cartesian coordinates. Among all of these

schemes, [Luh, Walker and Paul 80] reports a sampling rate of 16-20 ms for computation which is not adequate for high speed direct-drive manipulators. [Kanade, Khosla and Tanaka 84], however, achieved a sampling rate of 1 ms for a direct-drive manipulator with a computation hardware customized for the manipulator dynamics.

An alternative approach, which is proposed in this thesis, is to simplify the manipulator dynamics by modifying the *arm design; structure* and *mass distribution.* Using an adequate mass distribution for the arm links, a form of the inertia tensor for which coupling is significantly reduced can be obtained. Consequently, the manipulator dynamics is simplified and the computation burden is relaxed. This design technique is an extension of dynamic mass balancing and force balancing. Force balance deals with the redistribution of mass to reduce the shaking forces transmitted from the mechanism to the frame (ground). Most of this research has been directed to planar mechanisms [Tepper and Lowen 72, Tepper and Lowen 73, Tepper and Lowen 75, Walker and Oldham 78]. In our context, arm structure design and mass redistribution are used to modify the dynamics of multi-degree-of-freedom linkage system with multiple actuators. The inertia tensor of the linkage system is to be *decoupled.* This decoupled dynamic behavior is particularly desirable in manipulators performing high-speed and high-accuracy path control tasks. Furthermore a decoupled dynamics aids in the control of direct-drive manipulators where coupling and wide range load conditions for each actuator are significant [Asada, Kanade and Takeyama 83]. The control problem is then reduced to the one of independent joint control with possibly constant gains [Asada and Youcef-Toumi 83, Asada and Youcef-Toumi 84].

3.3 The Decoupled and Configuration-Invariant Arm Dynamics

The dynamic equation of a direct-drive arm with respect to actuator torque τ_i and joint motion θ_i is given by

$$\tau_i = h_{ii}\,\ddot{\theta}_i + \sum_{j\neq i} h_{ij}\,\ddot{\theta}_j + \sum_j \sum_k \left(\frac{\partial h_{ij}}{\partial \theta_j} - \frac{1}{2}\frac{\partial h_{ik}}{\partial \theta_i} \right) \dot{\theta}_j \dot{\theta}_k + \tau_{gi} \qquad (3.1)$$

The first term on the right hand side represents the inertia torque; the second term is the interactive inertia torque, which is linearly proportional with acceleration. It is ususally referred to as the *linear acceleration torques.* The third term is the *nonlinear velocity torque* due to Coriolis and centrifugal effects; and the last term is the gravity torque. In general, all of these torques are dependent on the arm configuration.

In the case where the inertia tensor **H** of the manipulator is diagonal, the second term vanishes and consequently no interactive inertial torques appear. In this case, the manipulator inertia tensor is referred to as a *decoupled* inertia tensor. The third term, representing the velocity torques, arises when the elements of the inertia tensor change with configuration. The significance of this term depends not only on the magnitude of velocities but also on the spatial rate of change of the elements of the inertia tensor. If the inertia tensor is decoupled, then nonlinear velocity torques present will result from only those diagonal elements that are space dependent. Therefore, by decoupling the inertia tensor, we not only eliminate the interactive acceleration torques but also reduce the effects of the nonlinear velocity torques effects. Under this condition, equ.(3.1) reduces to

$$\tau_i = h_{ii}\,\ddot{\theta}_i + \sum_k \left(\frac{\partial h_{ii}}{\partial \theta_k}\,\dot{\theta}_i\,\dot{\theta}_k - \frac{1}{2}\frac{\partial h_{kk}}{\partial \theta_i}\,\dot{\theta}_k^{\,2} \right) + \tau_{gi} \qquad (3.2)$$

Now, for a manipulator with a *configuration-invariant* inertia tensor, namely each element h_{ij} of the inertia tensor is constant, the spatial derivatives of the elements of **H** vanish and so do the nonlinear velocity torques. In this case, equ.(3.1) becomes

$$\tau_i = h_{ii} \ddot{\theta}_i + \sum_{j \neq i} h_{ij} \ddot{\theta}_j + \tau_{gi} \tag{3.3}$$

Thus, when the inertia tensor is both decoupled and configuration-invariant, the dynamic equation simplifies greatly;

$$\tau_i = h_{ii} \ddot{\theta}_i + \tau_{gi} \tag{3.4}$$

3.4 Necessary Conditions for Decoupling Serial Spatial Mechanisms

The goal of this section is to determine a fundamental kinematic condition that is necessary to decouple the inertia tensor. We analyze spatial serial mechanisms with all revolute joints[1] . In deriving the necessary condition, we examine the torques and forces resulting from acceleration only. The torques to be examined are the acceleration torques generated by the motion of one link and their effects on the remaining joints. Specifically, we start with the analysis of the last link, *n*, and find the effects of its acceleration upon the motion of link n-1. In deriving the necessary condition for decoupling, it suffices then to examine the torques due to acceleration only since the linear acceleration torques are dependent on the off-diagonal elements of the inertia tensor.

---

[1]Prismatic joints are a special case of revolute joints. The decoupling can be achieved easily for the prismatic case in general.

Consider the serial manipulator shown in Figure 3-1, where link n is accelerating with an acceleration $\ddot{\theta}_n$. In what follows, we derive the necessary conditions for decoupling a serial manipulator. The notations used in this derivation are listed below and illustrated in Figure 3-1,

- M_{ci} = mass center location of all links j , $i \leq j \leq n$, when all joints are immobilized except for joint i-1 .
- m_i = mass of link i
- I_i = moment of inertia of link i about joint axis i-1
- $\mathbf{b}_j$= unit vector along the j-th joint axis of rotation for link j+1
- A_{i-1} = projection of mass center M_{ci} onto joint axis i-1
- B_j^i= projection of A_i onto joint axis j
- $\mathbf{r}_{ci}$= vector directed from A_i to M_{ci}
- $\mathbf{r}^*_{ci}$= a reference position of $\mathbf{r}_{ci}$ taken at θ_i=0,
- $\mathbf{r}^i_j$= vector directed from B_j^i to A_i
- θ_j = joint angle j defined according to the Denavit and Hartenberg notation, [Denavit and Hartenberg 55].

The main assumptions used in the derivation are :

- All revolute actuators are mounted at joints between adjacent links of a serial linkage.
- Each link i possesses a principal direction along joint axis $\mathbf{b}_{i-1}$ for an arbitrary arm configuration.

Theorem 1: For a serial manipulator with all revolute joints where the actuators are mounted at the joints between adjacent links and one of the principal directions of link i is parallel to joint axis $\mathbf{b}_{i-1}$, a necessary condition for the manipulator inertia tensor to be decoupled is given by

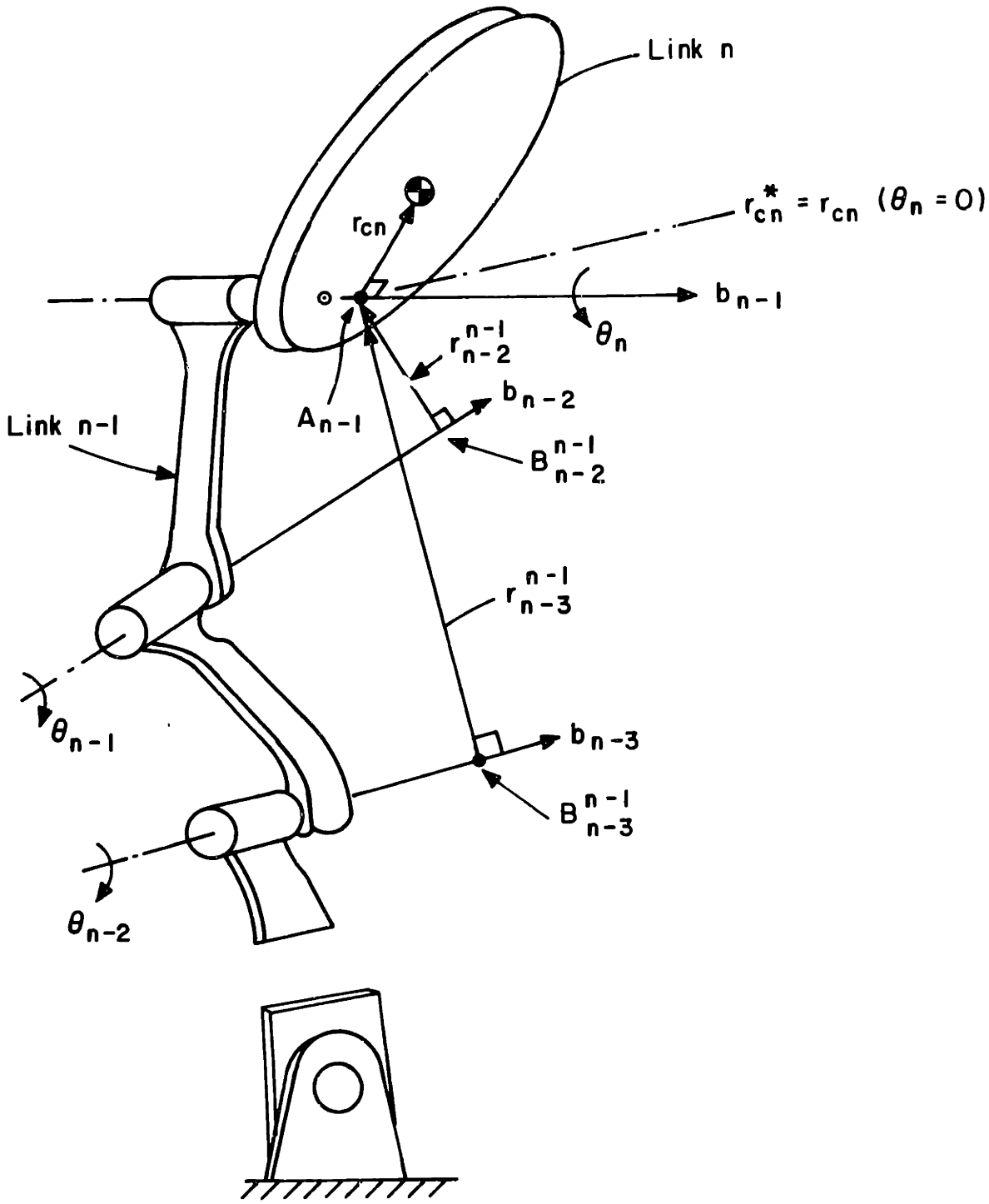

Figure 3-1: A serial manipulator

For $i = 2, \ldots, n$

(a) $\mathbf{b}_{i-1}{}^{t}\,\mathbf{b}_{j} = 0 \qquad$ for $j = 0, 1, 2, \ldots, i\text{-}2$

and

(b) $\mathbf{b}_{i-1}{}^{t}\,\mathbf{r}^{i-1}{}_{j} = 0 \quad$ or $\quad \mathbf{r}_{ci} = 0 \qquad$ for $j = 0, 1, 2, \ldots, i\text{-}2$

Proof

In order that the manipulator inertia tensor is decoupled for all the arm configurations, the linear interactive torques must vanish for arbitrary accelerations as well as for an arbitrary configuration. Therefore the interactive torques must be zero for the following special cases: (I) When only the last link is accelerating and, all velocities and other accelerations are zero; (II) When only the second to last link is accelerating and, all velocities and other accelerations are zero.

Case I: Link n accelerating only

We begin with the last link, link n, and derive the necessary conditions that must be satisfied in order to eliminate the interactive acceleration torques generated by the motion of link n that are transmitted to the other joints. Let link n accelerate with an acceleration $\ddot{\theta}_{n}$ as shown in Figure 3-1. From the definitions given, both vectors $\mathbf{r}_{cn}$ and $\mathbf{r}^{*}_{cn}$ are perpendicular to $\mathbf{b}_{n-1}$ so that

$$\mathbf{r}^{t}_{cn}\,\mathbf{b}_{n-1} = \mathbf{r}^{*t}_{cn}\,\mathbf{b}_{n-1} = 0 \tag{3.5}$$

$(.)^{t}$ represents the transpose vector operation. Let τ_{rn} be the inertial torque resulting from the angular acceleration of link n about joint axis n-1, and $\mathbf{F}_{n}$ be the inertial force due to the linear acceleration of the mass center of link n. In the special case described in (I), τ_{rn} and $\mathbf{F}_{n}$ are the only relevant dynamic forces

present. The strategy is to determine the condition for which the total reaction torque experienced by joint axis $\mathbf{b}_{n-2}$ vanishes. This analysis provides the necessary condition because if the two joint axes were decoupled, they would be decoupled for this special motion also. Since $\mathbf{b}_{n-1}$ is in the direction of the principal moment of inertia for link n, the inertial torque τ_{rn} due to angular acceleration is aligned with $\mathbf{b}_{n-1}$. In this case, the inertial torque τ_{rn} and the inertial force $\mathbf{F}_n$ due to the rotational and translational motions of link n are given by

$$\tau_{rn} = I_n \ddot{\theta}_n \mathbf{b}_{n-1} \tag{3.6}$$

and

$$\mathbf{F}_n = m_n(\mathbf{b}_{n-1} \mathrm{X} \mathbf{r}_{cn} \ddot{\theta}_n) \tag{3.7}$$

where the vector operation (.)X(.) represents the cross-product, m_n is the mass of link n, and I_n is the scalar moment of inertia of link n about $\mathbf{b}_{n-1}$ which is constant.

From Figure 3-1, the reaction torque that joint axis n-2 experiences when link n accelerates about joint axis n-1 is of magnitude $\tau^{n-1}{}_{n-2}$,

$$\tau^{n-1}{}_{n-2} = [\tau_{rn} + (\mathbf{r}_{cn} + \mathbf{r}^{n-1}{}_{n-2}) \mathrm{X} \mathbf{F}_n]^t \mathbf{b}_{n-2} \tag{3.8}$$

where the subscript, in $\tau^{n-1}{}_{n-2}$, denotes the joint axis experiencing the reaction torque due to an angular acceleration about a joint axis denoted by the superscript. $\tau^{n-1}{}_{n-2}$ is then the projection of link n inertial torques onto joint axis n-2. Similarly, any other joint j will be subject to a torque of magnitude $\tau^{n-1}{}_{j}$

$$\tau^{n-1}{}_{j} = [\tau_{rn} + (\mathbf{r}_{cn} + \mathbf{r}^{n-1}{}_{j}) \mathrm{X} \mathbf{F}_n]^t \mathbf{b}_j \tag{3.9}$$

In order for the motion of link n, when under acceleration, not to disturb the motion of any joint j, $\tau^{n-1}{}_j$ must vanish for all j that satisfy

$$1 \leq j \leq n-2$$

For j = n-2, substituting equs. (3.6) and equ.(3.7) into equ.(3.9) leads

$$\tau^{n-1}{}_{n-2} = [\, I_n \, \mathbf{b}_{n-1} + m_n(\mathbf{r}_{cn} + \mathbf{r}^{n-1}{}_{n-2}) \, X \, (\, \mathbf{b}_{n-1} \, X \, \mathbf{r}_{cn} \,) \,]^t \, \mathbf{b}_{n-2} \, \ddot{\theta}_n \qquad (3.10)$$

The first term between brackets is the torque due to the rotational motion of link n about its center of mass. We will refer to this motion as the *centroidal rotation.* The second term represents the torque due to the motion of the center of mass. This motion will be referred to as the *motion of the centroid.* Since the torque due to the centroidal rotation in equ.(3.10) does not depend on θ_n, the necessary condition for $\tau^{n-1}{}_{n-2}$ to be zero for all accelerations $\ddot{\theta}_n$ is

$$\frac{\partial \tau^{n-1}{}_{n-2}}{\partial \theta_n} = \frac{\partial}{\partial \theta_n} \, [\, (\mathbf{r}_{cn} + \mathbf{r}^{n-1}{}_{n-2}) \, X \, (\, \mathbf{b}_{n-1} \, X \, \mathbf{r}_{cn} \,) \,]^t \, \mathbf{b}_{n-2} = 0 \qquad (3.11)$$

where $\mathbf{r}_{cn}$ varies depending upon θ_n. Since we defined $\mathbf{r}_{cn}$ to be a vector perpendicular to $\mathbf{b}_{n-1}$, thus $\mathbf{r}_{cn}$ sweeps a circle in a plane perpendicular to $\mathbf{b}_{n-1}$ when θ_n changes. Furthermore, $\dfrac{\partial \mathbf{r}_{cn}}{\partial \theta_n}$ lies in the same plane traced by $\mathbf{r}_{cn}$, and consequently it is perpendicular to $\mathbf{b}_{n-1}$ for all θ_n. This is illustrated in Figure 3-2. The vectors $\mathbf{b}_{n-1} \, X \, \mathbf{r}_{cn}$ and $\dfrac{\partial \mathbf{r}_{cn}}{\partial \theta_n}$ are collinear in a plane that is perpendicular to $\mathbf{r}_{cn}$. Thus Equ.(3.11) reduces to

$$[\, (\mathbf{r}_{cn} + \mathbf{r}^{n-1}{}_{n-2}) \, X \, (\, \mathbf{b}_{n-1} \, X \, \frac{\partial \mathbf{r}_{cn}}{\partial \theta_n} \,) \,]^t \, \mathbf{b}_{n-2} = 0 \qquad (3.12)$$

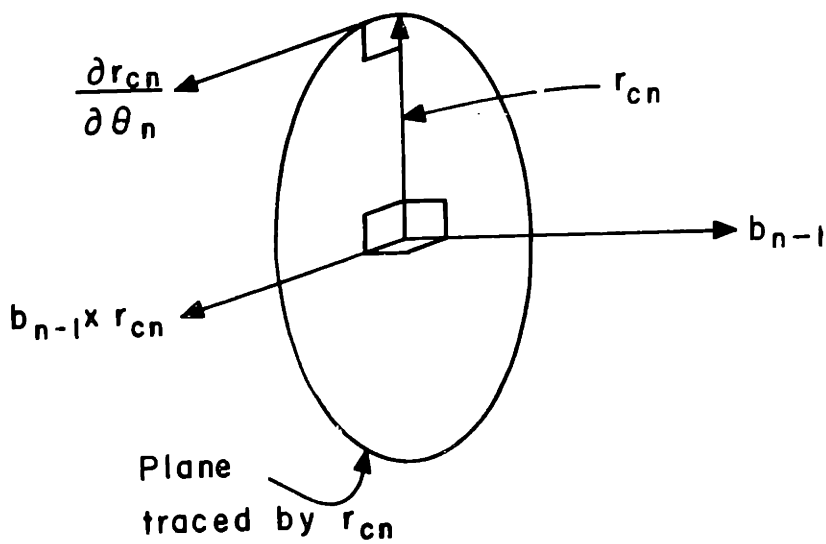

Figure 3-2: Plane of motion of $\mathbf{r}_{cn}$

We derive conditions for equ.(3.12) to be zero for all θ_n in each of the following cases; $\frac{\partial \mathbf{r}_{cn}}{\partial \theta_n} = \mathbf{0}$, and $\frac{\partial \mathbf{r}_{cn}}{\partial \theta_n} \neq \mathbf{0}$.

Case A: $\frac{\partial \mathbf{r}_{cn}}{\partial \theta_n} = \mathbf{0}$ **for all** θ_n

If $\frac{\partial \mathbf{r}_{cn}}{\partial \theta_n} = \mathbf{0}$ for all θ_n, then $\mathbf{r}_{cn}$ is independent of θ_n. However, this is possible only if $\mathbf{r}_{cn}$ is zero, that is the mass center of link n lies on joint axis $\mathbf{b}_{n-1}$. In this case, equ.(3.12) is zero and the torque due to the motion of the centroid is also zero. The only term that remains is the torque due to the centroidal rotation and Equ.(3.10) reduces to

$$\tau^{n-1}_{n-2} = I_n \ddot{\theta}_n \, \mathbf{b}_{n-1}{}^t \mathbf{b}_{n-2} = 0 \tag{3.13}$$

Since the moment of inertia I_n is always positive then equ.(3.13) holds for an arbitrary $\ddot{\theta}_n$ only if the dot product is zero. The necessary condition in this case is

$$\mathbf{b}_{n-1}{}^t \mathbf{b}_{n-2} = 0 \quad \text{and} \quad \mathbf{r}_{cn} = \mathbf{0} \tag{3.14}$$

The above relations state that the joint axes $\mathbf{b}_{n-1}$ and $\mathbf{b}_{n-2}$ must be perpendicular and that the mass center of link n lies on joint axis $\mathbf{b}_{n-1}$.

Case B: $\frac{\partial \mathbf{r}_{cn}}{\partial \theta_n} \neq \mathbf{0}$ **for all** θ_n

From the discussion given above on Figure 3-2, it follows that $\mathbf{b}_{n-1} \, X \, \frac{\partial \mathbf{r}_{cn}}{\partial \theta_n}$ is collinear with $\mathbf{r}_{cn}$ and equ.(3.12) reduces to

$$[\,(\,\mathbf{r}_{cn} + \mathbf{r}^{n-1}_{n-2}\,)\,X\,(\,k\,\mathbf{r}_{cn}\,)\,]^t\,\mathbf{b}_{n-2} = 0$$

where k is a constant and $\mathbf{b}_{n-1} \mathrm{X} \dfrac{\partial \mathbf{r}_{cn}}{\partial \theta_n}$ is replaced by $k.\mathbf{r}_{cn}$. The above relation can be simplified to

$$[\, \mathbf{r}^{n-1}{}_{n-2} \mathrm{X}\, \mathbf{r}_{cn} \,]^t \, \mathbf{b}_{n-2} = 0 \tag{3.15}$$

Equ.(3.15) is satisfied if $\mathbf{r}^{n-1}{}_{n-2}$ is zero or the whole scalar triple product is zero.

Case B.1 : $\mathbf{r}^{n-1}{}_{n-2} = \mathbf{0}$

If $\mathbf{r}^{n-1}{}_{n-2} = \mathbf{0}$, then equ.(3.15) is satisfied and equ.(3.8) reduces to

$$\begin{aligned} \tau^{n-1}{}_{n-2} &= [\, \mathbf{I}_n \mathbf{b}_{n-1} + m_n \mathbf{r}_{cn} \mathrm{X} (\mathbf{b}_{n-1} \mathrm{X} \mathbf{r}_{cn})]^t \, \mathbf{b}_{n-2} \, \ddot{\theta}_n \\ &= [\, \mathbf{I}_n \mathbf{b}_{n-1} + m_n \, k' \, \mathbf{b}_{n-1} \,]^t \, \mathbf{b}_{n-2} \, \ddot{\theta}_n \\ &= (\, \mathbf{I}_n + m_n \, k' \,) \, \ddot{\theta}_n \, \mathbf{b}^t{}_{n-1} \, \mathbf{b}_{n-2} \end{aligned} \tag{3.16}$$

Since the vector $\mathbf{r}_{cn} \mathrm{X} (\mathbf{b}_{n-1} \mathrm{X} \mathbf{r}_{cn})$ is always in the same direction as $\mathbf{b}_{n-1}$, the constant k' is always positive. Thus the torque transmitted, as given by equ.(3.16), is zero if and only if the dot product is zero , that is

$$\mathbf{b}_{n-1}{}^t \, \mathbf{b}_{n-2} = 0 \;\text{ and }\; \mathbf{r}^{n-1}{}_{n-2} = \mathbf{0} \tag{3.17}$$

These conditions mean that the joint axes $\mathbf{b}_{n-1}$ and $\mathbf{b}_{n-2}$ must be orthogonal and must intersect at the projection of the mass center of link n onto joint axis n-1, namely point A_{n-1}, as shown in Figure 3-1.

Case B.2 : $\mathbf{r}^{n-1}{}_{n-2} \neq \mathbf{0}$

In the case where the vector $\mathbf{r}^{n-1}{}_{n-2}$ is not zero, then the necessary and sufficient condition for the scalar triple product to vanish is that all three vectors

$\mathbf{r}^{n-1}{}_{n-2}$, $\mathbf{r}_{cn}$ and $\mathbf{b}_{n-2}$ in equ.(3.15) must be coplanar, [Wilson 60]. Since $\mathbf{r}_{cn}$ is pependicular to $\mathbf{b}_{n-1}$ by definition, then $\mathbf{r}^{n-1}{}_{n-2}$ and $\mathbf{b}_{n-2}$ must be perpendicular to $\mathbf{b}_{n-1}$ to satisfy the coplanarity condition. Using this result, equs.(3.15) and (3.12) are zero. We can focus now on the term resulting from to the motion of the centroid in equ.(3.10) and the relevant part is

$$[\,(\,\mathbf{r}_{cn} + \mathbf{r}^{n-1}{}_{n-2}\,)\,X\,(\,\mathbf{b}_{n-1}\,X\,\mathbf{r}_{cn}\,)\,]^t\,\mathbf{b}_{n-2}$$

or

$$[\,\mathbf{r}_{cn}\,X\,(\,\mathbf{b}_{n-1}\,X\,\mathbf{r}_{cn}\,)\,]^t\,\mathbf{b}_{n-2} + [\,\mathbf{r}^{n-1}{}_{n-2}\,X\,(\,\mathbf{b}_{n-1}\,X\,\mathbf{r}_{cn}\,)\,]^t\,\mathbf{b}_{n-2}$$

The vector $\mathbf{b}_{n-1}\,X\,\mathbf{r}_{cn}$ is perpendicular to $\mathbf{r}_{cn}$ and is in the plane traced by $\mathbf{r}_{cn}$ as θ_n changes. Therefore the cross product $\mathbf{r}_{cn}\,X\,(\,\mathbf{b}_{n-1}\,X\,\mathbf{r}_{cn}\,)$ is collinear with $\mathbf{b}_{n-1}$ and the first dot product in the above equation vanishes. As for the second term, the coplanarity condition requires that $\mathbf{r}^{n-1}{}_{n-2}$ is perpendicular to $\mathbf{b}_{n-1}$ which is always perpendicular to the plane traced by $\mathbf{r}_{cn}$, therefore the vector $\mathbf{r}^{n-1}{}_{n-2}\,X\,(\,\mathbf{b}_{n-1}\,X\,\mathbf{r}_{cn}\,)$ is collinear with $\mathbf{b}_{n-1}$ and consequently the second term vanishes. Thus, the effects due to the motion of the mass center in equ.(3.10) are also zero, and the only remaining torque is due to the centroidal rotation as given by equ.(3.13). The necessary condition in this case is

$$\mathbf{b}_{n-1}{}^t\,\mathbf{b}_{n-2} = 0\,, \quad \text{and} \quad \mathbf{r}^{n-1}{}_{n-2}{}^t\,\mathbf{b}_{n-1} = 0 \tag{3.18}$$

These conditions require that the joint axes $\mathbf{b}_{n-1}$ and $\mathbf{b}_{n-2}$ must be orthogonal and their common normal must pass through the projection of the mass center of link n onto joint axis n-1, namely point A_{n-1}.

We now examine the effects of the motion of link n on joint n-3. If we assume

that joints n-1 and n-2, with their corresponding links, have been designed according to the necessary conditions of (3.14), (3.17) or (3.18), then the torque τ_{rn} and force $\mathbf{F}_n$ would create a torque of magnitude ${\tau^{n-1}}_{n-3}$ given by

$$ {\tau^{n-1}}_{n-3} = [\, \tau_{rn} + (\mathbf{r}_{cn} + {\mathbf{r}^{n-1}}_{n-3}) \times \mathbf{F}_n \,]^t \mathbf{b}_{n-3} \tag{3.19} $$

This relation is similar to equ. (3.8) and therefore the results should be similar to those of equs. (3.14), (3.17) or (3.18) after substituting n-3 for n-2. Thus recursively, in order to decouple link n form all other joints, we must have

$$ \begin{aligned} &\text{(a) } \mathbf{b}_{n-1} \text{ being a pinciple direction for link n} \\ &{\mathbf{b}_{n-1}}^t \mathbf{b}_j = 0 \text{ for } j=1, 2, \ldots, n-2 \\ &\text{and} \\ &\text{(b) } {\mathbf{b}_{n-1}}^t {\mathbf{r}^{n-1}}_j = 0 \quad \text{or} \quad \mathbf{r}_{cn} = 0 \end{aligned} \tag{3.20} $$

Case II: Link n-1 accelerating only

Let us now assume that the conditions of equs. (3.14), (3.17) or (3.18) are satisfied, and proceed to determine the conditions that must be satisfied for decoupling the motion of link n-1 from the rest of the manipulator. The approach is similar to that in the previous case, case I, where we focus on the torques resulting from acceleration only. In order to examine this, we calculate the total inertia $\mathbf{I}_t^{(n-1)}$ of both links n and n-1 in body coordinates of link n-1,

$$ \mathbf{I}_t^{(n-1)} = {\mathbf{I}^{(n-1)}}_{n-1} + \mathbf{R}^t {\mathbf{I}^{(n)}}_n \mathbf{R} \tag{3.21} $$

where ${\mathbf{I}^{(n-1)}}_{n-1}$ is the inertia tensor of link n-1 in body coordinates of link n-1, ${\mathbf{I}^{(n)}}_n$

is the inertia tensor of link n in body coordinates of link n and **R** is the rotation matrix that aligns joint axis $\mathbf{b}_{n-1}$ with a principal direction of link n-1. To derive the necessary condition for which the motion of link n-1 does not affect the motion of the other joints, we first assume that the necessary conditions derived in the previous case, equ.(3.20). Also, we immobilize link n, after rotating it an angle θ_n equal to θ^*_n, for which the total inertia tensor $\mathbf{I}_t^{(n-1)}$ has a principal direction along $\mathbf{b}_{n-1}$. Thus if we accelerate link n-1 while link n is at this position, the necessary conditions would be similar to those derived for decoupling link n, that is

$$\mathbf{b}_{n-2}{}^t \mathbf{b}_j = 0 \quad \text{for} \quad j = 1, 2, \ldots, n-3$$

and

$$\mathbf{b}_{n-2}{}^t \mathbf{r}^{n-2}{}_j = 0 \quad \text{or} \quad \mathbf{r}_{cn-1} = 0$$

It is possible to repeat this process recursively for the rest of the links and obtain the result stated in the theorem. **Q.E.D**

3.5 The Necessary and Sufficient Conditions for Decoupling

The previous section revealed that all unit vectors in the directions of the joint axes must be orthogonal in order to achieve a decoupled inertia tensor. Since in practice more than two vectors can be maintained orthogonal only for a limited number of configurations, thus we can state the following corollary,

> **Corollary 1:** For a serial manipulator with all revolute joints where the actuators are mounted at the joints between adjacent links and one of the principal directions of link i is parallel to joint axis $\mathbf{b}_{i-1}$, decoupling can be achieved for no more than two degrees-of-freedom.

For two d.o.f serial linkage manipulators, it is possible to provide the necessary and sufficient conditions for decoupling.

Theorem 2: The necessary and sufficient conditions for decoupling a two degree-of-freedom serial linkage manipulator whose second link possesses a principal direction along joint axis 1, are

$$\text{(a) } \mathbf{b}_0{}^t \mathbf{b}_1 = 0 \tag{3.22}$$

and

$$\text{(b) } \mathbf{r}_{c2} = \mathbf{0} \quad \text{or} \quad \mathbf{b}^t{}_1 \mathbf{r}^1{}_0 = 0$$

Proof

Necessity:

The conditions listed above are simply an application of the general result to a two d.o.f serial linkage. Thus, these are also the necessary conditions for the two degree-of-freedom case. It remains to show that these conditions are also sufficient.

Sufficiency:

The two possible cases that satisfy the necessary conditions are illustrated in Figures 3-3 and 3-4. These were obtained by arranging the two links of each case according to the requirements of the necessary conditions. In each case, we have orthogonal joint axes, as stated by part (a) of the necessary conditions, and then we implement part (b) of the necessary condition separately, namely $\mathbf{r}_{c2} = \mathbf{0}$ for Figure 3-3 , or $\mathbf{b}^t{}_1 \mathbf{r}^1{}_0 = 0$ for Figure 3-4.

In order to prove the sufficiency, we use two facts :(i) the inertia tensor of the manipulator is symmetric, (ii) the inertia torque due to the angular acceleration of the second link is aligned with $\mathbf{b}_1$ since it is a principal axis.

In Figure 3-3, the mass center of the second link is on joint axis $\mathbf{b}_1$ and therefore will remain stationary when link 2 accelerates. Consequently, the inertial torque is entirely due to the rotation of link 2 about joint axis $\mathbf{b}_1$. Since $\mathbf{b}_1$ is orthogonal to $\mathbf{b}_0$, the base joint experiences no disturbing torque.

In Figures 3-4, the linear motion of the mass center of the second link causes no torque about the base joint axis since this motion is in a plane that contains the base joint. Note in case 2 the mass center of link 2 does not have to be on joint axis $\mathbf{b}_1$.

In both cases, when the base joint accelerates, no torque is induced about joint axis $\mathbf{b}_1$ due to the symmetry of the manipulator inertia tensor.

The sufficiency can be proven simply by substituting the conditions given in theorem 2 in the general expression of the elements of the inertia tensor;

$$h_{11} = m_1(\mathbf{b}_0 X \mathbf{r}_{c1})^t(\mathbf{b}_0 X \mathbf{r}_{c1}) + m_2(\mathbf{b}_0 X(\mathbf{r}^1_0 + \mathbf{r}_{c2}))^t(\mathbf{b}_0 X(\mathbf{r}^1_0 + \mathbf{r}_{c2})) + \mathbf{b}^t_0 I_1 \mathbf{b}_0 + \mathbf{b}^t_0 I_2 \mathbf{b}_0$$

$$h_{22} = m_2(\mathbf{b}_1 X \mathbf{r}_{c2})^t(\mathbf{b}_1 X \mathbf{r}_{c2}) + \mathbf{b}^t_1 I_2 \mathbf{b}_1$$

$$h_{12} = m_2[(\mathbf{b}_0 X \mathbf{r}^1_0)^t \mathbf{b}_1 X \mathbf{r}_{c2} + (\mathbf{b}_0 X \mathbf{r}_{c2})^t \mathbf{b}_1 X \mathbf{r}_{c2}] + \mathbf{b}^t_0 I_2 \mathbf{b}_1$$

The term $\mathbf{b}^t_0 I_2 \mathbf{b}_1$ is zero since $\mathbf{b}_1$ is a principal direction for the link inertia tensor I_2, and the unit vectors $\mathbf{b}_0$ and $\mathbf{b}_1$ are orthogonal. The coefficient of m_2 in h_{12} is zero when $\mathbf{r}_{c2}$ is zero. In the case where $\mathbf{r}_{c2}$ is different from zero, the coefficient of m_2 is still zero since the following vectors are orthogonal: $\mathbf{b}_0$ and $\mathbf{b}_1$, $\mathbf{b}_1$ and $\mathbf{r}^1_0$, $\mathbf{b}_1$ and $\mathbf{r}_{c2}$. This concludes the proof of the necessary and sufficient conditions that decouple the inertia tensor of two degree-of-freedom arms.

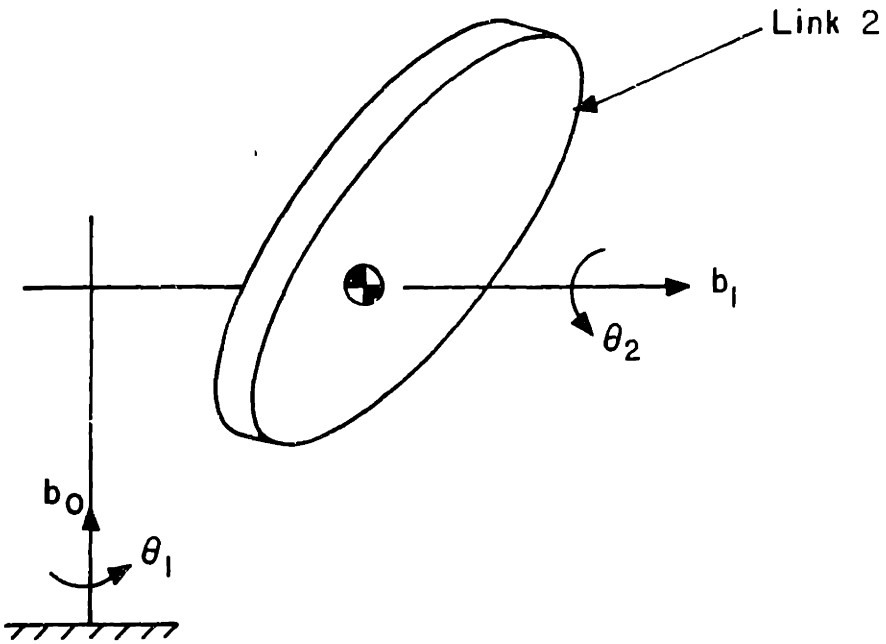

Figure 3-3: Case 1: $\mathbf{b_0}^t \mathbf{b_1} = 0$ and $\mathbf{r_{c2}} = \mathbf{0}$

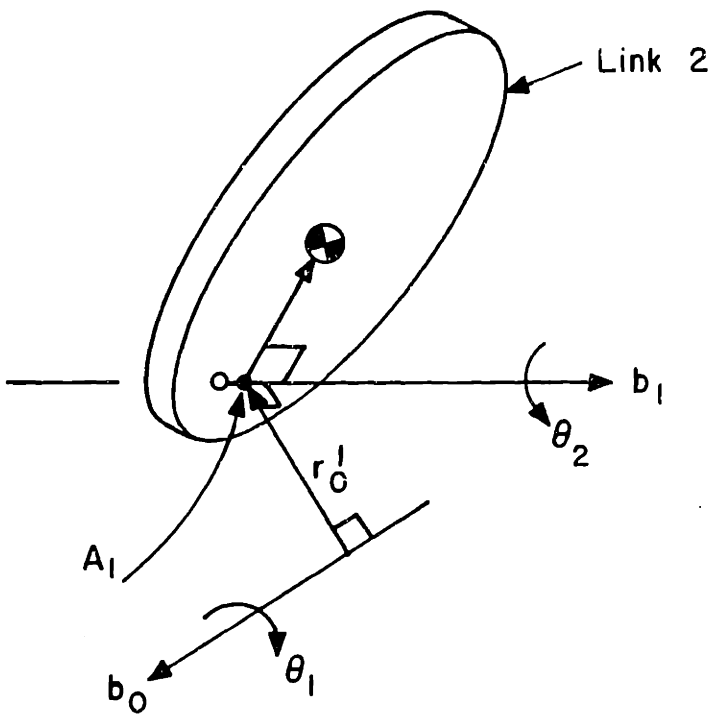

Figure 3-4: Case 2: $\mathbf{b_0}^t \mathbf{b_1} = 0$ and $\mathbf{b}^t{}_1 \mathbf{r}^1{}_0 = 0$

3.6 Discussions on the Decoupling Conditions

In this section, we discuss the necessary conditions derived previously in order to find the design guidelines for decoupling serial spatial mechanisms. The first requirement in the necessary conditions of equ.(3.20) is the orthogonality of the joint axes. In all cases studied during the derivation of the necessary conditions, the orthogonality of joint axes was required to eliminate the torque due to the centroidal rotation. We can conclude that the coupling between the joints of a serial spatial mechanism is dictated by the centroidal rotations of the links. The reason for this is the following. The reaction torques due to the motion of the centroid can be cancelled using both mass distribution or modifying the arm structure as part (b) of the necessary conditions suggest. However, the rotational effects are cancelled only by having orthogonal joint axes, as dictated explicitly by equs.(3.13) and (3.16). Therefore, the motions due to the centroidal rotation limit the decoupling of serial spatial mechanisms by mass distribution only, and we must resort to an additional tool in order to decouple more than two d.o.f.

Since the centroidal rotation of links is the limiting factor, it can be stated, from the mass properties point of view, that the moments of inertia characterize the decoupling by mass distribution. Thus in serial drive mechanisms, in order to achieve decoupling, the rotational effects must be eliminated. The orthogonality of joint axes as given by the necessary condition (a), does eliminate the effects of pure rotation of the links. Therefore, any other means that can eliminate the effects of centroidal rotation will be equivalent to the orthogonality condition. The following proposition can be stated

Proposition 1: Decoupling of the manipulator inertia tensor for more than two degrees of freedom cannot be accomplished merely by

redistributing mass, but the structure of the arm mechanism itself needs to be modified.

In addition, the orthogonality condition as required by the necessary condition cannot be satisfied for serial planar mechanisms where all joint axes are parallel, thus a corollary to theorem 1 is

> **Corollary 2:** It is impossible to decouple the inertia tensor of planar open loop kinematic chains that use revolute joints with actuators mounted at joints between adjacent links.

3.7 Conclusion

This Chapter first introduced the concept of decoupled and invariant manipulator inertia tensors and showed how this reduces the dynamics complexity. Derivations were then presented of the necessary, and the necessary and sufficient conditions that must be satisfied in order to decouple a serial manipulator with all revolute joints. Using the necessary conditions, the effects due to centroidal rotation of the links were shown to be the limiting factor in the decoupling of manipulator inertia tensors by mass distribution. It was also pointed out that decoupling of more than two degrees of freedom can be achieved by a method that eliminates the effects of centroidal rotation but does not use joint axes orthogonality. This will be discussed in detail in the next Chapter.

Chapter 4
ACTUATOR RELOCATION

4.1 Introduction

In the previous Chapter, we assumed that each actuator was located at the corresponding joint and that it exerts a torque between the adjacent links. The actuator, however can be located on other links if an appropriate transmission can be used. In this Chapter, we discuss the decoupling problem for a mechanism where the actuators are relocated to other links with the use of a transmission. It will be shown that the decoupling condition as previously obtained can be significantly relaxed by the relocation of actuators. When actuators are mounted remotely and joints are driven through a transmission, the torque exerted by one actuator is not necessarily applied to one joint but can affect several joints. Similarly, the displacement of one actuator may cause a displacement in more than one joint axis. Thus, we need to study the effects of relocating the actuators on the manipulator kinematics and dynamics. First we set up the relationship between the actuator displacements and their corresponding joint displacements . Then we determine the linear and angular velocity vectors of every link in order to examine the new manipulator dynamics. Second we focus on the manipulator mass properties. We recall that the effects of the centroidal rotation of links were the limiting factor in decoupling serial drive manipulators. Therefore, it is important to determine which link mass properties effect the coupling between any two given actuators. Specifically, the moments of inertia are of special interest since they in effect limit the decoupling. A useful set notation is introduced to facilitate the analysis and

help in the understanding of coupling.

4.2 Modeling of Transmission

The class of manipulators examined consists of serial linkages with all revolute joints. We assume that the actuator displacements ($\alpha_1, \alpha_2, \ldots, \alpha_n$) are a complete and independent set of generalized coordinates that are able to locate the manipulator uniquely and completely. This section presents a model of the transmission for this class of manipulators and introduces the following notations,

- α_l : the l-th actuator displacement
- θ_m : the m-th joint displacement defined according to the Denavit and Hartenberg notation.
- $\mathbf{b}_m$: unit vector in the direction of the m-th joint axis

Thus, the l-th actuator produces an actuator displacement α_l which induces link m to rotate, through a transmission, by a displacement θ_m about joint axis $\mathbf{b}_m$. In the analysis, we assume that the inertia of the transmission is negligible and we deal only with static forces transmitted. The actuator displacement vector, α, and the joint displacement vector, Θ, are assumed to be related by the vector function $\mathbf{f}$[2] ,

$$\Theta = \mathbf{f}\{\ \alpha\ \} \tag{4.1}$$

and the actuator velocities $\dot{\alpha}$ and joint velocities $\dot{\Theta}$ are related by

$$\dot{\Theta} = \mathbf{K}(\ \alpha\ )\ \dot{\alpha} \tag{4.2}$$

---

[2]It may be more appropriate to write $\alpha = \mathbf{f}(\ \theta\ )$ when the dim(θ) > dim(α).

where $\mathbf{K}(\alpha)$ is the Jacobian matrix associated with $\mathbf{f}$, and depends on the arm configuration in general. We will refer to the matrix $\mathbf{K}$ as the tranmission matrix. For a serial arm with actuators mounted at the joints between adjacent links, the transmission matrix $\mathbf{K}$ is a diagonal constant matrix with diagonal elements equal to the inverse of the gear ratios. Figures 4-1 and 4-2 show two two-degree-of-freedom manipulators where the actuators are mounted at the joints and at the base, respectively. As shown in the Figures, the transmission matrices $\mathbf{K}$ depend on the location of the actuators. In what follows, we derive the expression for the angular and the linear velocity vectors.

4.2.1 Link Angular Velocity Vector

In general, the angular velocity of link i, $\mathbf{w}_i$ is given by

$$\mathbf{w}_i = \sum_{l=1}^{n} \frac{\partial \mathbf{w}_i}{\partial \dot{\alpha}_l} \dot{\alpha}_l \tag{4.3}$$

where $\dot{\alpha}_l$ is the velocity of actuator l, and $\partial \mathbf{w}_i / \partial \dot{\alpha}_l$ is Kane's partial rate of change of orientation with respect to α_l [Kane 68]. This partial rate is denoted by $\mathbf{a}_{il}$. In the case where $\partial \mathbf{w}_i / \partial \dot{\alpha}_l$ is zero, actuator l induces no angular velocity to link i. Thus, we can define a set S_i of all actuators j that induce rotation to link i

$$S_i = \{ j / \quad \frac{\partial \mathbf{w}_i}{\partial \dot{\alpha}_j} \neq 0 \} \tag{4.4}$$

and

$$\mathbf{w}_i = \sum_{l \in S_i} \frac{\partial \mathbf{w}_i}{\partial \dot{\alpha}_l} \dot{\alpha}_l$$

For a serial manipulator, the velocity vector $\mathbf{w}_i$ is given by

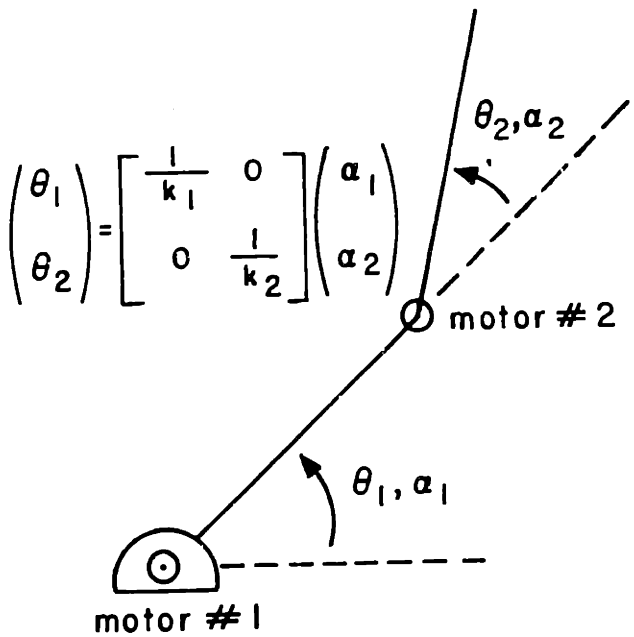

Figure 4-1: A 2 d.o.f serial manipulator with motors at the joints

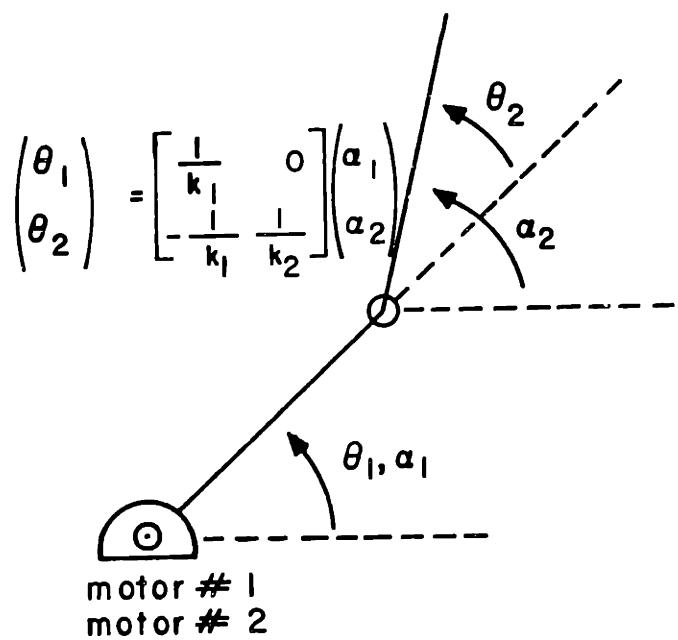

Figure 4-2: A 2 d.o.f serial manipulator with motors at the base

$$\mathbf{w}_i = \sum_{j=1}^{i} \mathbf{b}_j(\theta)\,\dot{\theta}_j$$

Using the relationship between the joint velocities and actuator velocities equ.(4.2),

$$\dot{\theta}_j = \sum_{l=1}^{n} K_{jl}\,\dot{\alpha}_l \tag{4.5}$$

therefore,

$$\mathbf{w}_i = \sum_{j=1}^{i} \mathbf{b}_j \sum_{l=1}^{n} K_{jl}\,\dot{\alpha}_l \;=\; \sum_{l=1}^{n} \Big(\sum_{j=1}^{i} \mathbf{b}_j\, K_{jl}\Big)\,\dot{\alpha}_l \;=\; \sum_{l\,\epsilon\,S_i} \mathbf{a}_{il}\,\dot{\alpha}_l \tag{4.6}$$

Now, we can write explicitly the expression for the partial rate of orientation $\mathbf{a}_{il}$ with respect to α_l,

$$\frac{\partial \mathbf{w}_i}{\partial \dot{\alpha}_l} = \mathbf{a}_{il} = \sum_{j=1}^{i} \mathbf{b}_j\, K_{jl} \tag{4.7}$$

Thus in this case, if it is desired that an actuator l is to have no contribution to the rotation of link i, $\mathbf{a}_{il}$ must be zero. This means that the linear combination of the unit vectors $\mathbf{b}_j$ weighted by the the elements of the transmission matrix, **K**, must be zero. If the vectors $\mathbf{b}_j$ are linearly dependent, we need to choose some nonzero K_{jl}'s so that equ.(4.7) vanishes.

The definition of S_i for a serial manipulator becomes

$$S_{i_{serial}} = \{\, l \;/\; \sum_{j=1}^{i} \mathbf{b}_j\, K_{jl} \neq 0 \,\} \tag{4.8}$$

4.2.2 Link Linear Velocity Vector

The linear velocity vector $\mathbf{v}_i$ of the mass center (ic) of link i, is

$$\mathbf{v}_i = \sum_{l=1}^{n} \frac{\partial \mathbf{v}_i}{\partial \dot{\alpha}_l} \dot{\alpha}_i \tag{4.9}$$

where $\partial \mathbf{v}_i / \partial \dot{\alpha}_l$ is Kane's partial rate of change of position with respect to α_l. This partial rate is denoted by $\mathbf{a}^*_{il}$. We define a new set S^*_i, similar to S_i, which is the set of all actuators that induce linear motion to the mass center of link i,

$$S^*_i = \{ j \; / \quad \frac{\partial \mathbf{v}_i}{\partial \dot{\alpha}_j} \neq 0 \} \tag{4.10}$$

and

$$\mathbf{v}_i = \sum_{l \in S^*_i} \frac{\partial \mathbf{v}_i}{\partial \dot{\alpha}_l} \dot{\alpha}_l$$

For a serial manipulator, the velocity vector $\mathbf{v}_i$ is

$$\mathbf{v}_i = \sum_{j=1}^{i} \mathbf{b}_j \, X \, \mathbf{r}^j_{ic} \, \dot{\theta}_j \tag{4.11}$$

where $\mathbf{r}^j_{ic}$ is a vector from joint axis j to the mass center of link i. Now using equ.(4.5), we have

$$\mathbf{v}_i = \sum_{j=1}^{i} \mathbf{b}_j \, X \, \mathbf{r}^j_{ic} \, (\sum_{l=1}^{n} K_{jl} \, \dot{\alpha}_l)$$

or

$$\mathbf{v}_i = \sum_{l=1}^{n} (\sum_{j=1}^{i} K_{jl} \, \mathbf{b}_j \, X \, \mathbf{r}^j_{ic}) \dot{\alpha}_l \tag{4.12}$$

By inspection, we recognize that the partial rate of change of position with respect to α_l is

$$\mathbf{a}^*_{il} = \frac{\partial \mathbf{v}_i}{\partial \dot{\alpha}_l} = \sum_{j=1}^{i} K_{jl} \, \mathbf{b}_j \, X \, \mathbf{r}^j_{ic}$$

The set S^*_i for a serial manipulator becomes

$$S^*_{i_{serial}} = \{ 1 / \sum_{j=1}^{i} K_{jl}\, \mathbf{b}_j X \mathbf{r}^j_{ic} \neq 0 \} \tag{4.13}$$

for all arm configurations.

4.3 Kinetic Energy

4.3.1 Arm Inertia Tensor

In this section we examine the total kinetic energy KE of an n degree-of-freedom mechanism with n links, in terms of the actuator displacements, in order to evaluate the effect of the transmission on the elements of the manipulator inertia tensor. The kinetic energy in terms of the actuator displacements α is

$$KE = \sum_{i=1}^{n} KE_i = \frac{1}{2} \sum_{i=1}^{n} (m_i \mathbf{v}_i{}^t \mathbf{v}_i + \mathbf{w}^t{}_i\, \mathbf{I}_i\, \mathbf{w}_i) \tag{4.14}$$

$$KE = \frac{1}{2}\, \dot{\alpha}^t\, \mathbf{G}\, \dot{\alpha}$$

where $\mathbf{v}_i$ and $\mathbf{w}_i$ are the linear and angular velocities of link i expressed in terms of the actuator velocities and; m_i and $\mathbf{I}_i$ the ith link mass and inertia tensor respectively. The kinetic energy can be rewritten in terms of the actuator velocities explicitely, matrix **G** is the inertia tensor for this expression. Let us derive **G**. Substituting the general expressions of the angular and linear velocities given by equ.(4.3) and equ.(4.9), in terms of the partial rates $\mathbf{a}_{il}$ and $\mathbf{a}^*_{il}$, the kinetic energy is

$$KE = \frac{1}{2}\sum_{i=1}^{n} [m_i (\sum_{l\epsilon S^*_i} \mathbf{a}^*_{il}\dot{\alpha}_l) ^t (\sum_{m\epsilon S^*_i} \mathbf{a}^*_{im}\, \dot{\alpha}_m) \qquad (4.15)$$

$$+ (\sum_{l\epsilon S_i} \mathbf{a}_{il}\, \dot{\alpha}_l) \, {}^tI_i \, (\sum_{m\epsilon S_i} \mathbf{a}_{im}\, \dot{\alpha}_m)]$$

and the l-m element, h_{lm} of the inertia tensor G can be identified as

$$h_{lm} = \sum_{i\,\epsilon\, S_{lm}} (\mathbf{a}_{il})^t \, I_i \, (\mathbf{a}_{im}) + \sum_{i\,\epsilon\, S^*_{lm}} m_i \, (\mathbf{a}^*_{il})^t \, (\mathbf{a}^*_{im}) \qquad (4.16)$$

where the sets S^*_{lm} and S_{lm} are defined as

$$S^*_{lm} = \{ i \,/\, l \epsilon S^*_i \text{ and } m \epsilon S^*_i \}$$
$$S_{lm} = \{ i \,/\, l \epsilon S_i \text{ and } m \epsilon S_i \} \qquad (4.17)$$

The set S_{lm} is the set of all links i that are rotated by both actuators l and m. On the other hand, the set S^*_{lm} is the set of all links i whose centroids motions are induced by both actuators l and m . These sets explicitly show how the inertia of the different links are distributed in the manipulator inertia tensor. The mass properties of these links will thus appear in the l-m element of the manipulator inertia tensor (without regard to cancelation of terms). If on the other hand, link i does not belong to either set S_{lm} or S^*_{lm}, then its mass properties are not involved in the l-m element of the manipulator inertia tensor.

Equation (4.16) is a general expression for the l-m element of the arm inertia tensor G. First we note that the elements of the transmission matrix K, namely K_{il}, are involved in this expression. They are additional design parameters that could be used to make the off-diagonal elements h_{lm}, $l \neq m$, zero. The first term in Equ. (4.16), is related to the reaction torque resulting from the centroidal rotation.

Similarly, the second term is related to the motion of the link's centroid. Using the proposition given in Chapter 3, we can state that the first term in h_{lm} must be eliminated by some means other than the orthogonality condition.

In general, the links whose mass properties would definetely have no contributions[3] to the value of h_{lm} are those links i for which the partial rates, corresponding to actuators l and m, are zero. Specifically, the mass (moments of inertia) of link i would not appear in h_{lm} when the partial rate $\mathbf{a}^*_{il}$ or $\mathbf{a}^*_{im}$ ($\mathbf{a}_{il}$ or $\mathbf{a}_{im}$) is zero for all arm configurations. In other words, actuator l or m does not induce motion (rotation) to (about) the mass center of link i;

$$l \notin S^*_i \text{ or } m \notin S^*_i \quad \text{that is } \mathbf{a}^*_{il} = \mathbf{0} \quad \text{or} \quad \mathbf{a}^*_{im} = \mathbf{0}$$

$$l \notin S_i \text{ or } m \notin S_i \quad \text{that is } \mathbf{a}_{il} = \mathbf{0} \quad \text{or} \quad \mathbf{a}_{im} = \mathbf{0}$$

4.3.2 Examples

Example 1:

Consider the manipulator shown in Figure 4-2 and assume that the drive systems have unity gear ratios. The influence of the velocity of actuator 1, $\dot{\alpha}_1$, on the angular velocity vector $\mathbf{w}_2$ of link 2 is

$$\mathbf{a}_{21} = \frac{\partial \mathbf{w}_2}{\partial \dot{\alpha}_1} = \mathbf{b}_1 K_{11} + \mathbf{b}_2 K_{21} = \mathbf{b}_1 (1) + \mathbf{b}_2 (-1) = 0$$

---

[3]Other possibilities for which a link's mass properties do not contribute to the value of h_{lm} are

- $(\mathbf{a}^*_{il})^t \mathbf{a}^*_{im} = 0$, that is orthogonal vectors.
- $(\mathbf{a}_{il})^t \mathbf{I}_i \mathbf{a}_{im} = 0$, that is $\mathbf{a}_{il}$ and $\mathbf{a}_{im}$ are $\mathbf{I}_i$ orthogonal.

Therefore, α_1 has no influence on $\mathbf{w}_2$ since the partial rate of change of orientation of link 2, with respect to α_1, is zero. In fact, the angular velocity vector $\mathbf{w}_2$ is

$$\mathbf{w}_2 = \mathbf{b}_2 \dot{\alpha}_2$$

making the set S_2 contain motor 2 only,

$$S_2 = \{ 2 \}$$

Example 2:

The manipulators of Figures 4-1 and 4-2 have an S^*_2 given by

$$S^*_2 = \{ 1, 2 \}$$

This means that the motion of the mass center of link 2 in both manipulators is induced by both motors 1 and 2.

Example 3:

If we apply the above to the manipulator of Figure 4-2, we obtain

$S_1 = \{1\}$ and $S_2 = \{2\}$, since motor 1 rotates link 1 only and motor 2 rotates link 2 only.

$S^*_1 = \{1\}$ and $S^*_2 = \{1, 2\}$, since the motion of the mass center of link 1 is caused by motor 1 only, and that of link 2 is caused by both actuators 1 and 2.

thus the sets S_{lm} and S^*_{lm} are:

$S_{11} = \{1\}$, $S_{12} = \phi$, $S_{22} = \{2\}$

$S^*_{11} = \{1, 2\}$, $S^*_{12} = \{2\}$, $S^*_{22} = \{2\}$

Therefore, the elements of the inertia tensor, as given by equ.(4.16) should involve the following mass properties

$h_{11} = h_{11}(m_1, m_2, I_1)$

$h_{12} = h_{12}(m_2)$

$h_{22} = h_{22}(m_2, I_2)$

Example 4:

Let us analyse the link mass properties of the parallel drive five-bar-link mechanism of Figure 2-5

Link rotations :

$S_1 = \{1\}, S_2 = \{2\}, S_3 = \{1\}, S_4 = \{2\}$

Link mass center motions :

$S^*_1 = \{1\}, S^*_2 = \{2\}, S^*_3 = \{1, 2\}, S^*_4 = \{1, 2\}$

The sets S_{lm} and S^*_{lm} are identified by

$S_{11} = \{1, 3\}$ and $S^*_{11} = \{1, 2, 3\}$

$S_{22} = \{2, 4\}$ and $S^*_{22} = \{2, 3, 4\}$

$S_{12} = \phi$ and $S^*_{12} = \{3, 4\}$

and consequently, the inertia tensor elements h_{lm} are

$h_{11} = h_{11}(m_1, m_3, m_4, I_1, I_3)$

$h_{22} = h_{22}(m_2, m_3, m_4, I_2, I_4)$

$$h_{12} = h_{12}(m_3, m_4)$$

The off-diagonal element h_{12} results only from the linear motion of links 3 and 4. The general expressions of the inertia tensor are

$$h_{11} = I_1 + I_3 + m_1 g^2_1 + m_3 g^2_3 + m_4 l^2_1$$

$$h_{22} = I_2 + I_4 + m_2 g^2_2 + m_3 l^2_2 + m_4 g^2_4$$

$$h_{12} = (m_3 l_2 g_3 - m_4 l_1 g_4) \cos(\theta_2 - \theta_1)$$

4.3.3 Transmission Matrices for Serial Manipulators

In this section we derive the general form of the transmission matrices for open loop revolute chains. The actuators can be mounted anywhere at the joints between the adjacent links. A typical transmission is shown in Figure 4-3, where motor i is mounted on link k, and drives link i. The joint displacements that are involved between the ith motor and the joint about which link i rotates range from k+1 to i-1. Following the Denavit and Hartenberg notation, that is link i rotates about joint axis i-1, we assign a value of zero to k to represent ground. In other words, link 1 rotates about joint axis indexed k=0. Now, the differential displacement $\delta \theta_i$ of link i is equal to the sum of the joint displacements ranging from k+1 to i-1, subtracted from the ith motor displacement $\delta \alpha_i$,

$$\delta \theta_i = \delta \alpha_i - \sum_{j=k+1}^{i-1} \delta \theta_j \tag{4.18}$$

which can be written as

$$\delta \alpha_i = \sum_{j=k+1}^{i} \delta \theta_j \tag{4.19}$$

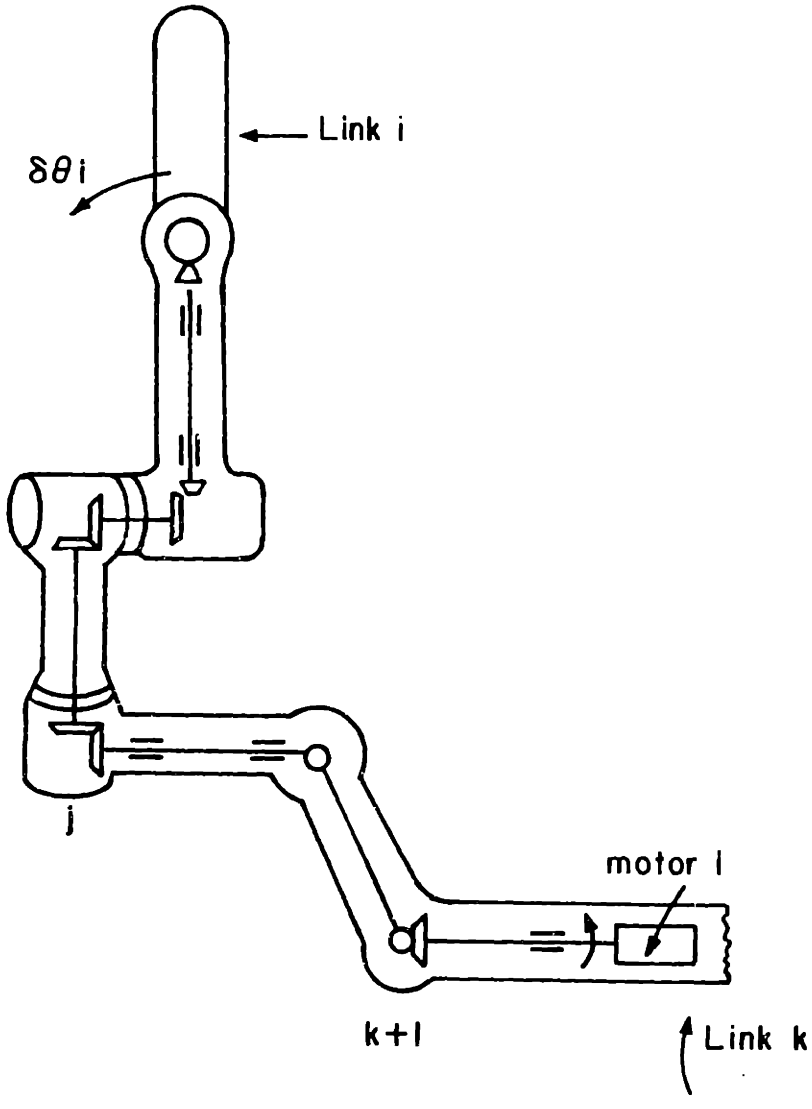

Figure 4-3: Transmission mechanism in a serial manipulator

4.4 Generalized Forces

In section 4.2 of this Chapter, we introduced a relationship between the generalized joint displacements θ and the generalized actuator displacements α, thus

$$\dot{\theta} = \mathbf{K}(\alpha)\,\dot{\alpha}$$

From the energy equation, the generalized joint forces τ and actuator forces $\mathbf{Q}$ should be related by the transpose of the transmission matrix $\mathbf{K}$,

$$\mathbf{Q} = \mathbf{K}^t \tau$$

4.5 Conclusion

This Chapter has focused on the kinematics and dynamics of mechanisms with transmissions. In particular, it emphasised the effects of actuator locations on the dynamics. Furthermore, a notation using sets was introduced to help understanding the dynamics. In this notation, link motions are represented by the sets S_i and S^*_i, and the link contributions to element h_{lm} of the inertia tensor by the sets S_{lm} and S^*_{lm}. These sets will be used later to set up conditions for decoupling.

Chapter 5
ARM STRUCTURE DESIGN FOR DECOUPLED AND CONFIGURATION-INVARIANT INERTIA

5.1 Introduction

This Chapter provides some decoupling design conditions which are based on the results of the theorem and corollaries of Chapter 3 and the set notation introduced in Chapter 4. Specifically, the centroidal rotation torque condition is expressed as a design rule for decoupling spatial serial mechanisms. This is then used in deriving the sufficient condition for a decoupled and invariant manipulator inertia tensor.

5.2 Decoupling of Serial Spatial Mechanisms with Actuator Relocation

The class of manipulators of interest are still the open kinematic chain type where the actuators can be located anywhere along the linkage. The goal is to utilize the fundamental result on decoupling, presented in section 3.5 of Chapter 3, namely that the reaction torques due to centroidal rotation must be eliminated. Thus to meet this binding necessary condition, it suffices to eliminate all of the rotational effects in each off-diagonal element, h_{lm}, of the manipulator inertia tensor. The links i that contribute moments of inertia to the element h_{lm} belong to the set S_{lm} as derived previously. The centroidal rotation effects, as given in

equ.(4.16), are reproduced below

$$h^{rot}_{lm} = \sum_{i \in S_{lm}} \mathbf{a}^{t}_{il}\, \mathbf{I}_i\, \mathbf{a}_{im} \tag{5.1}$$

To eliminate this term completely, we relocate the actuators and choose the mass properties of certain links so that : (i) the set S_{lm} is the empty set or; (ii) the entire sum is zero.

Design Guideline:

(1) $S_{lm} = \phi$

or

(2) $\mathbf{a}^{t}_{il}\, \mathbf{I}_i\, \mathbf{a}_{im} = 0 \qquad \forall i \in S_{lm}$, and for all arm configurations.

Proof

The first design guideline states that the set of links that are rotated by both actuators l and m must be the null set. Since we are interested in the off-diagonal element h_{lm}, $l \neq m$, one way to achieve this is by having the rotation of each link be induced by one and only one actuator, $S_i = \{ i \}$. Using the definition given by Equ.(4.17), it follows that $S_{lm} = \phi$, and no centroidal rotations are involved in h_{lm}, since h^{rot}_{lm} is zero.

One way to satisfy the second design rule, is for each link i that is rotated by both actuators l and m, we choose either partial rate of orientation $\mathbf{a}_{il}$ or $\mathbf{a}_{im}$ to be a principal direction for the inertia tensor $\mathbf{I}_i$ of link i for all arm configurations; and (ii) the partial rates of orientation $\mathbf{a}_{il}$ and $\mathbf{a}_{im}$, of actuators l and m that both induce rotation to link i, to be orthogonal for all arm configurations, namely

(5.2)

(i) For all $i \in S_{lm}$, $\mathbf{a}_{il}$ or $\mathbf{a}_{im}$ be a principal direction for link i[4] .

and

(ii) $\mathbf{a}_{il}^{t}\, \mathbf{a}_{im} = 0$ for $l \in S_i$ and $m \in S_i$ for all arm configurations

In other words, using the definition of the set S_i, this is equivalent to saying that all partial rate vectors, $\mathbf{a}_{il}$, that make up the angular velocity vector $\mathbf{w}_i$ of any link i must be mutually orthogonal. This design rule permits the elimination of all moments of inertia from the off-diagonal element h_{lm} in order to satisfy the necessary condition for decoupling serial spatial mechanisms.

Without loss of generatlity, we can assume that $\mathbf{a}_{im}$ is in a principal direction of $\mathbf{I}_i$. Let us assume a coordinate transformation so that the direction of $\mathbf{a}_{im}$ coincides with the z-axis of the new coordinate frame, then the inertia tensor can be expressed as

$$\mathbf{I}_i = \begin{bmatrix} I_{xx} & I_{xy} & 0 \\ I_{xy} & I_{yy} & 0 \\ 0 & 0 & I_{zz} \end{bmatrix}$$

Now we consider the quadratic form $\rho = \mathbf{a}_{il}^{t}\, \mathbf{I}_i\, \mathbf{a}_{im}$, where $\mathbf{a}_{im}$ is a principal axis for $\mathbf{I}_i$ and the partial rates are given by,

$$\mathbf{a}_{il}^{t} = (a \;\; b \;\; c)$$

$$\mathbf{a}_{im}^{t} = (\alpha \;\; \beta \;\; \gamma) = (0 \;\; 0 \;\; \gamma)$$

then

---

[4]In general, there is no rotational effect if $\mathbf{a}_{il}$ and $\mathbf{a}_{im}$ are $\mathbf{I}_i$ orthogonal for $l \neq m$.

$$\mathbf{a}_{il}^{t}\, \mathbf{I}_i\, \mathbf{a}_{im} = c\, \gamma\, I_{zz}$$

since $\mathbf{a}_{il}^{t}\, \mathbf{a}_{im} = 0$, then $\rho = 0$ and no moments of inertia should appear.

5.3 Decoupled and Invariant Inertia Tensor for Planar Mechanisms

5.3.1 Sufficient Conditions for a Decoupled and Invariant Inertia Tensor

Consider an open loop kinematic chain consisting of links 1 through n, driven by n independent actuators located at the base frame. The sufficient condition that the manipulator inertia tensor is decoupled and invariant for all arm configurations is given by:

(i)
$$\mathbf{K} = \begin{bmatrix} 1 & 0 & 0 & 0 & \ldots.. & 0 \\ -1 & 1 & 0 & 0 & \ldots.. & 0 \\ 0 & -1 & 1 & 0 & \ldots.. & 0 \\ 0 & 0 & -1 & 1 & \ldots.. & 0 \\ & & & \cdot & & \\ & & & & \cdot & \\ & & & & & \cdot \end{bmatrix}$$

(ii)
$$\mathbf{r}^{i-1}{}_{ic} = -\frac{1}{m_i} \sum_{j=i+1}^{n} m_j\, \mathbf{r}^{i-1}{}_{i} \qquad \text{for } i = 2, \ldots, n$$

where $\mathbf{r}^{i-1}{}_{ic}$ is the position vector from the origin of coordinate frame i-1 (on joint i) to the mass center of link i, $\mathbf{r}^{i-1}{}_{i}$ is the position vector from the origin of frame i-1 to the origin of frame i, and m_i is the mass of link i.

Proof

The transmission matrix **K**, as given by (i), is a matrix that corresponds to $S_i = \{ i \}$ for all $i=1,2,...,n$ and thus $S_{lm} = \phi$. The angular velocity vector $\mathbf{w}_i$ is given by

$$\mathbf{w}_i = \mathbf{b}_{i-1}\, \dot{\alpha}_i$$

Note that the partial rate $\mathbf{a}_{il}$ and the joint axis $\mathbf{b}_i$ are all parallel in this case.

The linear velocity vector $\mathbf{v}_i$, as given by equ. (4.12), becomes

$$\mathbf{v}_i = \sum_{j=1}^{i-1} \dot{\alpha}_j\, \mathbf{b}_{j-1} \times \mathbf{r}^{j-1}{}_j + \dot{\alpha}_i\, \mathbf{b}_{i-1} \times \mathbf{r}^{i-1}{}_{ic}$$

Using (ii), the linear velocity $\mathbf{v}_i$ becomes

$$\mathbf{v}_i = \sum_{j=1}^{i-1} \dot{\alpha}_j\, \mathbf{b}_{j-1} \times \mathbf{r}^{j-1}{}_j - \frac{1}{m_i}\, \dot{\alpha}_i \sum_{j=i+1}^{n} m_j\, \mathbf{b}_{i-1} \times \mathbf{r}^{i-1}{}_i$$

the kinetic energy is KE,

$$2\,KE = \sum_{i=1}^{n} m_i\, \mathbf{v}_i^t\, \mathbf{v}_i + I_i\, \mathbf{w}_i^t\, \mathbf{w}_i$$

$$= \sum_{i=1}^{n} m_i \sum_{j=1}^{i-1} \sum_{k=1}^{i-1} (\mathbf{b}_{j-1} \times \mathbf{r}^{j-1}{}_j)^t\, (\mathbf{b}_{k-1} \times \mathbf{r}^{k-1}{}_k)\, \dot{\alpha}_j \dot{\alpha}_k$$

$$- 2 \sum_{i=1}^{n} m_i \sum_{j=1}^{i-1} \dot{\alpha}_j\, \mathbf{b}_{j-1} \times \mathbf{r}^{j-1}{}_j \frac{1}{m_i}\, \dot{\alpha}_i \sum_{l=i+1}^{n} m_l\, \mathbf{b}_{i-1} \times \mathbf{r}^{i-1}{}_i$$

$$+ \sum_{i=1}^{n} m_i \frac{1}{m_i^2}\, \dot{\alpha}^2{}_i \Big(\sum_{l=i+1}^{n} m_l \Big)^2 (\mathbf{b}_{i-1} \times \mathbf{r}^{i-1}{}_i)^t\, (\mathbf{b}_{i-1} \times \mathbf{r}^{i-1}{}_i)$$

$$+ \sum_{i=1}^{n} \mathbf{b}_{i-1}\, {}^{t}\mathbf{I}_i\, \mathbf{b}_{i-1}\, \dot{\alpha}_i^2$$

The inner product of two vector products can be expanded as

$$(\mathbf{b}_{j-1} \times \mathbf{r}^{j-1}{}_j)^t (\mathbf{b}_{k-1} \times \mathbf{r}^{k-1}{}_k) =$$

$$(\mathbf{b}^t_{j-1}\, \mathbf{b}_{k-1})(\mathbf{r}^{j-1}{}_j{}^t\, \mathbf{r}^{k-1}{}_k) - (\mathbf{b}^t_{j-1}\, \mathbf{r}^{k-1}{}_k)(\mathbf{r}^{j-1}{}_j{}^t\, \mathbf{b}_{k-1})$$

Since the mechanism is planar, $\mathbf{b}_{j-1}$ is perpendicular to $\mathbf{r}^{k-1}{}_k$, and

$$\begin{aligned} (\mathbf{b}_{j-1} \times \mathbf{r}^{j-1}{}_j)^t (\mathbf{b}_{k-1} \times \mathbf{r}^{k-1}{}_k) &= (\mathbf{r}^{j-1}{}_j)^t\, \mathbf{r}^{k-1}{}_k \\ &= \mathbf{r}^{j-1}{}_j \cdot \mathbf{r}^{k-1}{}_k \cos(\beta_{jk}) \\ &= L_j \cdot L_k \cos(\beta_{jk}) \\ &= C_{jk} \end{aligned}$$

where L_j is the length of the vector $\mathbf{r}^{j-1}{}_j$ and β_{jk} is the angle between link j and link k. The kinetic energy now becomes

$$2\,KE = \sum_{i=1}^{n} m_i \sum_{j=1}^{i-1} \sum_{k=1}^{i-1} C_{jk}\, \dot{\alpha}_j\, \dot{\alpha}_k$$

$$- 2 \sum_{i=1}^{n} \sum_{j=1}^{i-1} \Big(\sum_{l=i+1}^{n} m_l \Big) C_{ji}\, \dot{\alpha}_j\, \dot{\alpha}_i$$

$$+ \sum_{i=1}^{n} \Big[\frac{1}{m_i} \Big(\sum_{l=i+1}^{n} m_l \Big)^2 C_{ii} + \mathbf{b}_{i-1}\, \mathbf{I}_i\, \mathbf{b}_{i-1} \Big] \dot{\alpha}^2{}_i$$

and by switching the order of summations, we obtain

$$2\,KE = \sum_{j=1,k=1,j=k}^{n} \left(\sum_{i=\max[j,k]+1}^{n} m_i \right) C_{jk}\,\dot{\alpha}_j\,\dot{\alpha}_k + \sum_{j=1}^{n} \left(\sum_{i=j+1}^{n} m_i \right) C_{jj}\,\dot{\alpha}^2_j$$

$$- 2 \sum_{j=1}^{n} \sum_{i=j+1}^{n} \left(\sum_{l=i+1}^{n} m_l \right) C_{ji}\,\dot{\alpha}_j\,\dot{\alpha}_i$$

$$+ \sum_{i=1}^{n} \left[\frac{1}{m_i} \left(\sum_{l=i+1}^{n} m_l \right)^2 C_{ii} + \mathbf{b}_{i-1}{}^t\, \mathbf{I}_i\, \mathbf{b}_{i-1} \right] \dot{\alpha}^2_i$$

$$= \left[\sum_{i=1}^{n} \left(\sum_{l=i+1}^{n} m_l \right) \left\{ \frac{1}{m_i} \left(\sum_{l=i+1}^{n} m_l + 1 \right\} \right. \right. C_{ii} + \mathbf{b}_{i-1}{}^t\, \mathbf{I}_i\, \mathbf{b}_{i-1} \left. \right] \dot{\alpha}^2_i$$

$$+ 2 \sum_{j=1}^{n} \sum_{k=j+1}^{n} \left(\sum_{l=k+1}^{n} m_l \right) C_{jk}\,\dot{\alpha}_j\,\dot{\alpha}_k$$

$$- 2 \sum_{j=1}^{n} \sum_{k=j+1}^{n} \left(\sum_{l=k+1}^{n} m_l \right) C_{jk}\,\dot{\alpha}_j\,\dot{\alpha}_k$$

or

$$= \left[\sum_{i=1}^{n} \left(\sum_{l=i+1}^{n} m_l \right) \frac{1}{m_i} \left(\sum_{l=i+1}^{n} m_l \right) . a^2_i + I_i \right] \dot{\alpha}^2_i$$

thus the elements of the inertia tensor are given by

$$h_{jk} = 0 \quad \text{for} \quad j \neq k$$

$$h_{ii} = \sum_{i=1}^{n} \left(\sum_{l=i+1}^{n} m_l \right) \frac{1}{m_i} \left(\sum_{l=i}^{n} m_l \right) . a^2_i + I_i \qquad \text{for } i = 2, 3, \ldots, n$$

Thus the inertia tensor is completely decoupled and invariant for all arm configurations.

5.4 Parallelogram Mechanisms

This section explores the differences in dynamic behavior that exist between two 2 d.o.f parallel drive mechanisms that use either a five-bar link mechanism or a chain. The two mechanisms examined first use parallel drive as shown in Figures 5-1 and 5-2 The set notation was applied to these two mechanisms in examples 3 and 4 of Chapter 4. It was found that the elements of the inertia tensor of the mechanism driven through a chain, Figure 5-1, depend on the following mass properties

$$h_{11} = h_{11}(m_1, m_4, I_1)$$

$$h_{22} = h_{22}(m_4, I_4)$$

$$h_{12} = h_{12}(m_4)$$

and they are explicitly given by

$$h_{11} = I_1 + m_1 g^2_1 + m_4 l^2_1$$

$$h_{22} = I_4 + m_4 g^2_4$$

$$h_{12} = m_4 l^2_1 g_4 \cos(\alpha_2 - \alpha_1)$$

On the other hand, The set notation was also applied to the mechanism which uses a five-bar-link mechanism in Chapter 4, to determine the mass properties that are involved in the elements of the inertia tensor. These implicit dependences are reproduced below

$$h^*_{11} = h_{11}(m_1, m_3, m_4, I_1, I_3)$$

$$h^*_{22} = h_{22}(m_4, m_2, m_3, I_2, I_4)$$

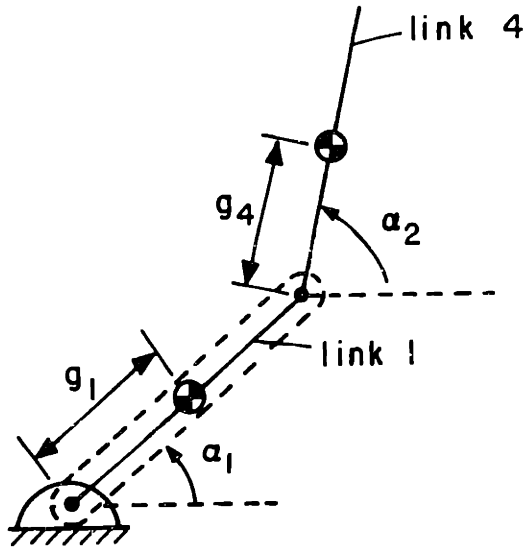

Figure 5-1: Parallel drive mechanism using a chain

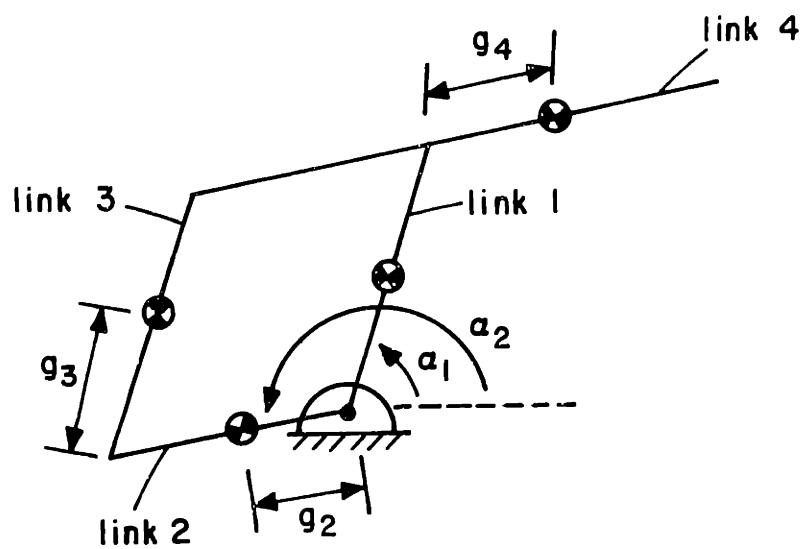

Figure 5-2: Parallel drive mechanism using a five-bar mechanism

$$h^*_{12} = h_{12}(m_3, m_4)$$

or explicitely,

$$h^*_{11} = I_1 + m_1 g^2_1 + I_3 + m_3 g^2_3 + m_4 l^2_1$$

$$h^*_{22} = I_4 + m_4 g^2_4 + I_2 + m_2 g^2_2 + m_3 l^2_2$$

$$h^*_{12} = (m_3 l_2 g_3 - m_4 l_1 g_4)\cos(\alpha_2 - \alpha_1)$$

Let us define a vector $\mathbf{p}^t = (m_2 \quad m_3)$ whose components are the masses of links 2 and 3, and let $I_i = m_i R^2_i$ for $i = 2 , 3$ where R_i is the radius of gyration of link i, then[5]

$$\lim_{p \to 0} h^*_{11} = h_{11}$$

$$\lim_{p \to 0} h^*_{22} = h_{22}$$

$$\lim_{p \to 0} h^*_{12} = h_{12}$$

The two inertia tensors are similar . Thus, the extra links merely transmit the motion from the actuator to the forearm, link 4, as expected.

As a counter example, consider the planar mechanism of Figure 2-3, where the actuators are at the base. There is no mass distribution that can decouple the inertia tensor of this mechanism since the angular velocity vector of link 3 is affected by the motions of both actuators. This example shows that simply placing the actuators at the base is not sufficient to achieve decoupling of the manipulator inertia tensor.

---

[5]Proper angles are used before taking the limit.

5.5 Conclusion

This Chapter provided some design conditions on decoupling using the results of the theorem and corollaries of Chapter 3 and the set notation introduced in Chapter 4. The reaction torque condition was expressed as a design rule for decoupling spatial serial mechanisms in terms of the partial rates of angular velocity and the sets S_i and S_{lm}. This was utilized in deriving the necessary and sufficient conditions for a decoupled and invariant inertia tensor of an n degree of freedom planar mechanism.

Chapter 6
DESIGN APPLICATION

6.1 Introduction

In this Chapter, we present the design of a 3-d.o.f revolute direct-drive manipulator and derive the mass redistribution conditions for which the 3 by 3 inertia tensor is diagonal. The planar dynamics, however, will be analyzed first.

6.2 Design Application - M.I.T Direct-Drive Arm

6.2.1 Arm Mechanism

The three-degree-of-freedom direct-drive arm to be analyzed is shown in Figures 6-1, 6-2 and 6-3. The arm uses a parallel drive mechanism consisting of a six-bar-link mechanism that forms a parallelogram. Reference [Asada and Youcef-Toumi 84] describes the first direct-drive arm prototype that uses a parallel drive mechanism. As seen in Figure 6-1, when joint 2 rotates link 2, the arm tip performs a reach motion. A lift motion is achieved by having joint 3 rotate link 3. A vertical planar motion of the arm tip can be accomplished by actuating joints 2 and 3 together. Finally, the base joint, joint 1, rotates the whole mechanism about the vertical axis allowing a three dimensional motion of the arm tip. This arm [Asada, Youcef-Toumi and Ramirez 84, Ramirez 84] uses the key feature of the parallel drive, as presented in [Asada and Youcef-Toumi 83, Asada and Youcef-Toumi 84], which allows the decoupling of the inertia tensor by mass distribution.

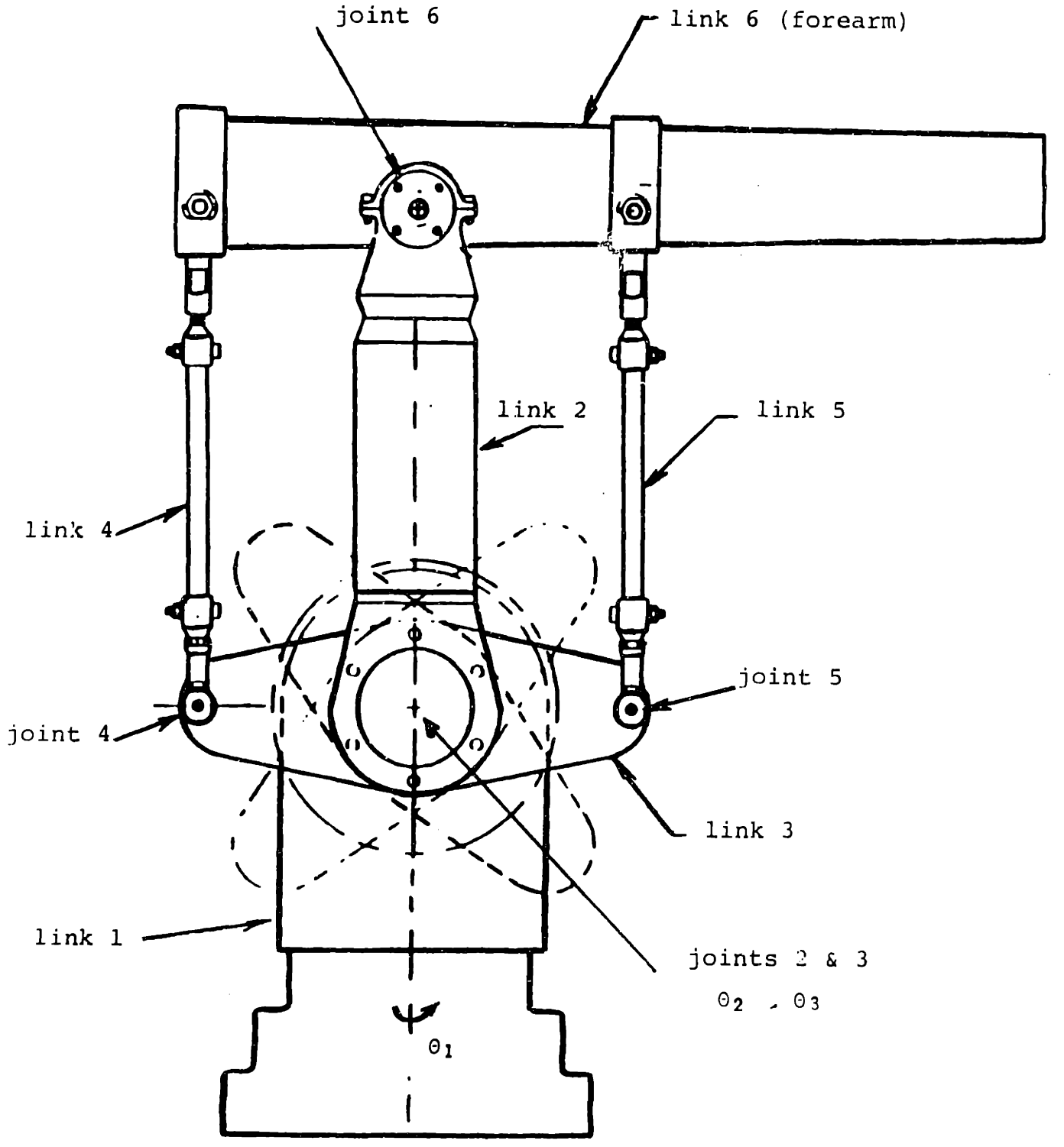

Figure 6-1: 3 d.o.f direct-drive manipulator side view

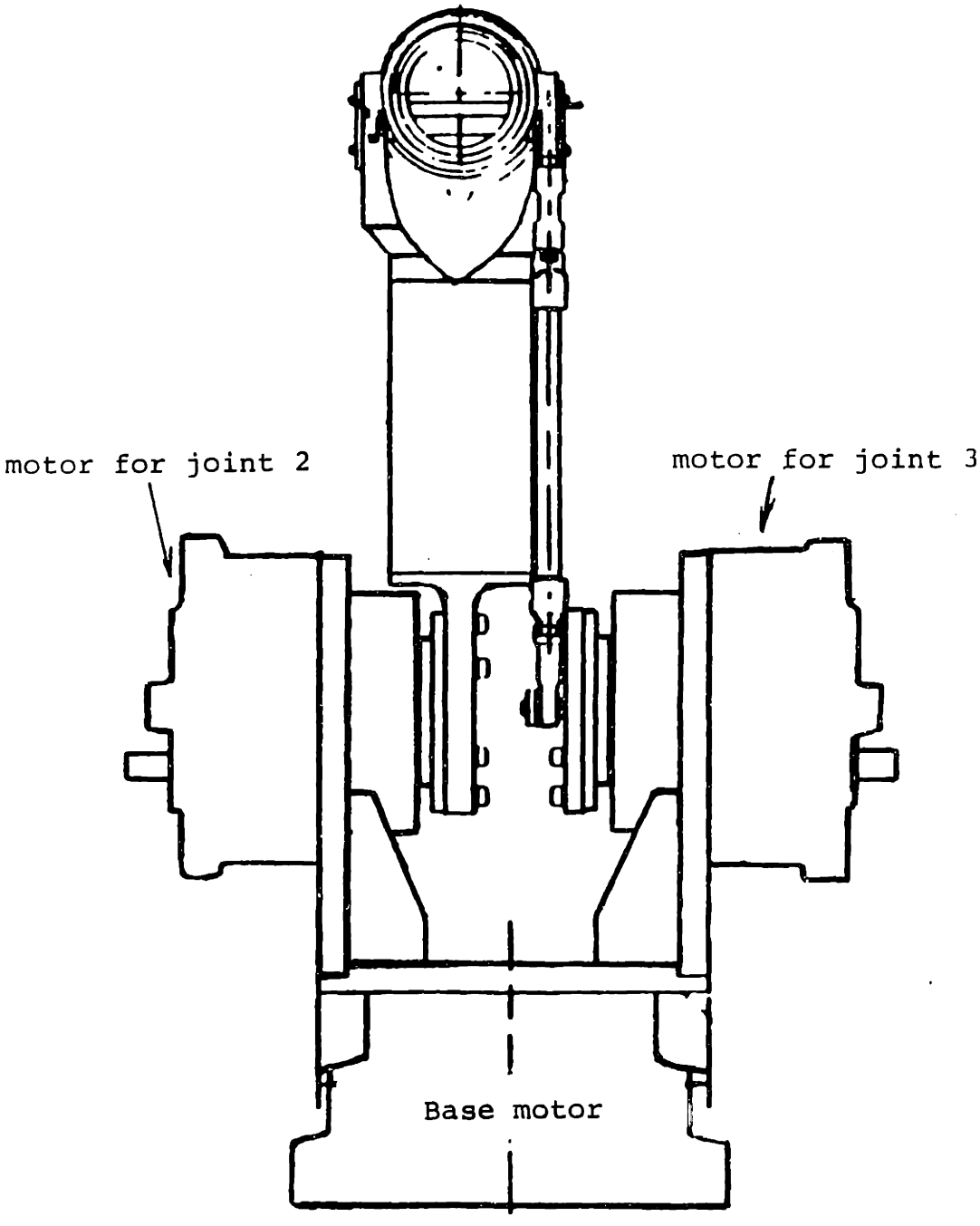

Figure 6-2: 3 d.o.f direct-drive manipulator front view

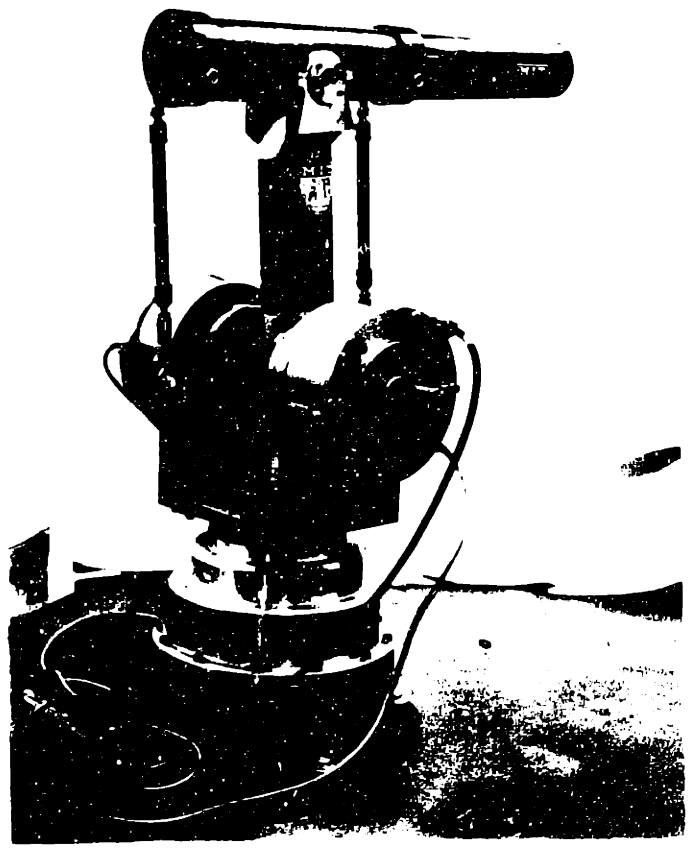

Figure 6-3: M.I.T 3 d.o.f direct-drive manipulator

6.2.2 Decoupling of Planar Dynamics

Let us immobilize the base joint so that joints 2 and 3 are the only active joints. This mechanism is equivalent to the five-bar-link mechanism described in Chapter 5, where we showed that the five-bar-link mechanism is equivalent to the parallel drive which uses a chain mechanism. Therefore, the necessary condition for decoupling should apply. Using the notation of Figure 6-4, the sets representing rotations are

$$S_2 = S_4 = S_5 = \{ 2 \} \qquad \text{and } S_3 = S_6 = \{ 3 \}$$

The set $S_{23} = \phi$, thus no link moment of inertia are involved in the off diagonal element h_{23}. The necessary condition for decoupling a planar mechanism,is then satisfied. The elements of the inertia tensor for the two-degree-of-freedom arm are given by

$$G_{23} = \begin{bmatrix} h_{22} & h_{23} \\ h_{23} & h_{33} \end{bmatrix}$$

where its elements are given by

$$h_{22} = I_2 + m_2 g_2^2 + I_4 + m_4 g_4^2 + I_5 + m_5 g_5^2 + m_6 l_2^2 \tag{6.1}$$

$$h_{33} = I_3 + m_3 g_3^2 + m_4 l_3^2 + m_5 l_3^2 + I_6 + m_6 g_6^2$$

$$h_{23} = (m_5 l_3 g_5 + m_6 l_2 g_6 - m_4 l_3 g_4) \cos(\alpha_3 - \alpha_2)$$

The parameters m_i, I_i represent the mass and mass moment of inertia about an axis going through the mass center of link i and parallel to the horizontal axis

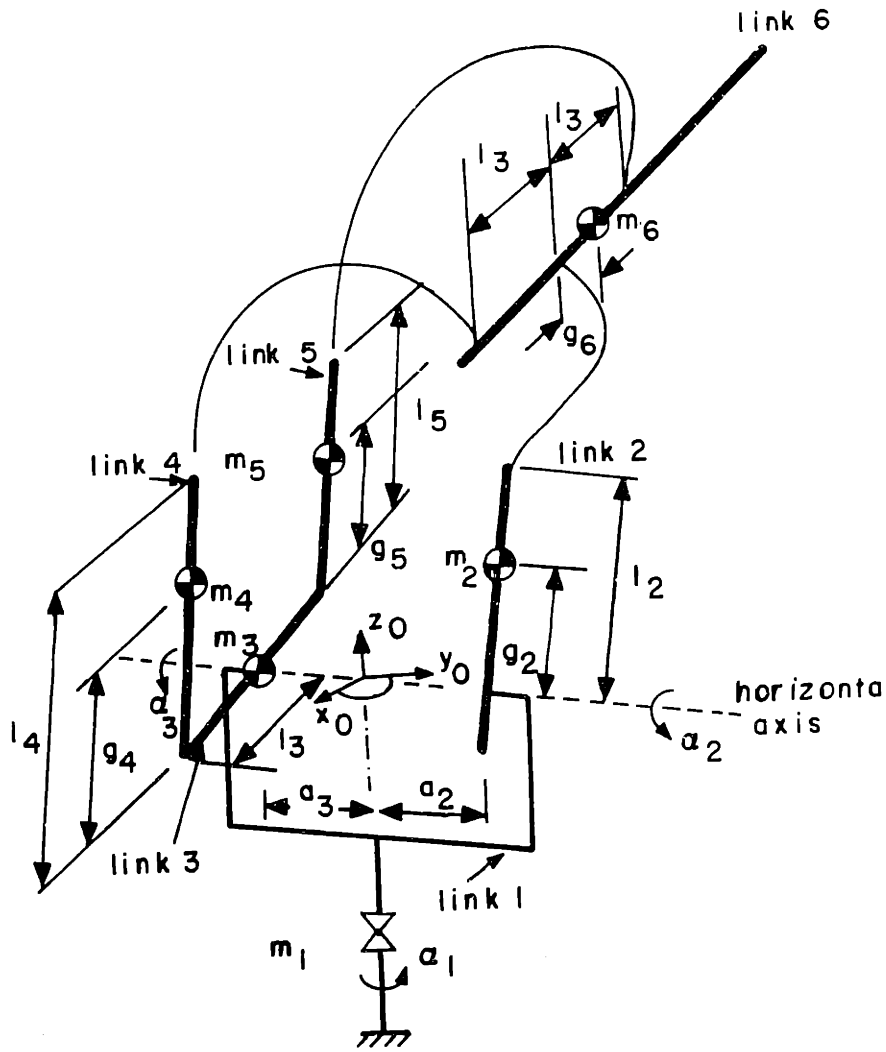

Figure 6-4: Skeleton of the 3 d.o.f manipulator

shown in Figure 6-4; l_i and g_i are its link length and the distance to the center of mass as defined in Figure 6-4.

It is apparent from equ.(6.1) that the diagonal elements of the inertia tensor, h_{22} and h_{33}, do not involve actuator displacements α_2 and α_3, hence they are invariant for all arm configurations. The coupling term h_{23} is caused mainly by the motion of the mass centers of links 4, 5 and 6. This term can be made equal to zero for all arm configurations when the following is satisfied,

$$m_5 l_3 g_5 + m_6 l_2 g_6 - m_4 l_3 g_4 = 0 \tag{6.2}$$

The above equation suggests the redistribution of the mass of links 4, 5 and 6 in order to decouple the arm inertia tensor. This can be achieved by changing the mass center locations, g_4, g_5 and g_6, or by changing the mass proportions of the three links; m_4:m_5:m_6 . One possible solution to equ.(6.2) occurs when links 4 and 5 are identical so that $m_5 l_3 g_5$ and $m_4 l_3 g_4$ cancel each other. The decoupling condition then reduces to

$$g_6 = 0 \tag{6.3}$$

Under this condition the mass center of the forearm coincides with joint 6. This is equivalent to static mass balancing of the forearm. For the six-bar-link mechanism, this is a condition for decoupling the inertia tensor.

6.2.3 Decoupling of Spatial Dynamics

The arm inertia tensor depends not only on the mass properties of each arm link but also on the kinematic structure of the arm linkage. As it was pointed out

earlier, the kinematic structure is critical for achieving a decoupled inertia tensor. For the manipulator shown in Figures 6-1 and 6-2, the parallelogram mechanism was used for decoupling the upper two joints, 2 and 3. It is also possible to decouple the arm inertia tensor in the 3 d.o.f case for all arm configurations. In this case, we use the design guideline of chapter 5 for spatial mechanisms, that is to eliminate the quadratic forms $\mathbf{a}_{il}\,\mathbf{I}_i\,\mathbf{a}_{im}$. The angular velocities of the links are

$$\mathbf{w}_1 = \mathbf{e}_1\,\dot{\alpha}_1$$

$$\mathbf{w}_2 = \mathbf{w}_4 = \mathbf{w}_5 = \mathbf{e}_1\,\dot{\alpha}_1 + \mathbf{e}_2\,\dot{\alpha}_2$$

$$\mathbf{w}_3 = \mathbf{w}_6 = \mathbf{e}_1\,\dot{\alpha}_1 + \mathbf{e}_2\,\dot{\alpha}_3$$

where Kane's partial rates $\mathbf{e}_1$ and $\mathbf{e}_2$ are

$$\mathbf{e}^t{}_1 = (\,0 \quad 0 \quad 1\,) \text{ and } \mathbf{e}^t{}_2 = (\,\cos\alpha_1 \quad \sin\alpha_1 \quad 0)$$

Note that the vectors $\mathbf{e}_1$ and $\mathbf{e}_2$ are orthogonal. Also, the principal direction of each link of the upper arm is in the direction of $\mathbf{e}_2$. Therefore, the necessary condition is satisfied since we eliminated all the moments of inertia from the off-diagonal elements of the manipulator inertia tensor.

In Figure 6-4, note that the axis of joint 1 is perpendicular to the axes of joints 2 and 3. Therefore, torques exerted by joints 2 and 3 would not act upon joint 1 for a balanced arm design. The elements of the inertia tensor of the 3 d.o.f manipulator are given by

$$\begin{aligned} h_{11} = {} & I^1{}_{zz} + m_2(\,a^2{}_2 + g^2{}_2\cos^2\alpha_2\,) + I^2{}_{zz}\sin^2\alpha_2 + I^2{}_{yy}\cos^2\alpha_2 + m_3a^2{}_3 \\ & + I^3{}_{yy}\sin^2\alpha_3 + I^3{}_{zz}\cos^2\alpha_3 + m_4(\,a^2{}_3 + l^2{}_3\cos^2\alpha_3 + g^2{}_4\cos^2\alpha_2\,) \\ & + I^4{}_{yy}\cos^2\alpha_2 + I^4{}_{zz}\sin^2\alpha_2 + m_5(\,a^2{}_3 + l^2{}_3\cos^2\alpha_3 + g^2{}_5\cos^2\alpha_2\,) \end{aligned}$$

$$+ I^5_{yy}\cos^2\alpha_2 + I^5_{zz}\sin^2\alpha_2 + m_6(a^2_2 + l^2_2\cos^2\alpha_2 + g^2_6\cos^2\alpha_3)$$

$$+ I^6_{yy}\sin^2\alpha_3 + I^6_{zz}\cos^2\alpha_3 + 2\, I^6_{yz}\sin\alpha_3\cos\alpha_3 - 2\, m_4 l_3 g_4 \cos\alpha_2\cos\alpha_3$$

$$+ 2\, m_5 l_3 g_5 \cos\alpha_2\cos\alpha_3 + 2\, m_6 l_2 g_6 \cos\alpha_2\cos\alpha_3$$

$$h_{22} = I^2_{xx} + m_2 g^2_2 + I^4_{xx} + m_4 g^2_4 + I^5_{xx} + m_5 g^2_5 + m_6 l^2_2$$

$$h_{33} = I^3_{xx} + m_4 l^2_3 + m_5 l^2_3 + m_6 g^2_6 + I^6_{xx}$$

$$h_{12} = (m_4 g_4 a_3 + m_5 g_5 a_3 - m_6 l_2 a_2 - m_2 g_2 a_2) \sin(\alpha_2)$$

$$h_{13} = (- m_4 l_3 a_3 + m_5 l_3 a_3 - m_6 g_6 a_2) \sin(\alpha_3)$$

$$h_{23} = (- m_4 l_3 g_4 + m_5 l_3 g_5 + m_6 l_2 g_6) \cos(\alpha_3 - \alpha_2)$$

where I^i_{xy} is the x-y moment of inertia of link i. As expected, no moments of inertia should be involved in the off-diagonal elements. The base joint inertia, h_{11}, is a function of the actuators displacements α_2 and α_3 as expected. The base motor would experience a high inertia when the upper arm is extended and a low inertia when it is retracted. The terms h_{22} and h_{33} are constants since their corresponding inertias are not affected by any of the joint motions. This results from the use of the parallel drive, as discussed previously. The off-diagonal elements are functions of configuration, however , they can be eliminated. The corresponding mass redistribution conditions that make the inertia tensor decoupled for all arm configurations are

$$m_4 g_4 a_3 + m_5 g_5 a_3 - m_6 l_2 a_2 - m_2 g_2 a_2 = 0 \qquad (6.4)$$

$$- m_4 l_3 a_3 + m_5 l_3 a_3 - m_6 g_6 a_2 = 0$$

$$- m_4 l_3 g_4 + m_5 l_3 g_5 + m_6 l_2 g_6 = 0$$

The acceleration of any link produces both translational inertial forces and rotational inertial forces at its mass center. The former depends only on the mass of the link and the latter on the moment of inertia. These conditions (6.4) are designed only to eliminate interactive torques resulting from the linear motion of the mass center of each link. The effects due to rotation are not present because we used design guideline (ii). The motion of each link, in the upper arm, is restricted to a vertical plane; as a result any acceleration torque resulting from rotation is orthogonal to the base joint axis and does not cause interactions Another result is that static balancing of all the links by making all g_i equal to zero does not alter the space dependency of the elements h_{12} and h_{13}.

If we assume that links 4 and 5 are the same, then the decoupling conditions become

$$2\, m_4\, g_4\, a_3 - (\, m_6\, l_2 + m_2\, g_2\,)\, a_2 = 0$$

$$g_6 = 0$$

If we balance link 2 such that, g_2 is zero, then the conditions reduce to

$$\frac{m_6}{m_4} \cdot \frac{l_2}{g_4} \cdot \frac{a_2}{a_3} = 2 \qquad (6.5)$$

$$g_2 = 0\ ,\ g_6 = 0$$

For the planar dynamics of the upper arm, the governing equation of each actuator does not include interactive acceleration torques, or nonlinear velocity torques since the inertia tensor G_{23} is decoupled and invariant . In the 3-d.o.f case, the inertia tensor is completely decoupled. However, the inertia of the base motor is a function of α_2 and α_3, hence some velocity torques are present. The resultant simplified

dynamic equations are

$$h_{11}(\alpha_2, \alpha_3)\,\ddot{\alpha}_1 + \frac{\partial h_{11}}{\partial \alpha_2}\dot{\alpha}_1\dot{\alpha}_2 + \frac{\partial h_{11}}{\partial \alpha_3}\dot{\alpha}_1\dot{\alpha}_3 + \tau_{g1} = \tau_1$$

$$h_{22}\,\ddot{\alpha}_2 \quad - \frac{1}{2}\frac{\partial h_{11}}{\partial \alpha_2}\dot{\alpha}^2_1 + \tau_{g2} = \tau_2$$

$$h_{33}\,\ddot{\alpha}_3 \quad - \frac{1}{2}\frac{\partial h_{11}}{\partial \alpha_3}\dot{\alpha}^2_1 + \tau_{g3} = \tau_3$$

6.3 Conclusion

This chapter has addressed the design of the M.I.T direct-drive manipulator with a decoupled inertia tensor by mass redistribution. The design guidelines of chapter 5 were used to make the decoupling possible.

Chapter 7
CONTROL SYSTEM DESIGN AND PERFORMANCE EVALUATION

7.1 Introduction

This chapter explores the overall control performance of the prototype direct-drive manipulator. Analytical and experimental evaluations are conducted for speed, acceleration, servo stiffnesses, actuator interactions and the torque control capability of the direct-drive robot.

7.2 Drive System Hardware

7.2.1 Actuators

The performance of the direct-drive arm is highly dependent on the performance of the motors at the active joints. An investigation has been conducted on actuators for the direct-drive arm [Asada,1981] . The motors used in this particular design are brushless DC motors which utilize a new type of rare-earth-cobalt permanent magnet. These magnets have an extremely large maximum magnetic energy product, BH(max)=26 MGOe. Since the magnets are not demagnetized in a normal operating range, a large current can be applied to the armature of the motor resulting in a large torque which can accelerate (decelerate) the arm joints very rapidly.

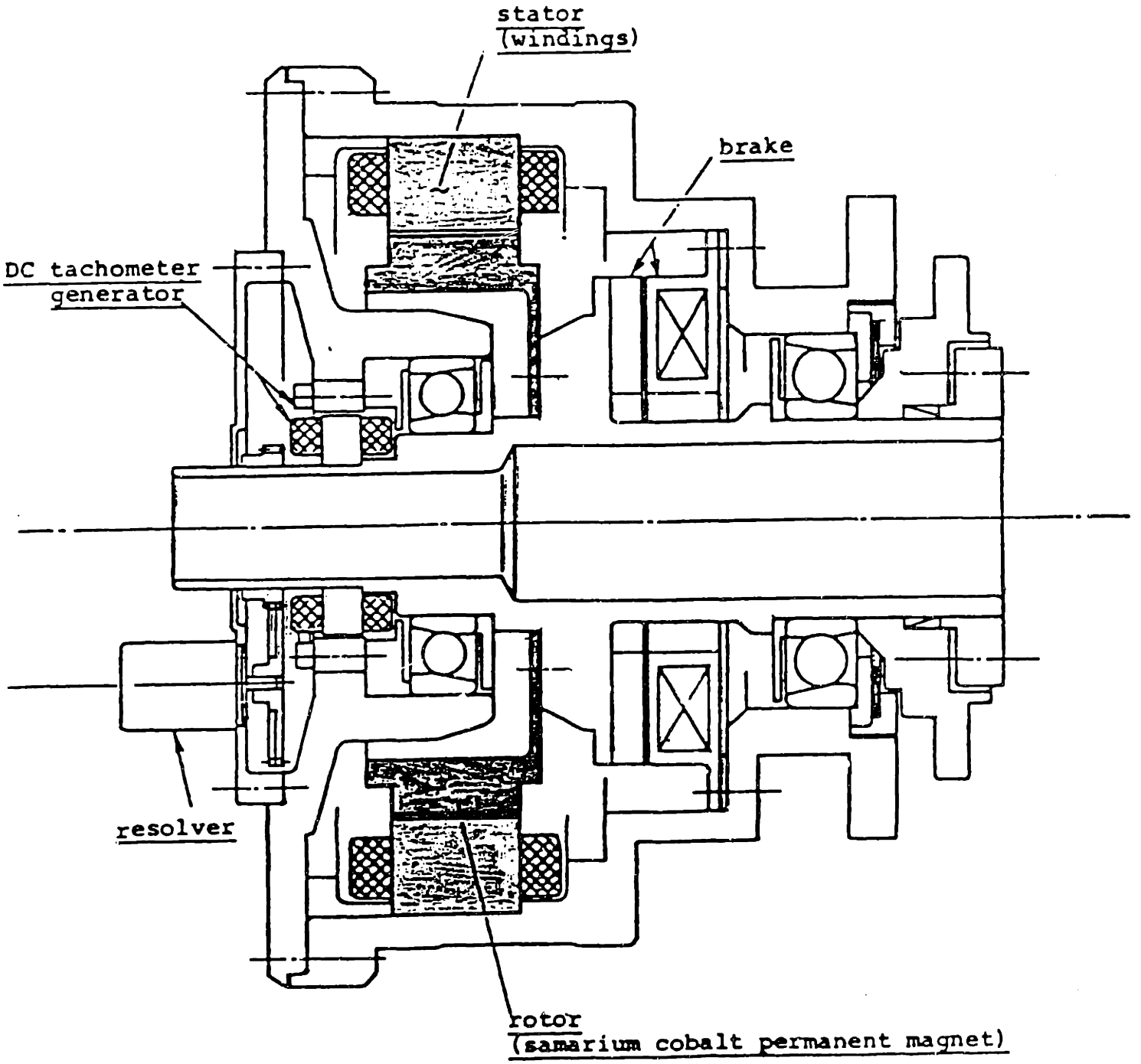

Figure 7-1: Brushless DC Motor

Figure 7-1 shows the brushless motor housed in a case. The rotor, which contains the magnets, is directly coupled to the joint axis. A magnetic brake and a tachometer generator with hallow shafts are also mounted in the case which is aligned with the joint axis. The windings are part of the stator (not the rotor) consequently the motor has a better heat dissipation than a DC torque motor [Asada,1981] because the heat generated is efficiently dissipated through the motor housing. Also, brushless motors can use high currents without causing sparks or mechanical wear .

Table 7-I lists the characteristics of the motors used in the M.I.T direct-drive arm. These characteristics are an order of magnitude better than the DC torquers in reference [Asada,1981] .

7.2.2 Sensors

A set of position and velocity sensors are mounted on each motor. A resolver generates two AC signals that are processed by a resolver to digital (R-to-D) converter to output a 16-bit signal representing position. This signal is used for commutating current in the three phases of the motor and also for position feedback. The three phase currents are measured by resistors in series with each of the phase windings. The torque exerted by the motor can be estimated from these currents. The tachometer shown in Figure 7-1 provides a measure of velocity.

7.2.3 Power Amplifier

The driving amplifiers used are Pulse Width Modulated (PWM), "H" bridge type with switching at a rate of 2 KHz . The motor voltage is switched at a high voltage, 340 volts, to provide high currents. The basic block diagram of the drive

Specifications of rare-earth brushless d-c motors

motor dia (cm)	peak torque (Nm)	rotor inertia (kg – m2)	# poles	maximum current (amp.)		mass (kg)	motor constant (Nm/√w)
				instantaneous	continuous		
35	660	0.181	30	50	15	20.39	7.5
25	230	0.0256	18	30	10	16.5	2.5

Table 7-I: RareEarth Brushless DC Motor

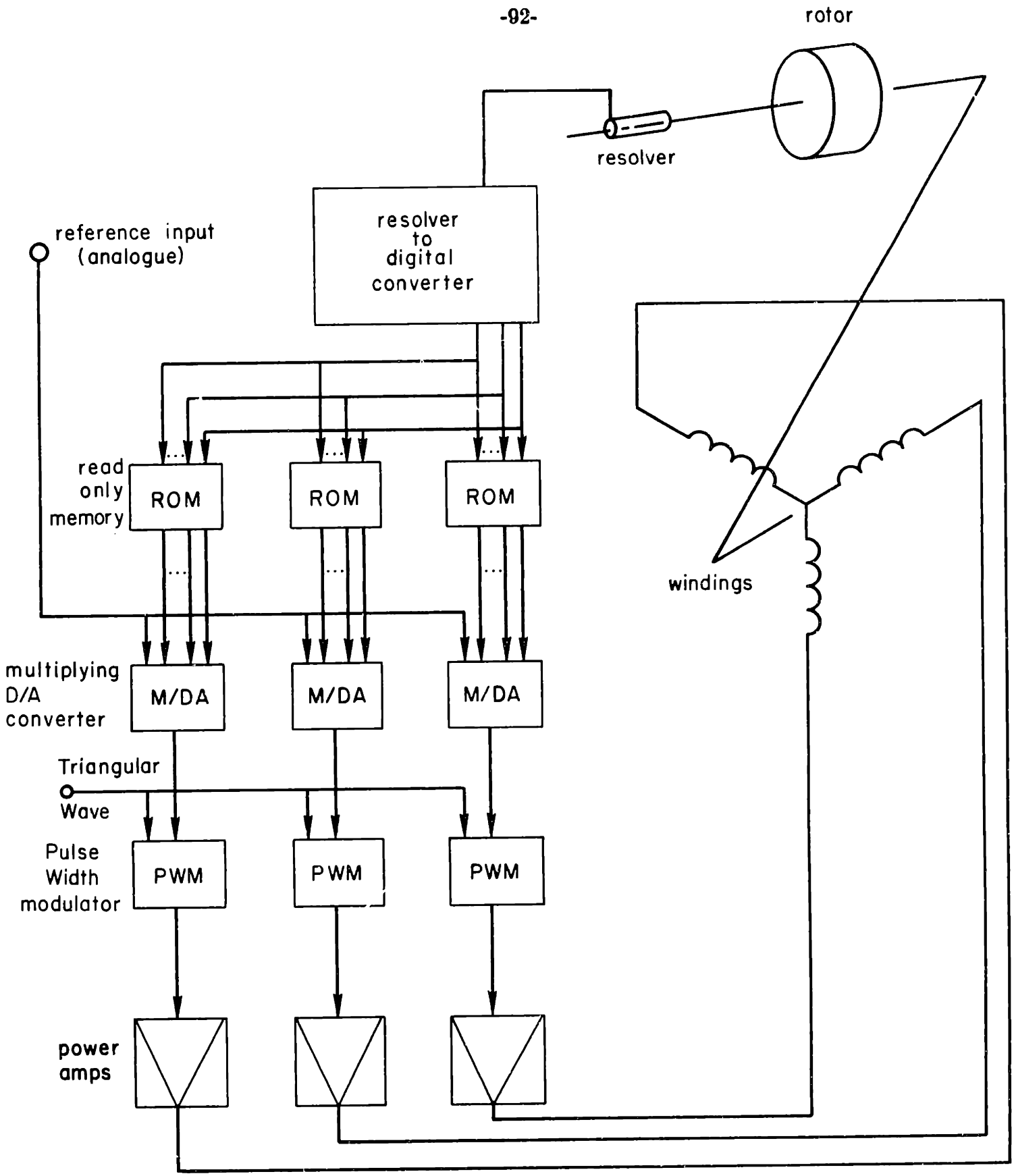

Figure 7-2: Block Diagram of Drive Amplifier

amplifier is shown in Figure 7-2. The R/D converter feeds a 10-bit signal representing the actual rotor position to the ROM's which output the sine scaling functions for each phase. These functions are in turn multiplied by the current request through the multiplying Digital/Analog converters to output the request current in each phase. Finally, the pulse width modulator and the output power stage work to bring the error between the request currents and the actual phase currents to zero.

7.3 Position Control Evaluation

7.3.1 Actuator Modeling and Identification

The direct coupling of the motor rotors to the load requires motors with high torque output. To achieve such high torque, one must increase the number of turns in the motor windings. However, the inductance is proportional to the square of the number of turns, hence the delay in motor response increases and the control task becomes difficult. The power amplifiers were designed with current feedback to minimize the inductance effects, improve control of the torque output, and avoid the effects of line voltage fluctuations.

The first goal is to evaluate the motor-amplifier combination in the direct-drive application. Figure 7-3 shows a block diagram of the PWM amplifier and its motor [Electro-Craft, Persson 1975 and 1976]. The differential command input ΔV is converted to a desired current by the gain k_1 . The PWM, modelled as a gain k_a, outputs a mean voltage V_m, the back EMF must be subtracted from this to yield an effective voltage V_{eff} across the motor windings. The phase resistance r and inductance l form the winding impedance, $r+ls$, where s stands for the Laplace operator. The motor torque τ_m which is the product of the torque constant and the

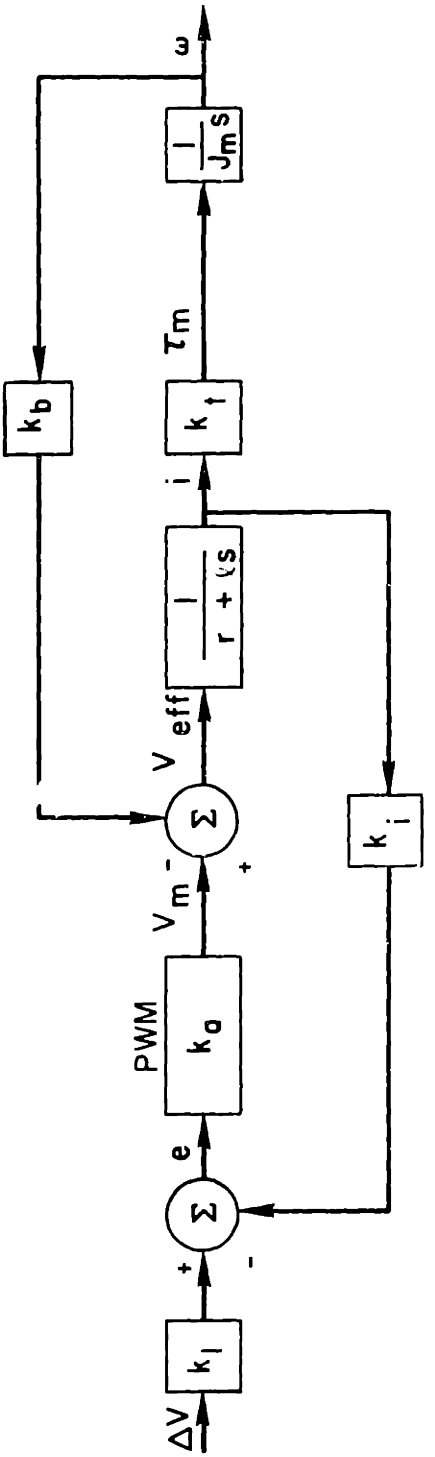

Figure 7-3: Block Diagram of PWM Drive Amplifier and motor

motor current i accelerates the motor inertia J_m. K_i is a current feedback constant. In this model, lower order effects due to mutual inductance windings, overlapping conduction angles and unequal rise and fall time of currents are neglected. The transfer function relating the input to the amplifier $\Delta V(s)$ and the angular velocity $\omega(s)$ is

$$\frac{\omega(s)}{\Delta V(s)} = \frac{\dfrac{k_1 k_a k_t}{J_m l}}{s^2 + \dfrac{r + k_i k_z}{l} s + \dfrac{k_t k_b}{J_m l}}$$

where k_b is the back EMF constant. The two poles are functions of the current gain k_i.

An experimental verification of the fundamental mathematical model presented is necessary to validate the analysis and amplifier design. A frequency response test was conducted on the amplifier-motor combination using a Spectrum Analyzer (H-P 5423A). The input/output variables considered were the differential input voltage to the amplifier and the motor velocity respectively. It was clear that the system has two real poles, thus it is second order. The slowest pole was identified as a load dependent parameter by repeating the frequency response test with different load conditions . The fastest pole was only affected slightly. A typical open loop frequency response is shown in Figure 7-4. Under zero load conditions, the amplifier-motor system had a DC gain of 35 db and two poles at 3.65 Hz and 68 Hz . This verifies the mathematical model for the amplifier-motor combination.

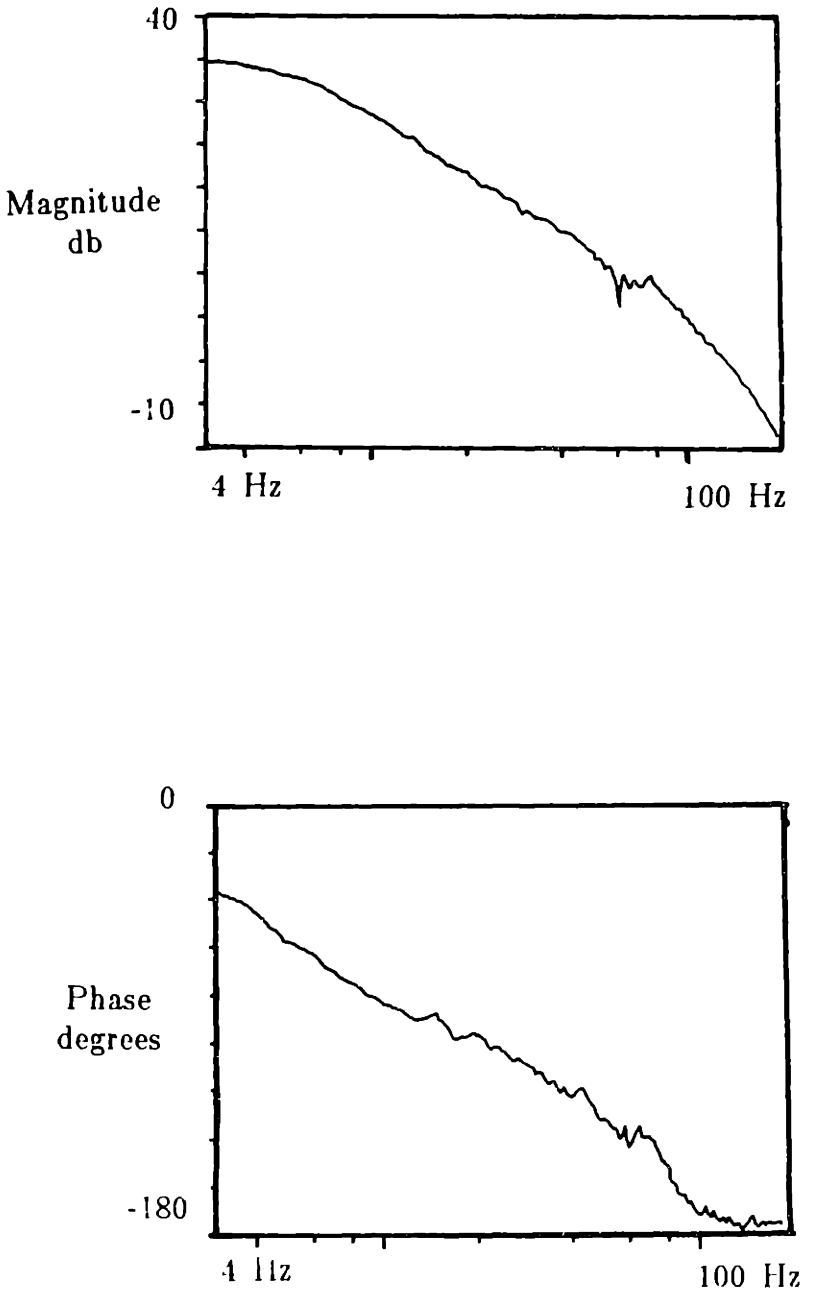

Figure 7-4: Open loop frequency response of Amplifier-motor system

7.3.2 Position Control System Design

Since the prototype arm's inertia is decoupled and nearly invariant, control problems reduce to single-axis control problems with fixed inertial loads. In this section, we present the design for the single-axis controller (refer to Appendix C)and evaluate its control performance.

Since we used large windings to exert a large torque, the motor has a significantly large inductance, which results in a lower frequency at the second pole. Unlike the conventional servomotor where inductance is negligibly small, the high torque brushless motor has a higher delay due to this large inductance, which leads to poor stability when the position loop is closed.

Figure 7-5 shows the step response when motor 1 drives the six-bar-link mechanism and position and velocity are fed back. The response ,with a delay time of 82 ms ,is fairly slow and poor in damping. When acceleration feedback was included, the response was significantly improved as shown in the same Figure. In this case the delay time is only 27 ms. Thus, the feedback of acceleration or equivalent higher order derivatives is necessary for proper control. Instead of using an accelerometer, motor currents monitored at the windings and the quasi-derivative of a tachometer signal were used to get the acceleration signal. The tachometer used was a pancake-type D.C. tachometer which has low ripple, less than 1 % of average reading, and a high sensitivity of 2.2 Volt/rad/s. The servo stiffnesses [Asada, Kanade and Takeyama 83] of the base motor and motors for the five-bar-link mechanism were measured by applying known loads and measuring the resultant displacements at the arm tip. The stiffnesses achieved were 300 N/mm for the base joint and 416 N/mm for the other two joints. These servo stiffnesses, which depend on the loop gains and link lengths, are 10 to 14 times larger than

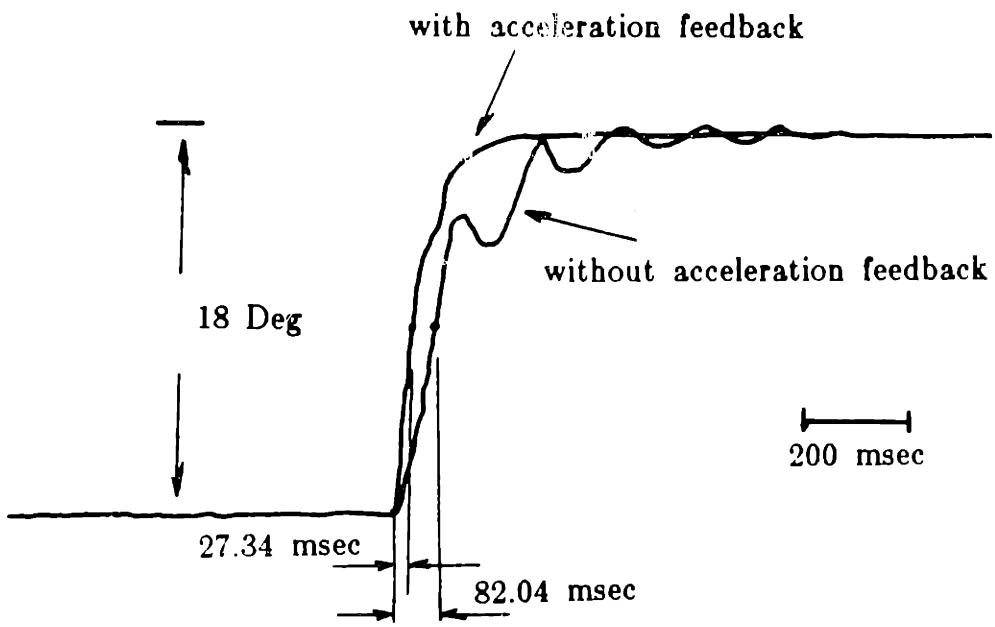

Figure 7-5: Position response of motor 1 driving the link mechanism

those of the direct-drive arm in reference [Asada, Kanade and Takeyama 83]. The bandwidths (at 3 decibels cutoff when the position loop is closed) were measured to be 3.17 Hz for the base and and 3.1 Hz the other motors respectively. These bandwidths, while measured for large amplitudes of about 90 degrees span, are comparable to the bandwidths of hydraulically driven robots.

Figure 7-6 shows a velocity profile when the base joint traveled a long distance from -90 deg to +90 deg. The arm was extended 0.75 m from the base center with no payload. The speed indicated is that of the end point. The end point was accelerated very rapidly and it reached the top speed. The maximum acceleration determined by the slope is 52 m/s^2, which is more than 5 G. Since most industrial robots currently used have at most 0.1 to 0.5 G, the developed direct-drive arm is an order-of-magnitude faster in acceleration. The top speed measured was 9.36 m/sec, which is also much faster than that of existing robots.

7.4 Dynamic Decoupling Evaluation

The following experiment was conducted to evaluate the coupling between the motors. One motor, tracking a sinusoidal position command, drives the link mechanism while the other motors are not servoing. The peak-to-peak ratios between the actual position signals of the driving motor and the other motors is a measure of the coupling for the arm dynamics. These ratios (in Db's) are listed in Table 7-II. The test was performed for two frequencies of the driving joint, 0.5 and 5 Hz, and for four different arm configurations. The experimental data shows a coupling of less than -30 Db for all arm configurations. Thus the arm is well decoupled.

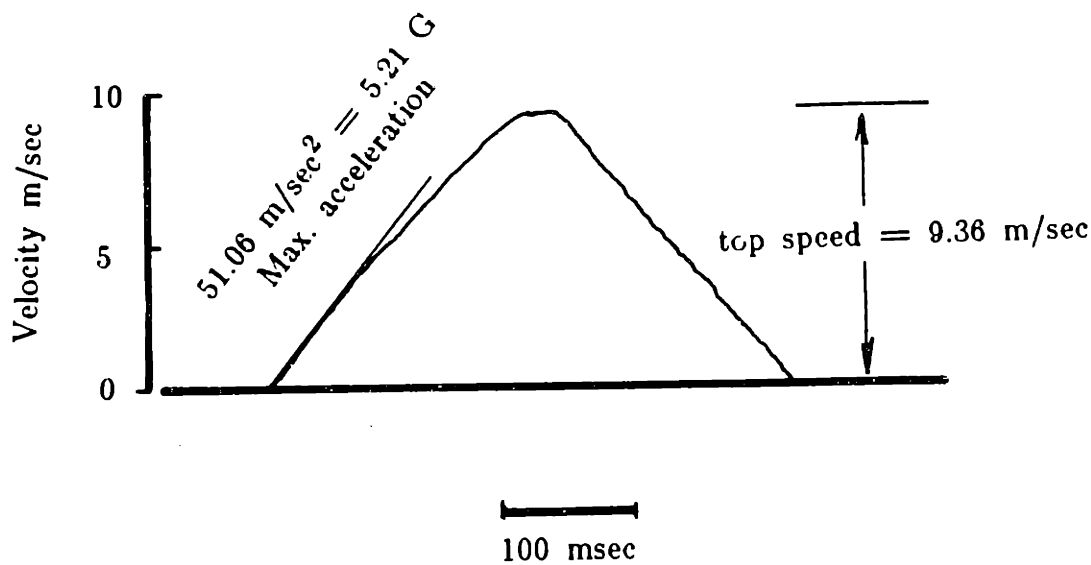

Figure 7-6: Velocity profile of base motor

	Arm configuration $\alpha_2 - \alpha_1$ Deg.	Oscillation Amplitude Ratio (Db) of Passive Axis to Active Axis	
		0.5 Hz	5 Hz
Effect of motor 2 on motor 1	95	-48	-31
	110	-57	-40
	130	-53	-39
	140	-52	-32
Effect of motor 2 on base motor	95	-57	-34
	110	-59	-38
Effect of motor 1 on base motor	95	-59	-49

Table 7-II: Experimental data on actuator dynamic interactions

7.5 Torque Control

7.5.1 Modeling and Estimation

The current in the motor windings generates a magnetic field in the air gap of the motor. This field interacts with the magnetic field from the magnets of the rotor and produces the output torque. The torque constant is the ratio of the output torque to the current. The magnetic field changes with the rotor position and causes variations in the torque constant. This results in torque ripple. Although the motors used for direct-drive arms are designed so that the torque constant is as uniform as possible for all the rotor positions, there still exists a significant torque ripple.

The torque generated is then transmitted to the joint axis through the motor shaft and the joint housing. In the case of a traditional joint mechanism, the torque is transmitted and amplified through a reducer, which causes the large torque disturbances produced by friction, backlash and dynamic deflections. The elimination of the gearing in the direct-drive arm greatly reduces these disturbances.

The motors, described previously, are three-phase variable frequency synchronous motors developed for the MIT direct-drive arm [Asada and Youcef-Toumi 83, Davis and Chen 84]. The motors are capable of exerting large torque so that the gearing can be completely eliminated. The motor is also designed to minimize the torque ripple. In the sinusoidal torque control generation scheme [Tal 81], the relationship between the output torque and the currents flowing into the three-phase windings is given by

$$\tau = K_t \left[I_{am} \sin(\theta) + I_{bm} \sin(\theta + 120) + I_{cm} \sin(\theta + 240) \right] \qquad (7.1)$$

where I_{am}, I_{bm} and I_{cm} are three phase currents, Θ is the angular position of the motor rotor and K_t is the torque constant.

From the above relationship, it follows that the output torque can be estimated by measuring the three phase currents and the angular position of the motor rotor. The three phase currents can be measured by inserting sensing resistors in series with the phases of the motor, and the rotor position can be measured by a position transducer attached to the rotor shaft. In the synchronous motor used, both the current and position information is already available, so that no additional sensors are necessary for implementing the torque measurement.

The joint torque estimator discussed in the previous sections was implemented and tested in terms of static and dynamic performances, [Asada, Youcef-Toumi and Lim 84] . The three phase currents were monitored with 0.01 Ohm sensing resistors through circuits which isolate the measured signals from the high voltage power lines of the drive amplifier. The computation of the output torque was accomplished with a computer by recording the measured currents and the rotor position information provided by a synchro resolver, refer to appendix B.

Figure 7-7 shows the results of an experiment using the current torque sensor in which applied and estimated torques were compared for the same rotor position. The estimated torques show no hysteresis and a linear relationship with the applied torques except around the origin. This discrepency is mainly due to the nonlinearity of the isolation circuitry. The sensitivities were 0.223 V/Nm and 0.260 V/Nm for applied torques in the clockwise and counterclockwise directions respectively. The difference in slopes is caused by a slight misadjustment of the resolver. The currents in each phase were also tested for repeatability and consistency. Various conditions were used for this test including (i) loading and unloading of the applied torques, (ii) moving away and back to the test position,

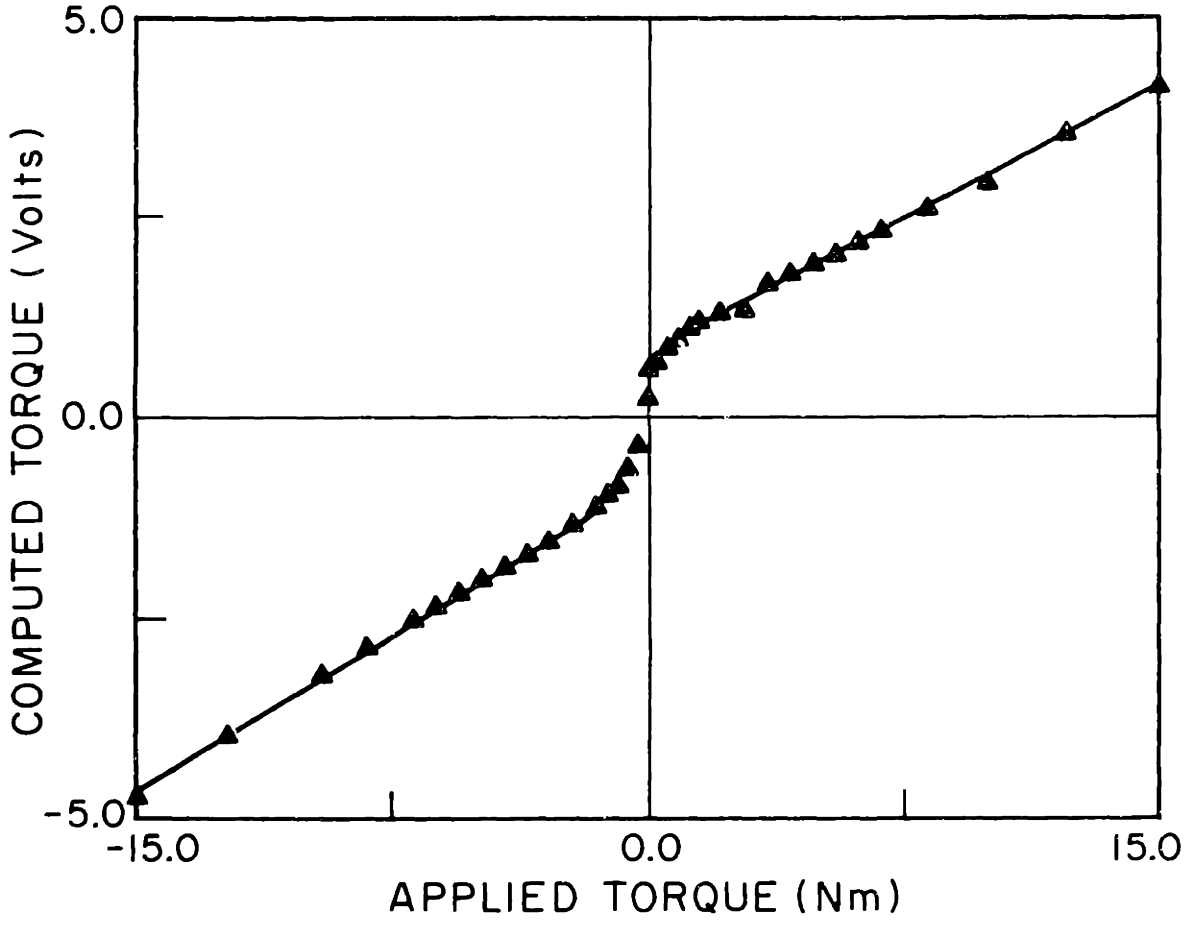

Figure 7-7: Calibration curve of the current torque estimator

(iii) and turning the system on and off. The repeatability in the current readings is due to the closed loop current controller in the amplifier that regulates current in each phase.

The accuracy of this method depends not only on the accuracy of the current and position tranducers but also on the variation of motor constant k_t. Since the magnetic field in the air gap varies slightly with the rotor position, the torque estimation based on equation (7.1) will also vary with the rotor position. Distortions of the sinusoidal motor phase currents I_{am}, I_{bm} and I_{cm} cause additional errors in the torque estimated. The experimental results in Figure 7-8 show the effects of these errors on the estimated torque. A constant torque was applied externally to the motor shaft for various rotor positions. The error in the computed torque was $\pm$ 10 % of the mean value. However, the estimated torque has a clear pattern where two main frequencies are dominant. The two lowest frequencies correspond with the number of rotor poles and the number of stator slots respectively. This error can be reduced by modifying equation (7.1) so that the errors due to the rotor and stator slot locations are compensated for. With this modification, the torque measurement error was reduced to $\pm$ 6 % of the mean value.

7.5.2 Torque Control

[Asada and Lim 85] evaluated the dynamic response of the torque control system. The step response showed a delay time and a settling time of 6 and 60 msec respectively. It was also found that the bandwidth of the torque control system was about 30 Hz. Thus a fast and accurate torque control system has been achieved.

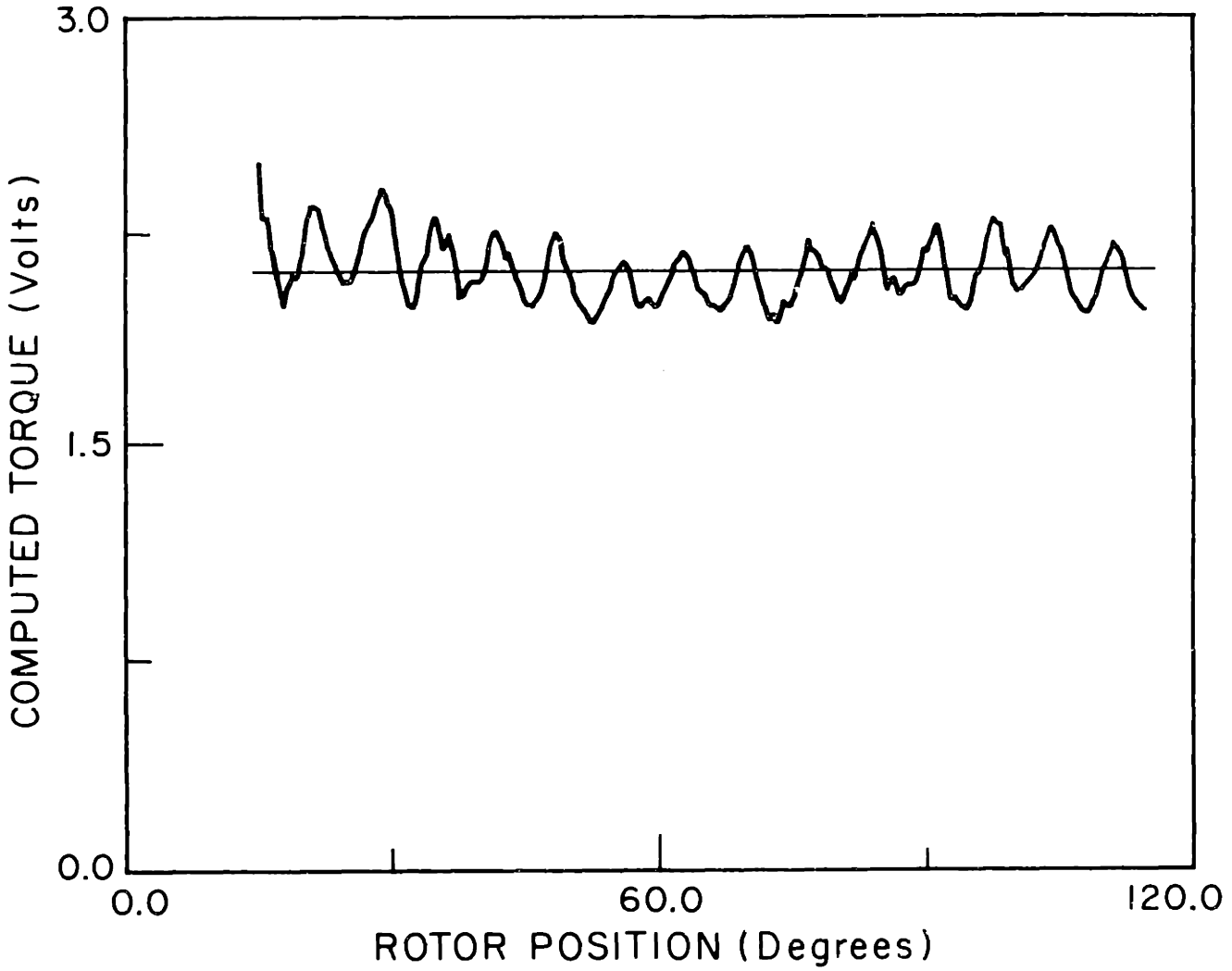

Figure 7-8: Variation in computed torque without correction

7.6 Conclusion

The control performances of the developed prototype direct-drive robot were considered. The manipulator, equipped with high torque brushless motors and a six-bar-link mechanism with a decoupled and nearly invariant arm inertia tensor, exhibits excellent performance. The delay time in the response is 27 ms, and the top speed and acceleration are on the order of 10 m/s and 5 G respectively. In addition, high servo stiffnesses were achieved. These characteristics are each an order of magnitude better than those of conventional robots. Also, the interactions between joints were also reduced to less than -30 Db's for all arm configurations. In addition, the torque developed by the direct-drive motor was estimated through the measurement of phase currents. Using a simple correction function, that depends on the pole and slot ripples, the estimated torque was found to be within $\pm$ 6 % of the mean.

Chapter 8
CONCLUSIONS AND RECOMMENDATIONS

The inherent problems of the direct-drive approach have been identified as: (i) heavy arm weight and small load capacity, (ii) motor overheating (iii) sensitivity to changes in load conditions and disturbances and, (iv) actuator stability. The potential advantages of the direct-drive concept are fully exploited by overcoming these inherent difficulties. This thesis presents effective design methods for articulated direct-drive arms, specifically for application to high-speed, high-accuracy trajectory control tasks. These design methods include a power efficiency analysis and a dynamic analysis of articulated direct-drive arms.

The power efficiency analysis, of chapter 2, was utilized to examine issues of (i) and (ii). Although, this analytical tool applies to static analysis only, it is helpful in evaluating the effectiveness of different kinematic structures in terms of the power dissipation in the actuators. For example, a parallel drive mechanism is shown to have lower power dissipation than a serial drive for the same motors and work space.

In dealing with problems (iii) and (iv), stated above, a new approach is developed for the arm linkage design. The goal is to simplify the controller design by reducing the effects of complicated manipulator dynamics and to further improve performance by increasing the load capacity. This is particularly useful for direct-drive manipulators used in high-speed, high-accuracy trajectory control

tasks, such as laser cutting. For such applications, two issues are of importance. Along a given trajectory, a high bandwidth drive system requires a high density of data points which can be independent of the end-effector speed. In addition; on-line updating of the joint angles corresponding to the end-effector command position and orientation can be required. These two requirements may limit the real time dynamic compensation that can be provided to the manipulator.

In chapter 3, a method for designing an arm linkage with small inertial load changes and small interactive and nonlinear forces is developed by analyzing the kinematic structure and mass properties. Using this design methodology, a decoupled and invariant manipulator inertia tensor in joint space can be achieved. With the resulting design each actuator experiences completely decoupled dynamics as well as a constant load which is independent of the arm configuration. First, decoupling conditions were derived for open loop kinematic chain structures under the following conditions : (i) revolute joints, (ii) actuators exert torques between adjacent links and, (iii) each link possesses a principal direction collinear with its corresponding joint axis. The last assumption is necessary to assure that the torque, resulting from angular acceleration, is directed along the joint axis of rotation. It was deduced from these conditions that structures of this type cannot be decoupled for more than 2 degrees-of-freedom. The group of 2 d.o.f structures that can be decoupled were identified. This does not apply to cartesian robots which use prismatic joints and can have 3 decoupled degrees of freedom. The limiting factor in decoupling was determined to result from the rotation of links about their centroids. These rotational effects can only be eliminated by introducing orthogonal joint axes. Consequently, the arm structure must be modified in order to decouple more than two degrees of freedom.

Relocation of actuators is introduced in chapter 4 as a method for relaxing

the decoupling conditions for serial drive manipulators. For example, there is no mass distribution that will decouple the inertia tensor of a planar open loop kinematic chain when actuators exert torques between adjacent links. Thus it is necessary to modify the arm structure. When actuators are mounted remotely, the torque exerted by one actuator can affect more than one joint. To analyze the effects of relocating actuators on the manipulator kinematics and dynamics, Kane's partial rates of positions and orientations are used. Furthermore, set notation is introduced to represent the manipulator dynamics. This notation concisely represents the causal relation between actuators and link motions. In addition, the contribution of a specific link's mass properties, in particular the moments of inertia, to a given element in the inertia tensor is directly apparent from this notation.

The results of the analyses of the decoupling of serial drive manipulators and the set notation are then used to provide design conditions for the decoupling of manipulators. Chapter 5 first presents some design guidelines to meet the necessary conditions for decoupling the manipulator inertia tensor. These guidelines, while strict, merely make the given structure characteristics meet the necessary conditions by eliminating all of the moments of inertia from the off-diagonal elements of the manipulator inertia tensor. Finally, the sufficient conditions for making the inertia tensor of an open loop kinematic chain completely decoupled and invariant were found to be : (i) the rotation of each link must result from one actuator only and, (ii) each link must be mass balanced. The mass balancing conditions are required for all links except the first link. While the mass added to meet the balancing conditions, in this case, is on the order of the number of links squared, the use of parallel drive mechanisms results in more practically achievable conditions. Using parallel drives, on the other hand requires the addition of extra

passive joints. For this case, clearance at the joints can be a problem [Dubowsky and Perreire 82]. In addition, decoupling of the mechanism's inertia tensor does not require the total mass center of the mechanism to be stationary as required in the case of force balance.

These design tools are applied in chapter 6 to the development of the 3 d.o.f M.I.T direct-drive arm. Complete decoupling of the manipulator dynamics is achieved. The total mass of the decoupled arm mechanism is about 15 Kg, which is excellent for the robot size considered. Also, the design can facilitate the identification of payload inertia characteristics since the manipulator is both decoupled and sensitive to load changes.

Chapter 7 presents an evaluation of the overall control performance of this prototype direct-drive manipulator. Analytical and experimental evaluations are conducted for speed, acceleration, servo stiffnesses, actuator interactions, and the torque control capability of the direct-drive robot. The manipulator, which is equipped with high torque brushless motors and a six-bar-link mechanism with a decoupled and nearly invariant arm inertia tensor, exhibits excellent performance characterized with an order of magnitude improvement in speed, 27 ms in delay time, about 10 m/s top speed, and 5 G accelerations as well as high servo stiffnesses.

Direct-drive applications still require improvements in direct-drive motors. The main issues are the dynamic performance, nonlinear effects in the drive system, heat dissipation and weight per torque output.

High speed high accuracy continuous path control applications require precise compensation for the dynamics. Investigations are needed to evaluate to what extent the simplification of the arm dynamics aids in the control performance. The

extension of the decoupling results of this thesis to general mechanisms and the use of the set notation to analyze the dynamic properties of mechanisms may be investigated. Other relevant areas are path planning and optimization, automatic calibration and parameter estimation.

Appendix A
FLOW CORRECTION IN CURRENT READING

The measurement of current in each phase of the windings, shown in Figure A-1, is in error because of the sensory limitations. The current readings need to be corrected before their use. The correction is based on satisfying the continuity of flow, or Kirchoff's current law. The measured currents I_{am} , I_{bm} and I_{cm}, are corrected as follows [Paynter 82],

$$\begin{aligned} I_{acorr} &= I_{am} - \frac{F}{F^*} Abs(I_{am}) \\ I_{bcorr} &= I_{bm} - \frac{F}{F^*} Abs(I_{bm}) \\ I_{ccorr} &= I_{cm} - \frac{F}{F^*} Abs(I_{cm}) \end{aligned} \qquad (A.1)$$

where

$$F = I_{am} + I_{bm} + I_{cm}$$

$$F^* = Abs(I_{am}) + Abs(I_{bm}) + Abs(I_{cm})$$

The above relations guarantee that continuity for the corrected currents is satisfied,

$$I_{acorr} + I_{bcorr} + I_{ccorr} = 0$$

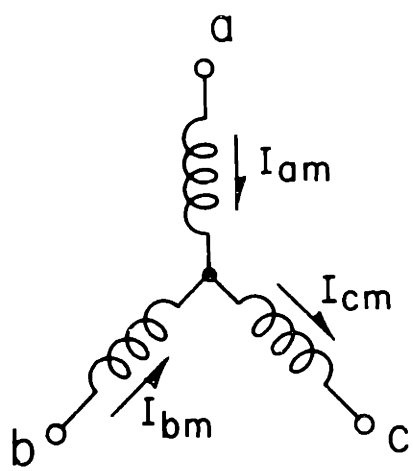

Figure A-1: 3 phase windings of the direct-drive motor

Appendix B
TORQUE CONTROL CALIBRATION AND SOFTWARE

B.1 Setup and Calibration

As presented in Chapter 7, the motor torque output is estimated from the phase currents. The relationship between the phase currents and torque output was given by Equ. (7.1),

$$\tau = K_t [I_{am} \sin(\theta) + I_{bm} \sin(\theta + 120) + I_{cm} \sin(\theta + 240)] \qquad (B.1)$$

where the currents I_{am}, I_{bm} and I_{cm} are the measured currents in phases a, b and c respectively; K_t is the torque constant. The amplifiers for the direct-drive motors use the sinusoidal torque generation approach [Electro-Craft 80]. Thus the phase currents are sinusoidal functions of rotor position θ. In practice, these are slightly distorted sinusoids. The weighting factors sin(θ), sin(θ + 120) and sin(θ + 240), Equ. (B.1), are generated by software or by hardware using ROM's and multiplying D/A's (M/DA) as shown in Figure 7-2. The key issue in using Equ. (B.1) is to make sure that the sinusoidal measured current I_{am}, I_{bm} and I_{cm} are <u>in phase</u> with the generated sinusoids sin(θ), sin(θ + 120) and sin(θ + 240) respectively. The torque constant K_t is determined experimentally from Equ. (B.1). The experimental setup is shown in Figure B-1.

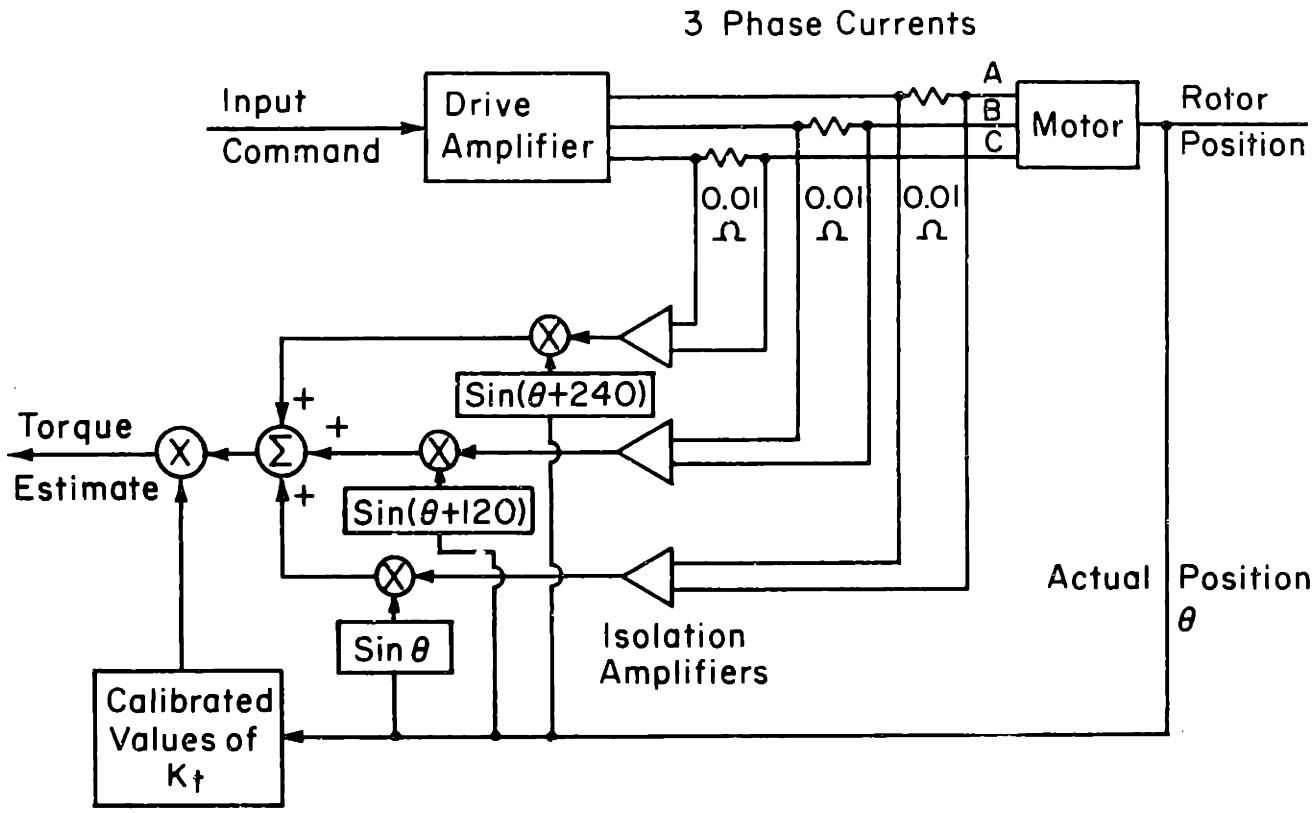

Figure B-1: Experimental setup for the torque estimator

B.2 Estimation and Control Software

```
C
C-----------------------------------------------------------------
C            TORQUE ESTIMATION AND CONTROL
C
C-----------------------------------------------------------------
C
C     IV(1) = volts for PHASE  A    ,
C     IV(2) = volts for PHASE  B    ,
C     IV(3) = volts for PHASE  C    ,
C
      DIMENSION IOSB(2),CURR(3)
      BYTE CHAR(6),TOP(2)
      DATA CHAR/27,91,50,74,27,56/
      DATA TOP/27,56/
      INTEGER  IV(3)
C
C-----------------------------------------------------------------
C      ATD CONVERSION CONSTANTS
C
C      DECIMAL READ IN = 204.8*(VOLTAGE INPUT TO A/D) + 2048.
C      AVG = SLOPE * V0LTS  + YINT
C
      SLOPE = 204.8
      YINT  = 2048.0
      IFLAG = 1
      TOREST = 100.0
C
C-------- INITIALIZE CONSTANTS
C
      PI    = 3.141592654
      CONV = 3.141592654/180.0
C      DT = 9.*360./1024. ! INCREMENT IN DEGREE, 10-BIT RES.
      DT = 9.*360./4096. ! INCREMENT IN DEGREE, 12-BIT RES.,
                         ! FOR COMMUTATION
      DTD = 360.0/4096.
      OFF7  = -0.135              ! offset in phase A
      OFF9  = -0.179              ! offset in phase B
      OFF11 = -0.193              ! offset in phase C
C
      ICH07 = 0      ! read phase A current thru chan.  0
```

```
      ICH09 = 2       ! read phase B current thru chan.  2
      ICH11 =10       ! read phase C current thru chan. 10
C
      IUNITO = 0                    ! OUPUT PORT control
      IUNITI = 2                   ! INPUT PORT position
      MASK   = -1                   ! MASK VALUE
C
C---- INQUIRE
C
      WRITE(5,5) CHAR         ! clear screen and reset cursor
 5    FORMAT(1X,4A1)
C
C-------------------------------------------------------------------
C----------------------- data aquisition -----------------------------
C
 300  continue
      CALL ADINP(IFLAG,ICH07,IVAL07)
      CALL ADINP(IFLAG,ICH09,IVAL09)
      CALL ADINP(IFLAG,ICH11,IVAL11)
      IV(1) = IVAL07              !phase A current = CURR(1)
      IV(2) = IVAL09              !phase B current = CURR(2)
      IV(3) = IVAL11              !phase C current = CURR(3)
C
C     CONVERT TO VOLTS AND CORRECT FOR OFFSETS
C
      DO 101 J = 1,3
      IVAL   = IV(J)
      CURR(J)= ( FLOAT( IVAL ) - YINT ) / SLOPE
 101   CONTINUE
C
      CURR(1) = CURR(1) - OFF7
      CURR(2) = CURR(2) - OFF9
      CURR(3) = CURR(3) - OFF11
C
C---------------------- CALCULATE COMMUTATION CONSTANTS---
C
      CALL DINP(IUNITI,MASK,IOSB,INP)        ! CURRENT POS.
      IPOS = INP.XOR.-1
C
C      POSD   = IPOS*DT
      X      = IPOS*DTD                    ! for 9 pairs of poles
      CA     = -SIN( (9.*X  + 60. )*CONV )    ! phase shifts to match
      CB     = -SIN( (9.*X  - 60. )*CONV )    ! generated sine waves
```

```
      CC    = -SIN( (9.*X  - 180.)*CONV )    ! to current sine waves
C
C---------------- CALCULATE TORQUE
C
      TOREST = CURR(1)*CA + CURR(2)*CB + CURR(3)*CC
      TOREST = -1.0*TOREST
      CALL TCONST(CKt,X)                  ! Fetch Torque constant
      TOREST = CKt*TOREST                    ! estimate torque
C
C-------------------------------------------------------
C            OUTPUT CONTROL SIGNAL
      CALL CONTROL(TOREST,IERR)
C
      IF ( IERR.GT. 2047 ) IERR =  2047
      IF ( IERR.LE.-2047 ) IERR = -2047
      ICONT = IERR.XOR.-32768              ! Change MSB (8000H)
      CALL DOUT(IUNITO,MASK,IOSB,ICONT)
C
      CALL STOP(ISTOP)
      IF ( ISTOP.EQ.1 )  GO TO 300
      CALL EXIT
      END
C
C
C
```

Appendix C
SINGLE JOINT DRIVE CONTROLLER

C.1 Controller

Considering the high noise environment, the controller for a single joints axis consists of an analog velocity loop and a digital position loop. the velocity loop was first optimized based on the actual response of the joint axis. The compensation for the velocity signal of motor 2 of figure 6-3 is shown in Figure C-1.

The position feedback loop was closed digitally. The 16 bits of actual rotor position are input to the PDP11/60 computer through the DR11K interface. The error between the reference position and the actual position in computed in real time. This setup facilitates the adjustment of the position gain depending on the arm configuration. Furthermore, a saturation algorithm allowed a high gain for the position loop. The controller uses the maximum (minimum) gain when the position error is greater (smaller) than some given limits, and a linear action otherwise. This algorithm was used in controlling the first M.I.T direct-drive arm [Asada and Youcef-Toumi 83]. With this arrangement, the 16 bit command signal is sent out through the DR11K, however, only a 12 bit Digital to Analog converter is needed. Figure C-2 shows the implementation block.

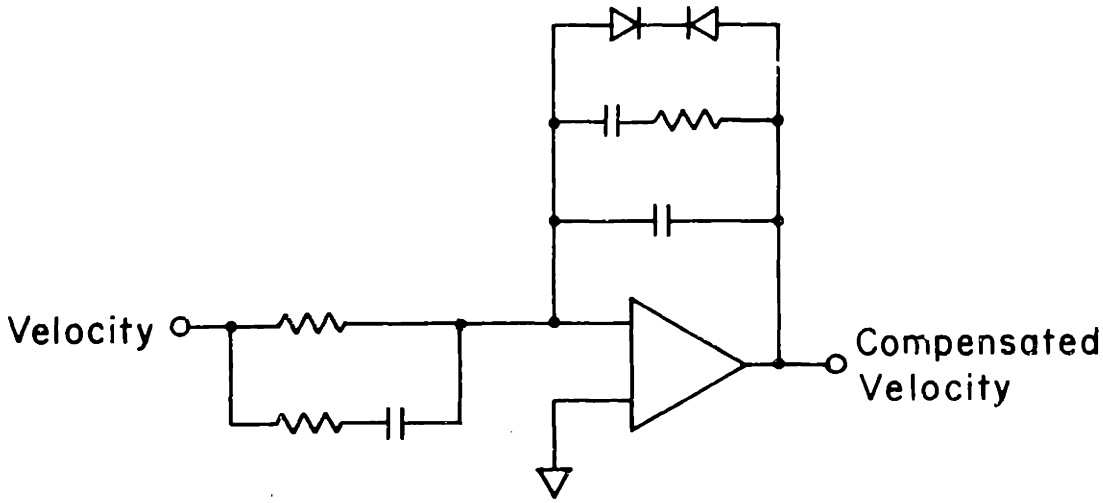

Figure C-1: Compensation circuit for velocity loop

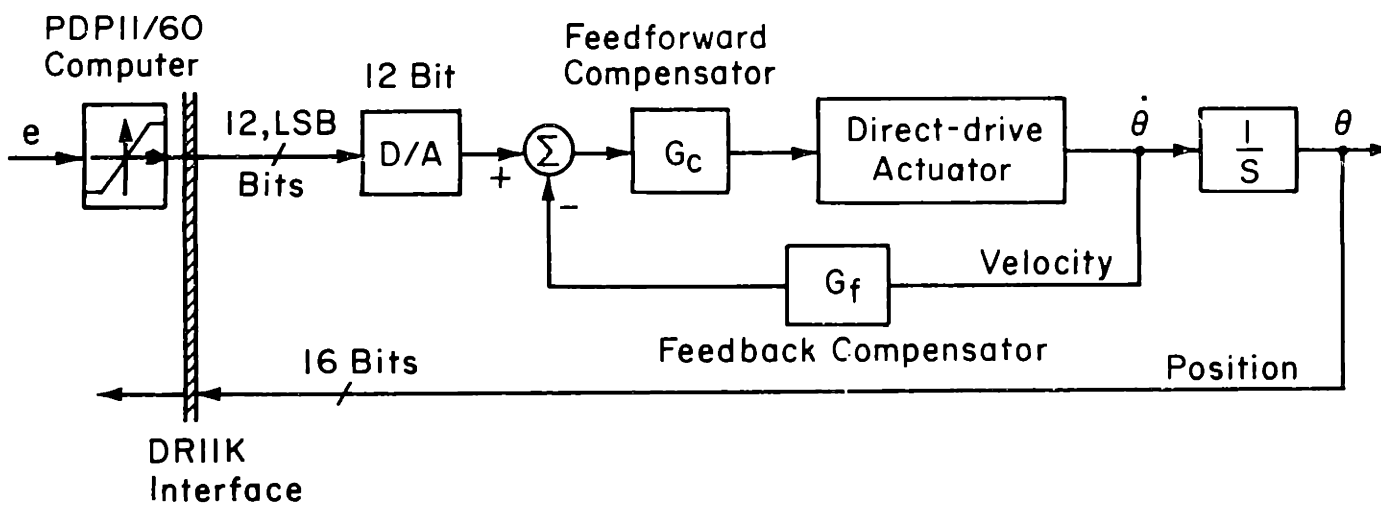

Figure C-2: Controller implementation

C.2 Software

```
C
C-----------------------------------------------------------------
C              DIRECT-DRIVE ARM CONTROL ROUTINE
C                  DIGITAL POSITION LOOP
C-----------------------------------------------------------------
C
      DIMENSION IOSB(2),IIREF(1000)
      BYTE CHAR(6),TOP(2)
      DATA CHAR/27,91,50,74,27,56/
      DATA TOP/27,56/
      CHARACTER*14 FIN
C
C
      WRITE(5,5) CHAR        ! clear screen and reset cursor
C
C-----------------------------------------------------------------
C              initialize
C-----------------------------------------------------------------
C
      TYPE*,'ENTER NUMBER OF LOOPS'
      ACCEPT*,LOOPS
      TYPE*,'ENTER SAMPLING IN SECONDS'
      ACCEPT*,TS
C
      TYPE*,' ENTER 1 FOR DISPLAY '
      ACCEPT*,IDIS
C
C 990    continue
      MASK = -1                          ! MASK VALUE
      IUNITI = 2
      IUNITO = 1
C
C---------------------- READ REFERENCE POSITIONS ----------------------
C
      TYPE*,'ENTER FILENAME'
      READ(5,55) FIN
 55    FORMAT(A14)
      OPEN(UNIT=4,STATUS='OLD',NAME=FIN)
      J = 1
 50    READ(4,*,END=501) I,I,IIREF(J)
```

```
C       WRITE(5,35) J,J,IIREF(J)
 35    FORMAT(1X,3I12)
       J = J + 1
       GO TO 50
501    NDATA = J -1
       CLOSE(UNIT=4)
C
C-----------------------------------------------------------------
C                    set up screen
C-----------------------------------------------------------------
C
       WRITE(5,5) CHAR        ! clear screen and reset cursor
 5     FORMAT(1X,4A1)
       WRITE(5,60)
 60    FORMAT(/,10X,
     1 '    <---REQUEST POSITION: integer     ',/,10X,
     1 '    <---POSITION ERROR  : integer     ',/,10X,
     1 '    <---ACTUAL  POSITION: integer     ',/,10X,
     1 '    <---counter                       ',/,10X,
     1 '    <---time                          ',/,10X,
     1 '       PRESS ANY KEY FOR NEXT POSITION')
c      WRITE(5,62) IREF,IERR,IPOS
c
 62    FORMAT(/,1X,I10,/,1X,I10,/,1X,I10,/,1X,I10,/,1X,F10.3,/,1x)
 63    FORMAT(1X,2A1)
C
C-----------------------------------------------------------------
C             READ AND WRITE POSITIONS
C                POSITION LOOP
C-----------------------------------------------------------------
C
       type*,'PRESS RETURN TO START CONTROLLER'
       READ(5,51)
 51    FORMAT(I1)
C
       JJ = 0
C
777    JJ = JJ + 1
C
C
        j = 1
666        IREF = IIREF(J)          ! SET HOME POSITION = 3737
C
```

```
          TI = SECNDS(0.0)
C
400                CONTINUE
                   CALL DINP(IUNITI,MASK,IOSB,IPOS)
                   IERR  =  IPOS - IREF
                   CALL GAIN(IPOS,KP)
                   ICONT =  IERR*KP
                   IF ( IERR.GT. 2047 ) IERR =  2047
                   IF ( IERR.LE.-2047 ) IERR = -2047
                   ICONT = IERR.XOR.-32768          ! change MSB (8000H)
                   CALL DOUT(IUNITO,MASK,IOSB,ICONT)
      IF (IDIS.EQ.1 ) THEN
      WRITE(5,63) TOP                ! reset cursor to home
      WRITE(5,62) IREF,IERR,IPOS,J,TF
      END IF
C
C
          TF = SECNDS(0.0) - TI
          IF ( TF.LE.TS ) GO TO 400
          IF ( J.EQ.NDATA.and.JJ.EQ.LOOPS ) GO TO 400
          IF ( J.EQ.NDATA.and.JJ.NE.LOOPS ) GO TO 777
          J = J + 1
        GO TO 666
C
C-------------------------------------------------------------------
C                    exit
C-------------------------------------------------------------------
C
C 991    TYPE*,'YOU HAVE PROBLEMS'
C        TYPE*,'STATUS CODE:    ',IOSB(1),IOSB(2)
C
 999    CALL EXIT
        END
C
C
```

References

[Asada and Kanade 83]
Asada, H., and Kanade, T.
Design of Direct-Drive Mechanical Arms.
ASME Journal of Vibration, Acoustics, Stress, and reliability in design 105(3):312-316, 1983.

[Asada and Lim 85]
Asada, H. and Lim, S.
Design of Joint Torque Sensor and Torque Feedback Control for Direct-Drive Arms.
In *To appear in the Proc. of the ASME, Winter Annual Meeting.* Miami, Florida, Nov., 1985.

[Asada and Youcef-Toumi 83]
Asada, H., and Youcef-Toumi, K.
Analysis and Design of Semi-Direct-Drive Robot Arms.
In *Proc. of 1983 American Control Conference*, pages 757-764. San Francisco, 1983.

[Asada and Youcef-Toumi 84]
Asada, H., and Youcef-Toumi, K.
Analysis and Design of a Direct-Drive Arm With a Five-Bar-Link Parallel Drive Mechanism.
ASME Journal of Dynamic Systems, Measurement and Control 106(3):225-230, 1984.

[Asada, Kanade and Takeyama 83]
Asada, H., Kanade, T., and Takeyama, I.
Control of a Direct-Drive Arm .
ASME Journal of Dynamic Systems, Measurement, and Control 105(3):136-142, 1983.

[Asada, Youcef-Toumi and Lim 84]
Asada, H., Youcef-Toumi, K. and Lim, S.
Joint Torque Measurement of a Direct-Drive Arm.
In *Proc. of the 23rd Conference on Decision and Control.* Las Vegas, NV., Dec., 1984.

[Asada, Youcef-Toumi and Ramirez 84]
Asada, H., Youcef-Toumi, K. and Ramirez, R.
Design of M.I.T Direct-Drive Arm.
In *International Symposium on Design and Synthesis, Japan Society of Precision Engineering.* Tokyo, Japan, July, 1984.

[Brady, Hollerbach et al 83]
Brady, M., Hollerbach, J. M., et al.
Robot Motion: Planning and Control.
M.I.T Press, Cambridge,Mass, 1983.

[Davis and Chen 84]
Davis, S. and Chen, D.
High Performance Brushless DC Motors for Direct-Drive Robot Arms.
In *Proceedings of IEEE.* , Oct., 1984.

[Denavit and Hartenberg 55]
Denavit, J. and Hartenberg, R. S.
A Kinematic Notation for Lower-Pair Mechanisms Based on Matrices.
ASME Journal of Applied Mechanics :215-221, 1955.

[Dubowsky 83] Dubowsky, S.
The Dynamics and Control of Robotic Manipulators.
In *of NATO, Advanced Study Institute.* Pisa, Italy, June, 1983.

[Dubowsky and Des Forges 79]
Dubowsky, S., and Des Forges, D. T.
The Application of Model-Referenced Adaptive Control to Robotic Manipulators.
ASME Journal of Dynamic Systems, Measurement and Control 101:193-200, 1979.

[Dubowsky and Perreire 82]
Dubowsky, S. and Perreire, N. D.
Noise and Vibration Genarated by Impacts in Linkage Systems: With Applications to Engines.
In *International Symposium Sponsored by General motors Research laboratories on Engine Noise. Edited by R. Hickling and M. Kamal.* Plenium Publishing CorporationHolt, 1982.

[Electro-Craft 80]
Electro-Craft.
DC Motors,Speed Controls,Servo-Systems .
Engineering Handbook by Electro-Craft Corporation, Minn., 1980.

[Freund 82] Freund, F.
Fast Nonlinear Control with Arbitrary Pole Placement for Industrial Robots and Manipulators.
Int. Journ. of Robotics Research 1(1):65-78, 1982.

[Hanafusa and Asada 77]
Hanafusa, H., Asada, H.
A Robot Hand with Elastic Fingers and Its Application to Assembly Process.
In *Proc. of IFAC First Symposium on Information Control Problems in Manufacturing Technology*, pages 127-138. Tokyo, 1977.

[Hogan 81] Hogan, N.
Impedance Control of a Robotic Manipulator.
In *Proc. of 1981 ASME, Winter Annual Meeting, WAshington DC.* NOV, 1981.

[Hollerbach 80] Hollerbach, J. M. .
A Recursive Lagrangian Formulation of Manipulator Dynamics and a Comparative Study of Dynamics Formulation complexity.
In *IEEE Trans. on Systems, Man, and Cybernetics*, pages 730-736. November, 1980.

[Inoue 71] Inoue, H.
Computer Controlled Bilateral Manipulator .
In *Bulletin*, pages 199-207. Japan Soc. Mech. Eng., 1971.

[Kanade, Khosla and Tanaka 84]
Kanade, T., Khosla, P. K. and Tanaka, N.
Real-Time Control of CMU Direct-Drive Arm II Using Customized Inverse Dynamics.
In *Conference on decision and Control.* december, 1984.

[Kane 68] Kane, T. R.
Dynamics.
Holt, Rinehart and Winston, Inc., 1968.

[Luh, Walker and Paul 80]
Luh, J. Y. S., Walker, M. W., Paul, R. P. C.
On Line Computational Scheme for Mechanical Manipulators.
ASME Journal of Dynamic Systems, Measurement and Control 102, 1980.

[Mason 81] Mason, M.
Compliance and Force Control for Computer Controlled Manipulators.
IEEE transactions on Systems, Man, and Cybernetics SMC-11(6), June, 1981.

[Nevins and Whitney 74]
Nevins, J. L., and Whitney, D. E.
The Force Vector Assembler Concept.
In *First IFToMM Symp. Theory, Practice of Robots, Manipulators.* 1974.

[Paul 81] Paul, R.
Robot Manipulators: mathematics, Programming, and Control.
M.I.T Press, 1981.

[Paynter 82] Paynter, H. M.
Modeling and Simulation of Dynamic Systems.
In *Course 2.141, Department of Mechanical Engineering, Massachusetts Institute of Technology.* Spring, 1982.

[Raibert and Craig 80]
Raibert M.H.,Craig J.J.
Hybrid Position/Force Control of Manipulators .
In *Dynamic Systems and Control Division of ASME, Winter Annual Meeting.* November, 1980.

[Ramirez 84] Ramirez, R. .
Design of High Speed Graphite Composite Robot Arm.
In *Master of Science Thesis, Department of Mechanical Engineering.* Massachusetts Institute of Technology, Feb., 1984.

[Strang 80] Strang, G.
Linear Algebra and its Applications.
Academic Pres, Inc., 1980.

[Takegaki and Arimoto 81]
Takegaki, M. and Arimoto,S.
An Adaptive Trajectory Control of Manipulators.
Int. Journal of Control 34(2):219-230, 1981.

[Tal 81] Tal, J.
Modeling Motors for Control Applications.
In *Proceedings of the First Int. MOTORCON Conf.*, pages 2A.1-1 - 2A.1-12. , June, 1981.

[Tepper and Lowen 72]
Tepper, F. R. and Lowen, G. G.
General Theorems Concerning Full Force Balancing of Planar Linkages by Mass Redistribution.
Journal of Eng. Ind. , Trans. of ASME Ser., B,94:780-796, 1972.

[Tepper and Lowen 73]
Tepper, F. R. and Lowen, G. G.
Two General Rules for Full Force Balancing of Planar Linkages.
In *Proc. 3rd. Appl. Mech. Conf., Paper No 10.*. Oklahoma State University, 1973.

[Tepper and Lowen 75]
Tepper, F. R. and Lowen, G. G.
Shaking Force Optimization of Four-Bar Linkages with Adjustable Constraints on Ground Bearing Forces.
Journal of Eng. Ind. , Trans. of ASME Ser., B,97:643-651, 1975.

[Unimation 80] Unimation Inc. .
Unimate PUMA Robot, Technical Manual
1980.

[Vukobratovic and Stokic 80]
Vukobratovic, K.M., and Stokic, D.M.
Contribution to the Decoupled Control of Large-Scale Mechanical Systems.
In *Automatica*, pages 9-21. January, 1980.

[Walker and Oldham 78]
Walker, M. J. and Oldham, K.
Mechanisms and Machine Theory.
, 1978, pages 175-185.

[Wilson 60] Wilson, E. B.
Vector Analysis.
Dover Publications, Inc., 1960.